UCLA

UCLA Electronic Theses and Dissertations

Title

Experimental Study on the Aerospace Applications of Photoreactive Nanomaterials

Permalink

https://escholarship.org/uc/item/10h2d60v

Author

Wirth, David M.

Publication Date

2012

Peer reviewed|Thesis/dissertation

UNIVERSITY OF CALIFORNIA

Los Angeles

Experimental Study on the Aerospace Applications of Photoreactive Nanomaterials

A thesis submitted in partial satisfaction

of the requirements for the degree Master of Science

in Aerospace Engineering

by

David M. Wirth

2012

ABSTRACT OF THE THESIS

Experimental Study on the Aerospace Applications of Photoreactive Nanomaterials

by

David M. Wirth

Master of Science in Aerospace Engineering

University of California, Los Angeles, 2012

Professor Laurent G. Pilon, Chair

This study was concerned with the aerospace applications of the photoignition of carbon nanotubes. First, experiments investigating the volumetric photoignition characteristics of single walled (SWCNTs) and multi walled (MWCNTs) carbon nanotubes were conducted. Photoignition of various SWCNTs, MWCNTs, and ammonium perchlorate/SWCNT mixtures was investigated. The minimum ignition energy (MIE) was measured as a function of bulk temperature using a custom made flash thermal energy sensor. Moreover, design and experiments were carried out to demonstrate individually photoignitable "rocket cells" using mixtures of MWCNTs and solid oxidizers. A number of these rocket cells were assembled and ignited in various arrangements and sequences to demonstrate volumetric photoignition of solid rocket fuel. A proof of concept demonstration of a re-ignitable, controllable, and thrust vectorable solid rocket motor using photoignitable MWCNTs as the ignition source was also constructed and tested. Finally, future work was suggested based on the current state of knowledge and on the results of this study.

The thesis of David M. Wirth is approved.

William E. Peris

Yong Chen

Laurent G. Pilon, Committee Chair

University of California, Los Angeles

2012

Table of Contents

List of Figures

viii

ix

LIST OF TABLES

Acknowledgments

I would like to acknowledge the following colleagues and faculty who supported the publication of this work. Prof. Laurent Pilon: for his time, dedication and patience when working with me throughout my time here at UCLA. Cadet Joshua Kim: for all his help and volunteer work in the lab. Prof. Richard Wirz: for allowing me to start my career in R&D, and for offering me a job in his Electric Propulsion lab. I also like to give my thanks to Prof. Wirz and Prof. Karagozian for their nomination for the Vishal Parikah Memorial Scholarship and internship at AFRL. Dr. Al Badakshan and Dr. Steve Danczyck: I had the pleasure of working with both of them at AFRL and I am appreciative of their support in bringing part of their project to UCLA. Prof. Yong Chen: for taking an interest in my work during my short time in his class, and for his collaboration and mentorship on a number of occasions. Lt Col Ajax Peris: I am grateful to have known him for 4 out of my 5 years at UCLA. I am grateful for his guidance, mentorship, and support of my efforts to pursue this degree, and for his nomination for the National Cadet Research Award.

I would like to extend my thanks to all students working in Prof Pilon's lab for tolerating the numerous small explosions, accidental detonations, Xe arc flashes, and substantial UV light exposure which resulted from my work.

Finally I would like to thank my Father (Milton Wirth) and my Grandfather (Robert Berman) for their enthusiasm of science and chemistry, respectively. I would like to believe some of their enthusiasm rubbed off on me.

CHAPTER 1

Introduction

"Where the telescope ends, the microscope begins.

Which of the two has the grander view?"

-Victor Hugo, 1862

The objective of this chapter is to present the motivations, applications, and background for the current study. First it examines the use of nanotechnology to address the current challenges in aerospace applications. It then discusses the properties and manufacturing processes of carbon nanotubes (CNTs), as well as the differences between single walled carbon nanotubes (SWCNTs) and multi walled carbon nanotubes (MWCNTs). The phenomenon of photoignition of CNTs is also introduced and its potential applications are discussed. Finally, the objectives of the present study and the scope of this thesis are presented.

1.1   Motivations

Currently, small rockets are ignited using a so-called "electric match". Figure 1.1 shows a standard electric match which typically consists of a small metallic wire through which current is passed causing Joule heating. Heating results in the ignition of a pyrogenic (flame producing) mixture which coats the tip of the electric match. This technology is very similar to the simple friction match which has been used for centuries.

In the 1950's, the disciplines of engineering, physics, biology, and chemistry were clearly defined and shared virtually no common subject ground. Figure 1.2 shows that today, all four of these subjects are converging on the nanoscale to exploit both physical laws and new
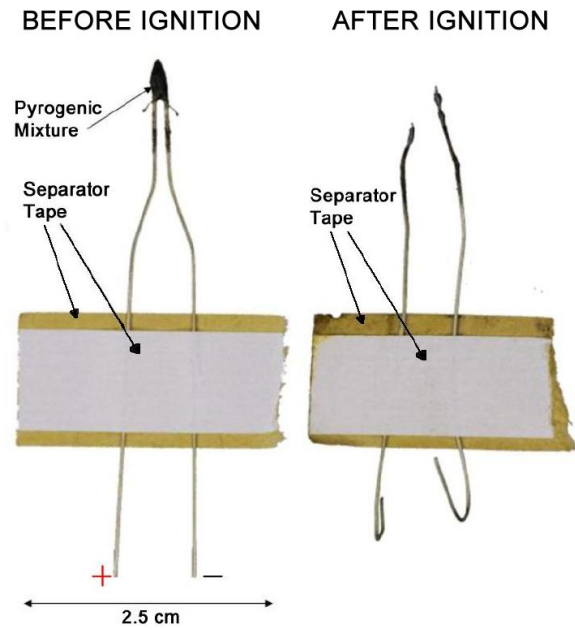
Figure 1.1: A simple wire "electric match" rocket igniter [1].

materials with unusual physicochemical properties [2]. Advances in nanotechnology may
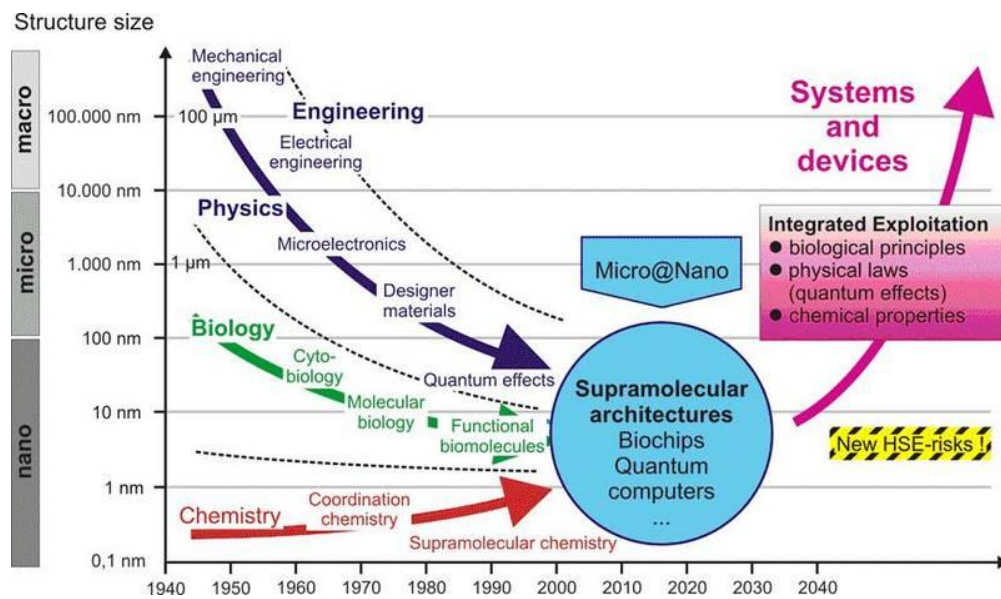
Figure 1.2: Nanotechnology, the convergence of scientific disciplines [2].

open up new avenues in propulsion applications for the aerospace industry.

1.2 Aerospace propulsion

A major challenge currently facing the aerospace industry is that there exists no spacecraft propulsion technology which has both high thrust and high specific impulse [22]. A rocket's specific impulse (I_{sp}) can be defined as the ratio of its thrust (N) to its fuel consumption (kg/s), divided by Earth's gravitational acceleration.

$$I_{sp} = \frac{F_{thrust}}{\dot{m}g_0} \tag{1.1}$$

where F_{thrust} is the rocket's thrust in (N), $\dot{m}$ is the mass flow rate in (kg/s) and g_0 is the Earth's gravity (9.81 m/s^2). Technologies have been proposed to attain both high I_{sp} and high thrust [23]. However, all propulsion technologies have both drawbacks and limitations. In fact, the technologies which produce the greatest vacuum specific impulse I_{sp} are electric propulsion such as ion engines, Hall effect thrusters, and other plasma based rockets which do not function well in Earth's atmosphere [24].

Also, the high thrust devices, such as chemical rockets (liquid, solid, and hybrid), have a limited burn time and are inefficient compared to electric propulsion [24, 25]. There is also a large need for single-stage to orbit (SSTO) capability in today's aerospace industry requiring high efficiency, long burning and controllable propulsion systems which have sufficient thrust to bare [26].

1.3 Carbon nanotubes

Carbon nanotubes (CNTs) are a form of carbon which exhibits many unusual properties and has been the subject of intense study since their discovery by Iijima *et al.* [3] in 1991. Figure 1.3 shows the difference in diameter and structure between double walled carbon nanotubes (DWCNTs) and multi walled carbon nanotubes (MWCNTs). DWCNTs have

two wall structures whereas MWCNTs have 3 or more wall structures. Similarly, SWCNTs consist of a single layer of graphene rolled into a tube whose diameter depends on the chirality of the nanotube.
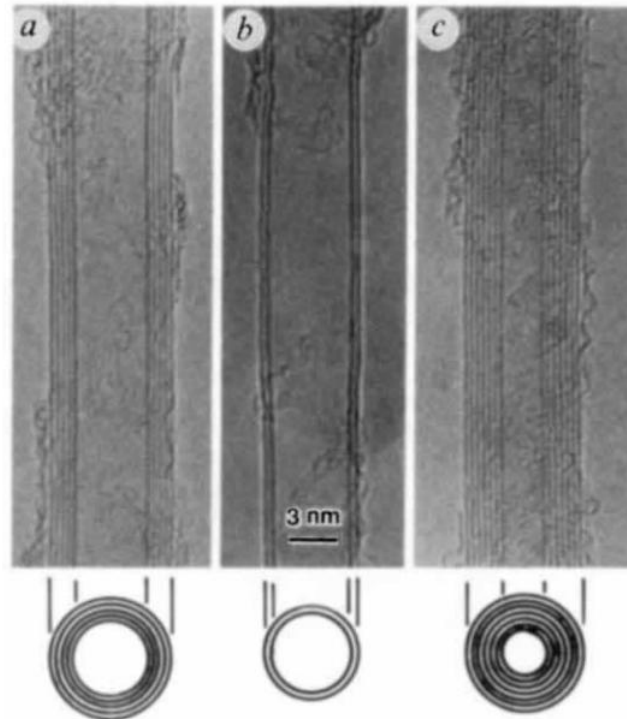
Figure 1.3: First electron micrograph highlighting the structure of (a) and (c) multi walled and (b) double walled carbon nanotubes [3].

1.3.1 Single walled carbon nanotubes (SWCNTs)

Single walled carbon nanotubes are extremely light and strong fibers made of carbon atoms arranged in a high aspect ratio tube with diameter ranging from 0.5 to 20 nm while their length can exceed 2 cm or 900,000 times their diameter [27]. The diameter of a SWCNT depends on its chiral vector $\vec{C}$, which can be expressed in terms of its components in the a_1 and a_2 directions along a graphene sheet. Figure 1.4 shows the a_1 and a_2 vector components on a graphene sheet as well as the chiral vectors C $= \langle n, m \rangle$ of some typical SWCNTs. The

diameter of a SWCNT is a function of its chiral vector and is given by 1.2:

$$d_{SWCNT} = \frac{b}{\pi}\sqrt{3(n^2 + mn + m^2)} \qquad (1.2)$$

where b is the C-C bond length equates to $b = 0.142$ nm [27].
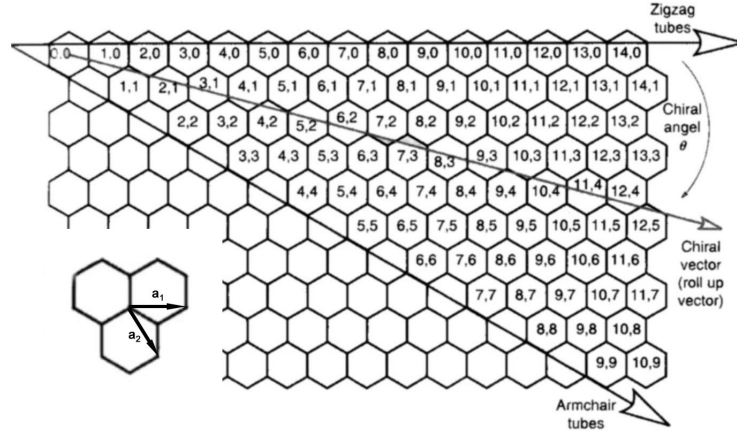
Figure 1.4: Schematic of a graphene sheet rolled along different directions to form various chiralities of SWCNT [4].

SWCNTs can be manufactured by a number of processes. We will focus on two of particular importance to this study, namely (i) chemical vapor deposition (CVD) and (ii) DC arc discharge.

Chemical vapor deposition

CVD synthesis of SWCNTs and MWCNTs is a process in which chemically active gasses in (i) a low pressure plasma deposition chamber or (ii) a high pressure CVD reactor. In the HiPco CVD process, CO gas is raised to high pressure [28]. In methane plasma PCVD, methane gas (CH_4) is injected into a low pressure plasma CVD chamber [29]. In both methods, the chambers are raised to high temperatures in the presence of a nanoparticle catalyst such as iron pentacarbonyl $Fe(CO)_5$ or ferrocene $Fe(C_5H_5)_2$. In the reaction chamber, the methane or carbon monoxide gas spontaneously reduces into H_2 and CO_2 gas, respectively. The resulting

carbon accumulates at the catalyst sites to form both SWCNTs and MWCNTs [28, 29] according to the reactions:

$$CH_{4(g)} \rightarrow C_{(s)} + 2H_{2(g)} \qquad \text{or} \qquad 2CO_{(g)} \rightarrow C_{(s)} + CO_{2(g)} \tag{1.3}$$

Figure 1.5 shows a diagram of a typical PCVD reactor used to grow SWCNTs. The diagram shows (a) the substrate consisting of silicon with adhered catalytic nanoparticles, (b) the CH_4 gas which will become ionized, and (c) the carrier gas, CH_4 [29].
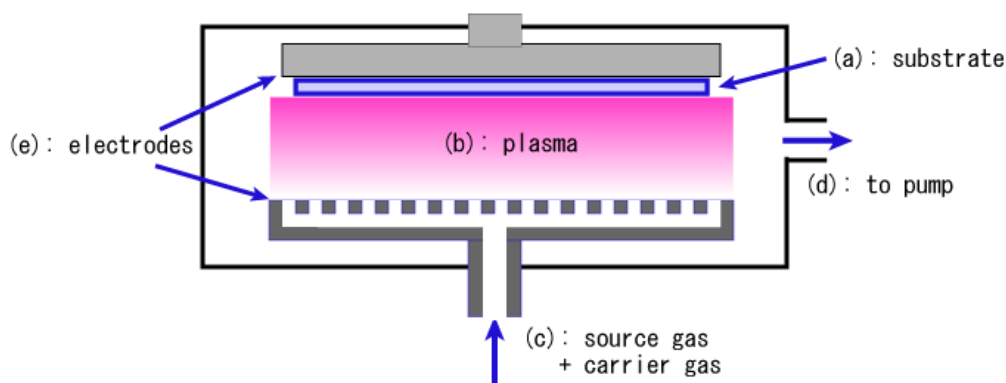
Figure 1.5: Diagram of a plasma CVD reactor used for the synthesis of SWCNT [5].

In methane catalyzed plasma CVD, the methane plasma decomposes at the catalyst sites to produce hydrogen gas and carbon nanotubes. In the HiPco process, due to the high pressure of the CO gas, the reaction proceeds in the direction which reduces the total number of moles of gas. This reaction is very effective at producing SWCNTs with specific diameters and physical properties. Chemical vapor deposition (CVD) is currently the cheapest and most widely adopted method to produce SWCNTs in the industry [27].

Xylene-ferrocene catalyzed CVD is one particular method of producing MWCNTs featuring small ferrocene impurities and large diameter nanotubes. The MWCNTs produced by this process have a diameter of between 100 and 200 nm, and contain deposits of ferrocene interspersed within the clusters of nanotubes.

6

DC arc discharge

Figure 1.6 shows a typical DC arc discharge reactor [16]. In the DC arc discharge process, high voltage is applied to graphite electrodes in an inert atmosphere. A plasma arc is created which ablates carbon atoms from a carbon-based electrode and electrostatically accelerates them towards the opposite electrode. These ablated carbon atoms adhere to the catalyst particles such as iron or nickel-yittrium (Ni-Y) [30]. Depending on the size of the catalyst particles, single, double, or multi-walled nanotubes can be formed. The SWCNTs made from DC arc discharge have a markedly different structure than the CVD-produced SWCNTs. Most notably, they are "fluffier" and much less dense than CVD-produced nanotubes whereas the CVD-produced SWCNTs and MWCNTs have higher density [15]. The production of SWCNTs via DC arc discharge is one of the oldest and most well understood production methods for small scale synthesis of CNTs [3]. However, it requires a strictly controlled inert atmosphere, expensive graphite/catalyst electrodes, and high amperage DC power [6].
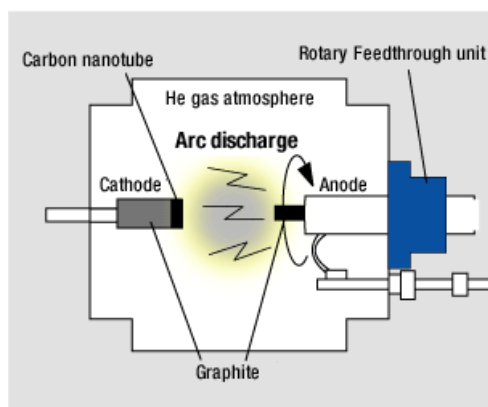
Figure 1.6: A typical DC arc discharge reaction chamber for the production of SWCNT [6].

1.3.2 Multi walled carbon nanotubes (MWCNTs)

Multi walled carbon nanotubes (MWCNTs) are light and strong fibers made of carbon atoms arranged in a series of concentric tubes, each with a diameter a few Angstroms larger than

the one nested inside. The final diameter of a MWCNT can range from that of relatively small DWCNT configurations 1.05 nm - 2.89 nm [27] to very large xylene-ferrocene catalyzed MWCNTs (used in this study) with diameters between 100 nm and 200 nm [27]. They are not as strong, conductive, or optically absorbing as SWCNTs due to their increased defect density [4]. However, MWCNTs are significantly cheaper to produce than SWCNTs and have found equivalent or comparable use in many applications.

Many of the structures produced in CVD or DC arc discharge reactors are amorphous carbon or MWCNTs. Amorphous carbon is the most abundant of the reaction products but it is of little use and is usually discarded. Then, the products are sorted according to diameter. The vast majority of the products are MWCNTs and a minority are SWCNTs. MWCNTs can be preferentially manufactured by a number of processes, but the prevailing method is CVD catalyzed with a multitude of different catalysts depending on the application [31].

1.4 Photoreactive nanomaterials

Photoignition is the property of a material to undergo combustion when exposed to light [8]. Photochemical reactions are key to understanding photoignition and many materials exhibit photoreactions. For example, potassium permanganate ($KMnO_4$) decomposes into potassium manganate ($KMnO_2$) and oxygen (O_2) when exposed to light [32]. Water splitting in evacuated CNTs has also been recently demonstrated [7]. Photoreactive nanomaterials are also the basis for all organic autotrophic life on Earth through photosynthesis [33].

1.4.1 Photochemical reactions

One key photochemical reaction, employed in the current study, is that of the photodecomposition of potassium permanganate ($KMnO_4$) to produce oxygen on demand. In 1937, Sundar Rao *et al.* [32] first reported the photodecomposition of $KMnO_4$ through the reaction:

$$MnO_4 + h\nu \rightarrow MnO_2 + 2O''$$
(1.4)
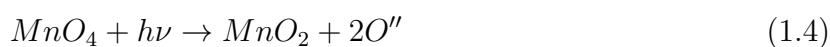
Moreover, photochemical reactions can result in the decomposition and combustion of CNTs. Indeed, when CNTs are flashed with light in vacuum instead of in an oxidizing environment, the temperature of the reaction increases dramatically and more dramatic structural reorganization can take place [8]. This was used by Guo *et al.* [7] to catalyze nano-thermolysis of water in SWCNTs under ultra-high vacuum. The authors found that when water vapor was introduced into a chamber containing SWCNTs which were maintained at ultra-high vacuum (10^{-7} Pa) and flashed with a Xe flash lamp, there was sharp pressure rise in the chamber and a release of hydrogen, helium, methane, and carbon monoxide which were produced by the reaction. Figure 1.7 reproduces the results measured with a quadrupole mass spectrometer (QMS) for the ultra-high vacuum system.
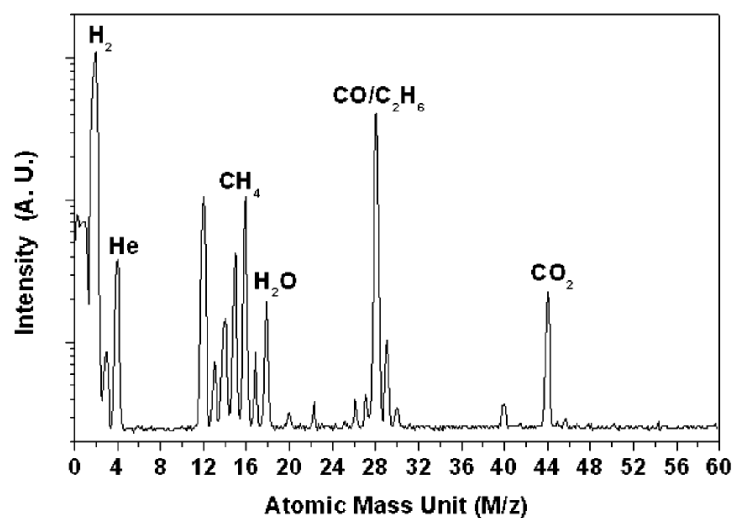
Figure 1.7: Quadrupole mass spectrometer (QMS) measurements of gas components generated from flash induced water-splitting in SWCNTs from one flash irradiation [7].

This illustrates the variety of gasses released from such a photoreaction and begs questions about the macromolecular chemistry responsible for the reactions.

1.4.2 Photoignitable nanomaterials

Photoignition has been observed in SWCNTs [8], MWCNTs [34], graphene oxide [35], silicon nanowires [36], polyanaline nanofibers [35], and certain types of metal-doped activated carbon [34]. Theoretically, any optically absorbing fuel in the presence of oxidizer can be photoignitable. However, the energy required may be extremely high for most materials. It is possible to impart sufficient light energy per unit area to achieve photoignition with any light source but with various levels of difficulty. In order for a material to undergo a combustion reaction, sufficient energy must be imparted to heat the fuel to its flash point and supply the activation energy for the combustion reactions to occur. This minimum energy required to start the light-initiated combustion reaction is called the minimum ignition energy (MIE) and is measured in mJ/pulse or mJ/cm^2 [15]. Some studies have also measured the flash power in W/cm^2 [10, 15].
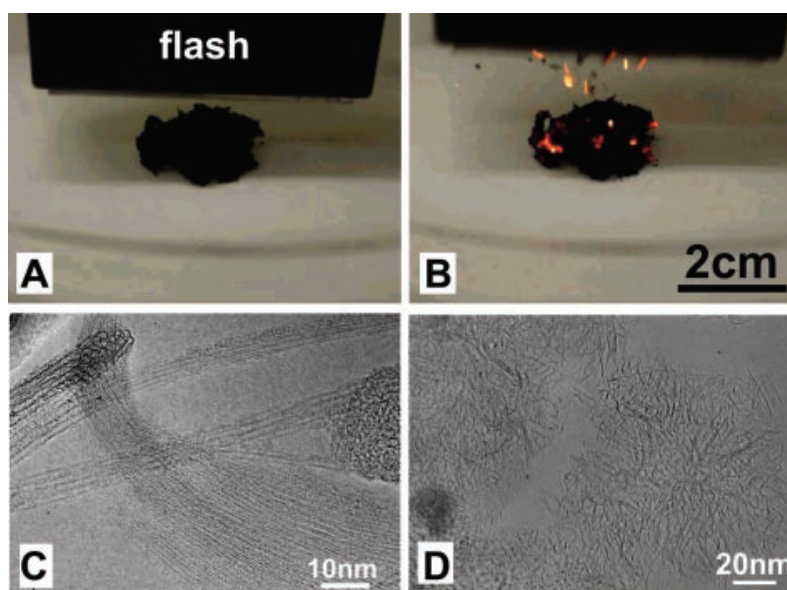
Figure 1.8: (A and B) Sequence of the burning of SWCNTs: (A) original sample (about 2 cm outer diameter) showing the flash on top; (B) sample soon after flashing exhibiting the ignited SWCNT material with burning red and yellow spots. (C) pristine SWCNTs seen under HRTEM. (D) SWCNTs after 1 flash in air seen under HRTEM [8].

Photoignition of CNT was first observed by Ajayan *et al.* [8] in 2002. The authors observed the spontaneous combustion of a sample of fluffy 50 wt.% Fe SWCNTs when exposed to an ordinary camera flash. Figure 1.8 shows a photograph of the SWCNT samples before (A) and after (B) flashing [8]. The authors also noted the structural change between the unflashed (C) and flashed (D) SWCNTs and in particular, the production of "nanohorns" using high resolution transmission electron microscope (HRTEM). These nanohorns indicated the presence of local temperatures in excess of 1500^oC [8].

Photoignition of SWCNTs can be used to ignite explosive materials [12], solid and liquid rocket fuels [11], as well as quiescent gaseous fuel-air mixtures [9]. Photoignition of CNTs is affected by a number of factors including (i) light flash energy [12, 15], (ii) atmospheric composition including air, oxygen, argon, helium, CO_2 [8, 15, 16], (iii) atmospheric pressure, (iv) sample compaction [9, 15, 37], (v) solid impurities such as iron nanoparticles, ferrocene, solid oxidizers, metallic powders [11, 37], and (vi) bulk temperature of the CNT bundle [16].

1.5   Photoreactive Nanomaterials for Aerospace Applications

The most convenient way to ignite an air/fuel mixture in a chamber is through a reusable spark plug. It consists of generating a spark causing combustion to propagate along a flame front. Figure 1.9 shows the propagation of a flame-front from a spark plug [9]. It is important to note the relatively slow propagation of the flame front, on the order of several milliseconds. Lasers can also be used as a source of photoignition but the high power lasers and delicate optics required renders them less practical for use in combustion engines [11]. The use of pyrophoric igniting compounds (such as triethylborane in the SR-71 aircraft engines) was found to be a reliable source of ignition [38] but they are non-reusable and dangerous to handle, making them difficult to adapt to civilian applications.

CNTs can also be used to ignite gaseous fuels in internal and external combustion engines much faster than spark plugs or lasers. This was recently demonstrated by Berkowitz *et al.* [9]. The application was first suggested by Chehroudi *et al.* [15] who studied the photoignition

11
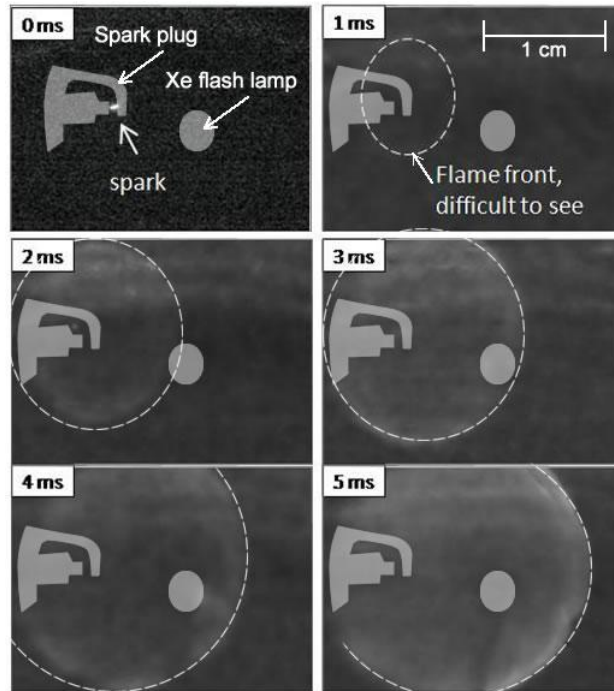
Figure 1.9: Flame-front (dashed line) propagating in a gaseous mixture of ethylene and air ignited with a conventional spark plug [9].

of liquid fuels with CNTs. The authors discovered that the presence of oxygen gas instead of air had a dramatic effect on SWCNT photoignition properties [15].

The photoignition properties of both SWCNTs and MWCNTs could enable low cost, highly reliable distributed ignition throughout combustion chambers. This would produce a steeper pressure rise, and faster combustion, allowing for internal combustion with larger chambers where an ordinary flame front may not be well suited such as in the case of liquid and hybrid rocket engines.

The efficiency in gasoline and liquid fueled rocket engines can also be improved through the use of CNT photoignition [9]. Figure 1.10 shows the peak pressure and rise time for a volumetric photoignition of 2 mg of SWCNTs dispersed in air and gaseous ethylene with a stoichiometric ratio of 1.0 at a chamber pressure of 1 bar. It indicates that the peak pressure within the reaction chamber is significantly higher than with an ordinary spark

12

at a comparable pressure and fuel/air ratio. The use of such an ignition mechanism could allow for more efficient internal combustion, jet, or rocket engines, as well as providing a vast improvement in the power and efficiency of pulse detonation engines which are currently being investigated for use in SSTO systems [39].
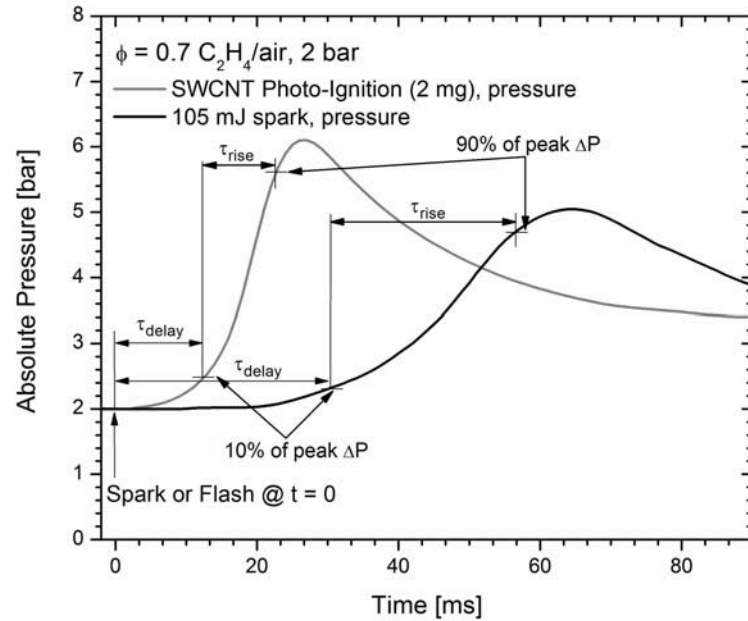
Figure 1.10: Comparison of pressure rise as a function of time between ordinary spark ignition and SWCNT photoignition. Volumetric ignition produces a much faster rise time and higher peak pressure [9].

1.6 Objectives of this study

This study aims to examine the use of photoignition of CNTs for direct spacecraft propulsion and solid fuel combustion initiation. The use of either SWCNTs or MWCNTs could enable distributed ignition in both solid rockets and combustion engines. Distributed ignition would enable (i) faster and more reliable ignition, (ii) throttling and re-ignition of solid rocket engines, as well as (iii) more efficient and powerful ignition of fuel-air mixtures. The objectives of the present study are as follows:

1. To assess the dependence of CNT photoignition on atmospheric composition, solid oxidizer addition, and bulk temperature of the CNT bundle.

2. To demonstration photoignition of SWCNTs and MWCNTs when used in solid mixtures with various oxidizers, fuels, and metallic powders.

3. To demonstrate proof of concept for spacecraft propulsion using CNT-based photoignitable materials and mixtures.

4. To demonstrate volumetric photoignition to be a safe and effective alternative to point ignition in prototypical rockets.

1.7   Scope of the document

Chapter 2 provides a review of the current state of knowledge on SWCNTs and MWCNTs as well as on solid and liquid propellant rockets, and photoignition of CNTs. Chapter 3 describes experimental setups and procedures to investigate SWCNT and MWCNT photoignition, photoignitable mixtures of fuel and oxidizer, and quantitative measurements for minimum ignition energy (MIE). It also explores the effect of sample surface area on MIE. Chapter 4 presents the design, assembly, and testing of prototypical photoignitable solid rockets. Chapter 5 summarizes our findings and proposes recommendations for future work.

CHAPTER 2

Current State of Knowledge

The objective of this chapter is to present the current state of knowledge for the different aspects of carbon nanotube photoignition for propulsion applications. This chapter introduces the basic concepts along with a detailed review of the literature.

2.1 Properties of CNTs

Carbon nanotubes (CNTs) can be metallic conductors with a theoretical electrical conductivity of 4×10^9 A/cm^2, or semiconductors, depending on the chirality of the carbon-carbon bonds with respect to the CNT axis [40]. CNTs also have very high mechanical strength measured to be in the tens of GPa (10^9 Pa) [4]. They were also found to have a high Young's modulus on the order of one TPa (10^{12} Pa) [41]. Both SWCNTs and MWCNTs behave nearly as blackbodies for optical wavelengths between far UV to far IR [42]. Table 2.1 shows a comparison of optical absorbance between SWCNTs, MWCNTs, "super black", black spray paint, and white spray paint. "Super black" is a synthetic material made of a nickel-phosphorous alloy which has similar optical properties to CNTs but reflects in the IR region of the spectrum [18, 19]. Figure 2.1 shows the absorptance of 30 and 43 wt.% Fe SWCNTs, between 400 and 1600 nm [10]. It indicates that CNTs absorb lower wavelength light such as UV more strongly than infrared.
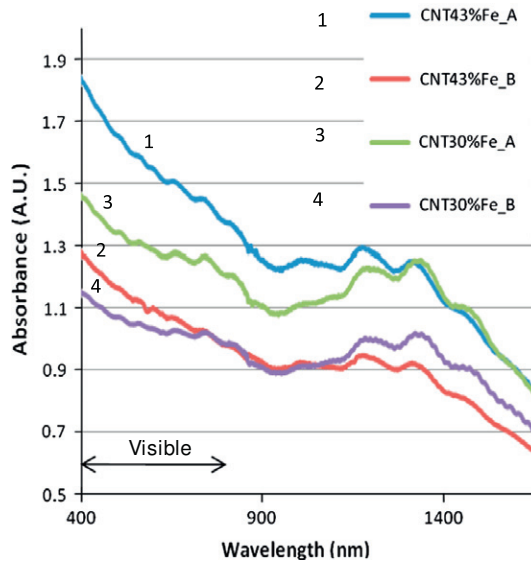
Figure 2.1: Absorbtion spectra of selected SWCNTs in arbitrary units (A.U.) over wavelengths from the edge of visible (400 nm) to NIR (1600 nm) [10].

2.2 Photoignition

Most materials require a large amount of energy to ignite and begin combustion. This ignition energy can be supplied by focused light, such as with a laser [43]. However, until recently, there was no material sensitive enough to be ignited by an unfocused beam or omnidirectional flash. Recently, Ajayan *et al.* [8] observed that some materials have the ability to ignite with much lower energy. They also noticed a loud photoacoustic effect accompanying the photoignition. *Photoignition* refers combustion which is initiated either as a direct or indirect result of photon energy absorption by a flammable material. The material may be ignited at a single point or many at once.

2.2.1 Principles of photoignition

SWCNTs containing ferrous impurities have a low activation energy for combustion and the highest optical absorbance of any known material [16, 42]. They are able be ignited with an

16

Table 2.1: Summary of absorbance of CNTs, and various other substances [18, 19].

Material	Absorbance (ε)
SWCNTs (far UV to far IR)	$\varepsilon \approx 0.99$
MWCNTs (far UV to far IR)	$\varepsilon \approx 0.98$
"Super black" (far UV to near IR)	$\varepsilon \approx 0.996$
Black spray paint (visible)	$\varepsilon \approx 0.96$
White spray paint (visible)	$\varepsilon \approx 0.16$

ordinary camera flash [8]. Similarly, nanoporous silicon [36], some forms of MWCNTs [34], and some forms of palladium-doped activated carbon [34] also exhibit photothermal heating and ignition properties with relatively low input energy. Many of these flash photoignitable materials release a photoacoustic "snap" following photoignition due to the rapid heating and expansion of air surrounding the material [8]. This photoacoustic effect is audible even when there is insignificant energy to ignite the material [8, 15]. The ability of a material to be ignited with a Xenon flash lamp is particularly important because, unlike a laser, flash lamps can cover a large surface area and thus can ignite multiple points on a material simultaneously. This phenomena is called *volumetric photoignition* and has been observed only recently in (i) gaseous fuels containing SWCNTs [9] and (ii) in liquid fuels containing SWCNTs [11].

2.2.2 Experimental evidences

Figure 2.2 shows a schematic of a reaction chamber and apparatus used by Berkowitz *et al.* [9] to ignite a SWCNT/gaseous ethylene/air mixture. A flash lamp (model 8951428-K, from disposable flash camera) which was placed in the center of the chamber was used to ignite 2 mg of SWCNTs dispersed in air with a stoichiometric ratio of 1.0 at a chamber pressure of 1 bar. Figure 2.3 shows the photoignition of gaseous ethylene and SWCNTs over 5.5 ms using a flash lamp in the center of the chamber.

Similarly, Figure 2.4 shows the photoignition of 50 wt.% Fe SWCNTs contained in a

17
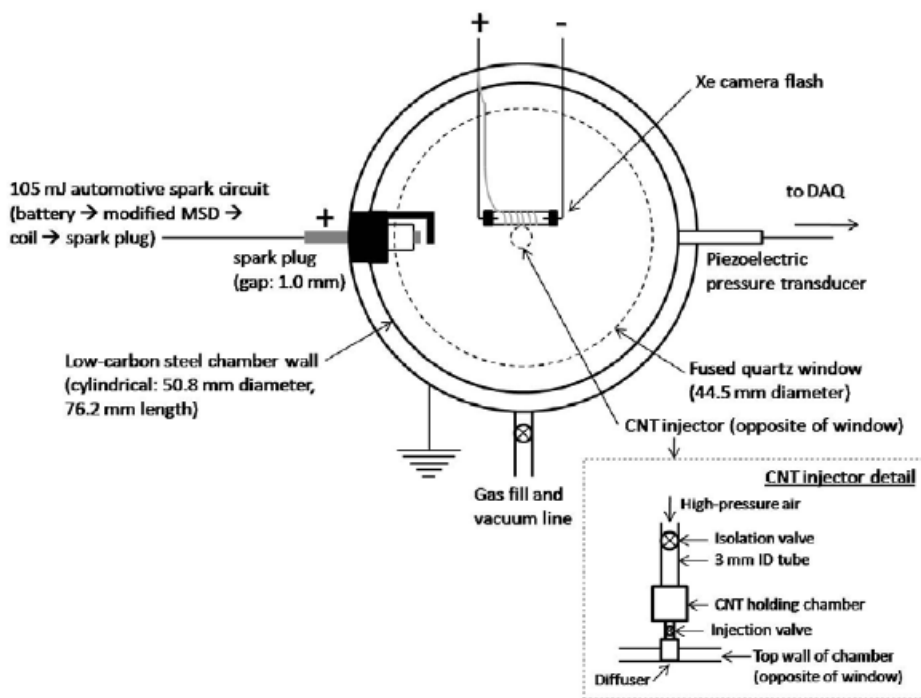
Figure 2.2: Volumetric ignition chamber experimental setup for photographs in Figure 2.3 [9].

gel capsule which led to the volumetric ignition of liquid fuel (50%/50% hexane/acetone) dispersed by an ultrasonic spray nozzle in the presence of pure oxygen [11]. The ignition capsule was flashed with a Canon camera flash model Speedlight 580 EXII compact Xe-arc with a pulse width of 7 ms and a flash energy of 5 J/cm^2.

In addition to the ability to initiate combustion in gaseous and liquid fuels, Manaa *et al.* [12] demonstrated the ability of SWCNTs to initiate detonations in solid fuels as well. They successfully photoignited pentaerythritol tetranitrate (PETN) and "K-6 explosive", leading to an explosive detonation. Figure 2.5 shows the setup and results of a SWCNT photoinitiated detonation reaction. The authors expressed interest for further research into (i) the ignition mechanism of SWCNT and (ii) determining which wavelengths of light are most effective at stimulating the ignition of SWCNTs [12].

In 2008, Desilets *et al.* [34] patented a flash-ignitable energetic material where they described a number of different mixture compositions which could be photoignited. Pho-
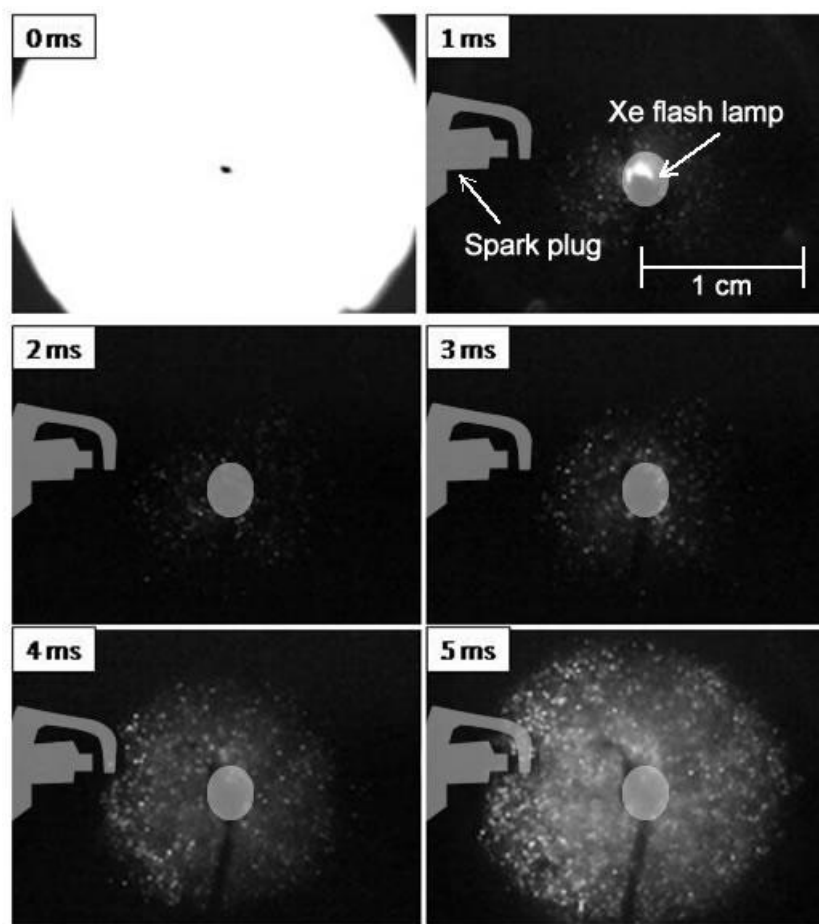
Figure 2.3: Demonstration of a gaseous volumetric photoignition of 70 wt.% Fe SWCNTs in an environment of gaseous ethylene and air [9].

toignition agents were ball milled with energetic materials for a period of time in order to homogenize the mixture. The novel findings and concepts in their patent were the following:

1. Mixtures contained a photoignition agent such as SWCNTs, MWCNTs, or palladium doped activated carbon, and an energetic material e.g., black powder, ammonium perchlorate (NH_4ClO_4), hexogen, or TNT. The authors found that the mixtures were capable of energetic high temperature photoignition.

2. Of these mixtures, SWCNTs were the preferred photoignition agent. Palladium doped activated carbon (with a ratio 97:3 activated carbon to palladium powder) was also

19
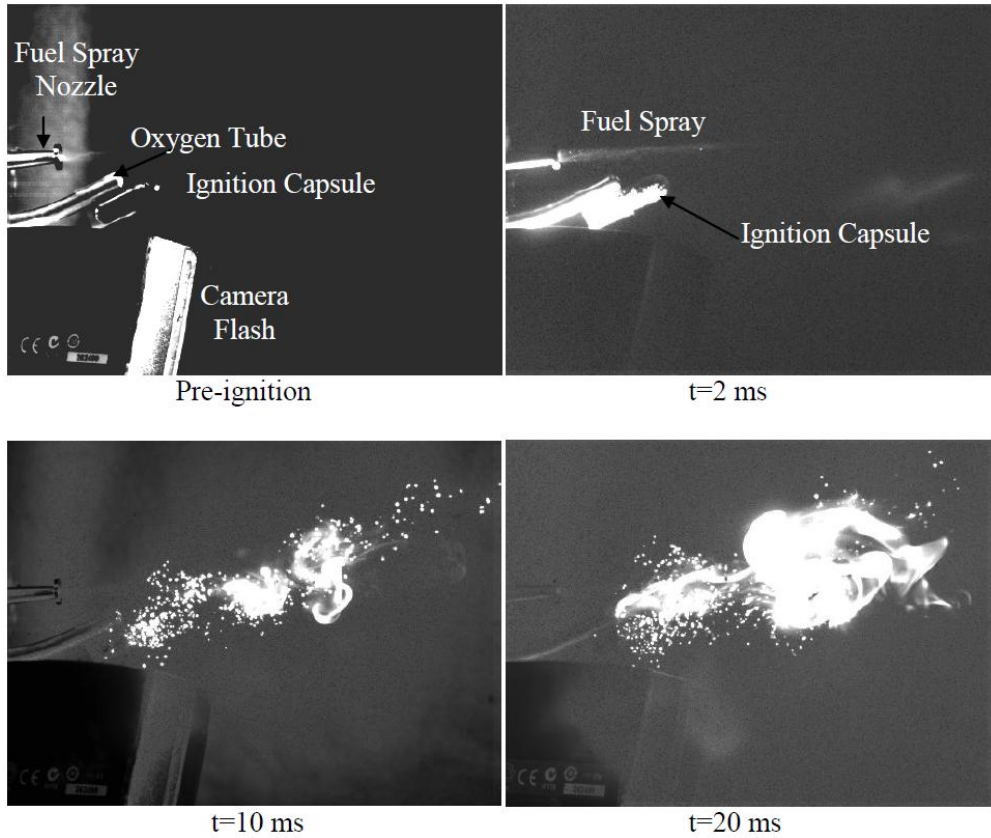
Figure 2.4: Demonstration of a liquid volumetric photoignition of a hexane/acetone mixture in the presence of pure oxygen using 50 wt.% Fe SWCNTs encapsulated in a gelatin capsule [11].

highly prone to photoignition. MWCNTs were described as inefficient but potentially usable as a photoignition agent.

3. The authors reported that effective mixtures contained 5 wt.% photoignition agent and 95 wt.% energetic material(s).

Re-ignitable solid rockets have also been proposed [13], but to date none have implemented a photoignition system. Figure 2.6 schematically shows the re-ignitable solid rocket motors patented by Bastian *et al.* [13]. The designs are based on separating one propellant grain section radially or vertically from the next with a non-flammable shield. The major
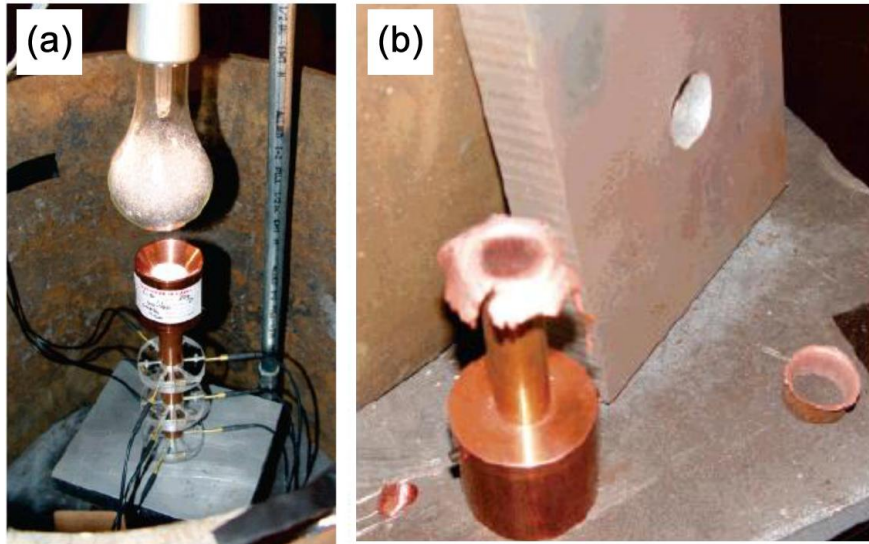
Figure 2.5: (a) A copper cylinder and a funnel containing "K-6 explosive" prior to the addition of 20 mg of 50 wt.% Fe SWCNTs. The mixture was flashed with an overhead flashbulb. (b) The copper cylinder after detonation of "K-6 explosive" and SWCNTs [12].

problem with such designs is the challenges in implementing an ignition system which can ignite a solid rocket repeatedly. Ignition of different sections of fuel grain requires ignition wires to be run near and around the hot burning propellant, risking failure due to gas leaks and broken wires. The solution may be to embed the ignition system within the fuel grain through use of a photoignitable material which can be ignited remotely via light pulse. The flashing mechanism could be placed behind a heat resistant alumina window, rather than being in direct contact with the fuel grain like all current ignition systems.

2.2.3   Photoacoustic considerations

Tseng *et al.* [14] studied the photoacoustic effect which accompanies the flashing of SWCNTs and MWCNTs, along with the physical mechanism(s) of photoignition. Figure 2.7 shows the sound pressure (Pa) as a function of frequency (Hz) for the photoacoustic signal recorded when flashing various carbon materials with a broad spectrum Xe flash lamp. It demonstrates
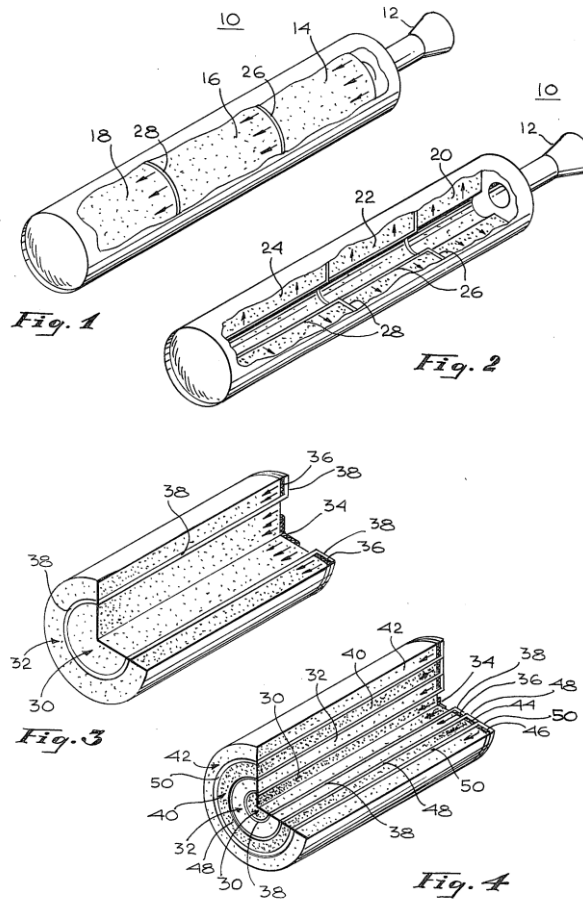
Figure 2.6: Designs for re-ignitable solid rocket motors. Shows concentric or vertically separated sections of propellant grain separated by non-flammable barriers [13].

that "fluffy" 30 wt.% Fe SWCNTs prepared using a modified HiPco process exhibit the largest photoacoustic effect when flashed with a Xe flash lamp. Other materials produced a lower photoacoustic response "Fluffy" MWCNTs, purified SWCNTs, compacted SWCNTs, carbon fiber, and carbon powder each demonstrated a successively decreasing photoacoustic effect.

Tseng *et al.* [14] also observed the effect of spraying ferrocene powder onto SWCNTs containing iron impurities. When flashed without ferrocene powder, the SWCNTs simply emitted hot sparks. However, with ferrocene powder the CNTs burst into flame. Figure 2.8
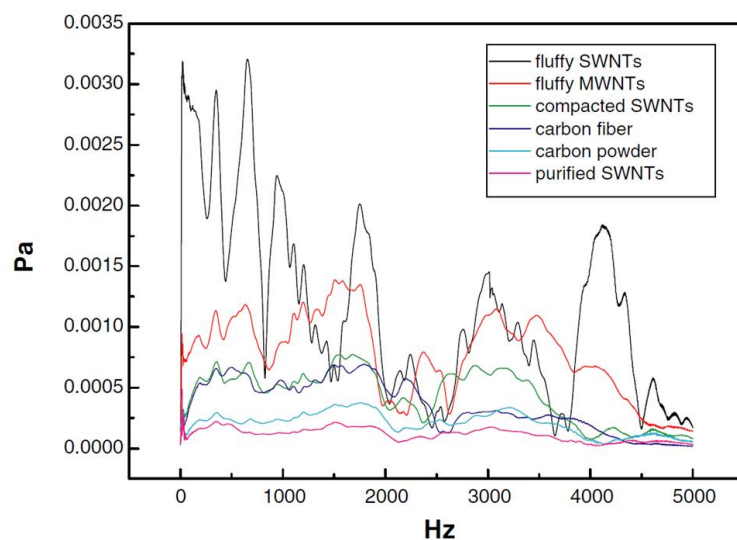
Figure 2.7: Pressure recorded as a function of frequency (Hz) when flashing carbon materials with a broad spectrum Xe flash lamp [14].

shows the enhanced ignition properties demonstrated when 1.0 g of ferrocene was sprayed onto the surface of "fluffy" SWCNTs and flashed. A visible flame is seen when ferrocene was added. This image should be compared with the SWCNTs seen in Figure 1.8 where only hot sparks could be observed.

2.2.4 Thermokinetics

Vignes *et al.* [16] performed a thermokinetic study on the self-heating of CNTs without regard to their photoignition. They measured the thermogravimetric properties of MWCNTs at high temperature, specifically the relative weight of a sample with respect to its bulk temperature. They determined the activation energy for self-ignition of raw MWCNTs to be $E_A = 155$ kJ/mol. They also hypothesized that SWCNTs have a lower ignition activation energy than MWCNT due to their smaller diameter and therefore higher surface area and reactivity to oxygen [16]. Finally, they noted that "industrial" MWCNTs have a significantly higher activation energy ($E_A = 290$ kJ/mol), than SWCNTs containing 3.5 wt.% Fe which have

Figure 2.8: Photoignition of HiPco synthesized "fluffy" SWCNTs containing 30 wt.% Fe after 1.0 g of ferrocene was sprayed uniformly onto the cluster of nanotubes [14].

an activation energy of $E_A = 119 \pm 5$ kJ/mol due to their defects and catalytic particles, respectively [16].

2.3 Parameters affecting photoignition

Chehroundi *et al.* [15] discussed a number of important aspects of CNT photoignition with respect to wavelength of light, MIE, atmospheric composition, and solid impurities in the CNTs. Their findings are discussed in the following sections.

2.3.1 Mechanism of CNT photoignition

Before we can examine the effect of various parameters on CNT photoignition, we must discuss the mechanism by which the CNTs photoignite. There are two different theories on

the photo-absorption mechanism of CNTs as discussed by Berkowitz *et al.* [9].

First, Ajayan *et al.* [8] suggested that the optically black SWCNT fibres absorbed visible and infrared light and transmitted that energy as heat into the Fe nanoparticle sites, which subsequently gained enough activation energy to oxidize and support a combustion reaction with the surrounding air.

An alternate theory was proposed by Smits *et al.* [37] who postulated that the Fe nanoparticles (not the SWCNTs) were the sites of photon absorption, and the SWCNTs acted to confine the heat through their low density and one-dimensional heat conducting properties. Due to the SWCNT's thermal properties, some Fe nanoparticle sites become insulated. The heat builds up and the Fe gains sufficient thermal energy to oxidize. The SWCNTs oxidize with the surrounding air and undergo significant structural modifications. Due to the optical and thermal properties of SWCNTs, Smits *et al.* [37] suggested that they act as a stabilizing agent preventing self-ignition of the Fe nanoparticles up to a certain critical energy (the MIE), after which, the heat flux into the nanotube clusters exceeds the heat flux out and thermal energy builds up until a redox reaction occurs.

2.3.2   Effect of light flash energy

The minimum ignition energy (MIE) of a sample of CNTs depends on (i) the light energy absorbed and (ii) the wavelength of the incident light [12]. Table 2.2 summarizes the MIE measured for different commercial filters. Slight deviations in MIE with respect to wavelength are present. This can be explained by examining the SWCNT's absorption spectrum (figure 2.1) and the Xe flashlamp emission spectra (figure 3.5). The flash lamp emits most strongly in the NIR wavelengths while the SWCNTs absorb most strongly in the ultraviolet region. However, the data taken by Chehroudi *et al.* [15] has a large experimental uncertainty and further studies are needed to clarify the results.

The data summarized in Table 2.2 shows a consistent trend that MIE decreases as the flash power (W/cm^2) increases [15]. This is most likely due to heat building up faster than

Table 2.2: Measured MIE per flash and calculated radiation flux on sample for different wavelengths [15]. Wavelength range taken from filter supplier's website [20, 21].

Filter (nm)	MIE (mJ/pulse)	Max light output (mJ/pulse)	Flash power (W/cm^2)	Flash duration (ms)	Light filter (supplier)
None 400 − 1600	85 ± 10	620	7.3 ± 1.4	7	
Long Pass 490 − 1600	83 ± 15	460	7.5 ± 1.4	7	CVI (Griot) (LP 495)
Long Pass 560 − 1600	97 ± 15	425	8.7 ± 1.4	7	CVI (Griot) (LP 550)
Long Pass 725 − 1600	83 ± 15	440	7.1 ± 1.4	7	Edmund Optics (LP 700)
Short Pass 510 − 1050	79 ± 15	505	7.1 ± 1.4	7	Edmund Optics (SP 1100)
Short Pass 425 − 865	85 ± 15	385	7.7 ± 1.4	7	Edmund Optics (SP 900)
None 400 − 1600	32 ± 5	54	255 ± 40	0.2	
Long Pass 490 − 1600	36 ± 5	44	290 ± 40	0.2	CVI (Griot) (LP 495)
Long Pass 560 − 1600	33 ± 5	34	260 ± 40	0.2	CVI (Griot) (LP 550)
Long Pass 725 − 1600	32 ± 5	39	255 ± 40	0.2	Edmund Optics (LP 700)
Short Pass 510 − 1050	29 ± 5	45	230 ± 40	0.2	Edmund Optics (SP 1100)
Short Pass 425 − 865	32 ± 5	34	255 ± 40	0.1	Edmund Optics (SP 900)

it can be re-emitted away from the CNTs in the form of infrared radiation. Therefore, a lower total energy needs to be delivered to the sample before it reaches the necessary ignition temperature for the combustion reaction to propagate.

2.3.3   Effect of atmospheric composition

Atmospheric composition also plays a large part in the photoignition properties of CNTs. First, photoignition is not possible in the absence of an oxidizing atmosphere. However,
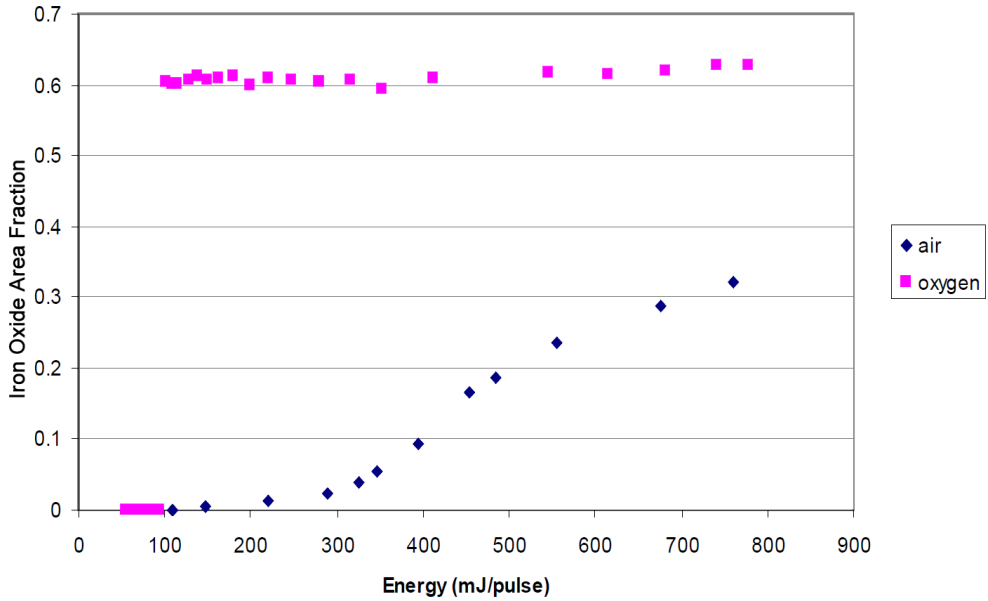
Figure 2.9: Photoignition response of a 5 lbf compacted sample of 50 wt.% Fe SWCNT under air and O_2 environments, flashed with light at successively higher energies from 50-750 mJ/pulse [15].

photo-heating may be greatly enhanced in atmospheres which are less thermally conductive [8]. Table 2.3 summarizes the effects of atmosphere composition on the structural and photo-heating characteristics of CNTs. Chehroudi *et al.* [15] noted that the MIE necessary to cause photoignition is dramatically lower in oxygen compared with air. Figure 2.9 shows the increasing "area fraction" of iron oxide with respect to increasing flash energy in environments of oxygen and air. The "area fraction" is defined as the area of oxidized SWCNTs divided by the total area of SWCNTs. This area fraction is an indicator of the completeness of the oxidization reaction resulting from SWCNT photoignition.

It is notable that in pure oxygen, there is a clear threshold point where the entire sample spontaneously oxidizes and releases a large amount of heat. However, in air, the threshold point is not as clearly defined. Figure 2.9 shows the MIE of SWCNTs in air and O_2 is around 100 mJ for both atmospheres, but the ignition response at higher flash energies is far

Table 2.3: Summary of the effects of atmosphere composition on photoignition of SWCNTs [8].

Atmosphere	Thermal conductivity of atmosphere $(mW/(m \cdot K))$	Temp. (K)	Structural Effects
Vacuum	0.0	1500+	"Substantial reconstruction" and graphitization
Argon (1 bar)	18	1500+	"Substantial reconstruction" and graphitization
Air (1 bar)	24	600-700	Oxidization and ignition of ferrous impurities, reconstruction of SWCNT into "nanohorns"
Oxygen (1 bar)	24	700+	Vigorous oxidization and ignition of SWCNT, combustion of SWCNT
CO_2 (1 bar)	80	?	Minor structural "fraying", no observable "nanohorns" on SEM image
Helium (1 bar)	152	?	Few remaining nanotube structures, large amounts of "nanohorns"
Acetone (1 bar)	160	N/A	No ignition or reconstruction
Liquid water (1 bar)	600	N/A	No ignition or reconstruction

different. If a sample was flashed in air, after the MIE is reached the area fraction increases slowly as the flash energy is increased. However, if the sample was flashed in oxygen, when the MIE is reached the entire sample oxidized fully and further oxidization with higher flash energy was not possible. Figure 2.10 shows photographs of (a) SWCNTs after 25 flashes in air. (b) SWCNTs after 5 addition flashes in air. (c) SWCNTs after the 8 flashes in pure O_2. (d) SWCNTs after the 9th flash in pure O_2. The experiment demonstrates that when flashed 25 times in air followed by an additional 5 flashes with all flashes above the MIE, there was little change in oxidization. However, when flashed in pure oxygen, even one flash above the MIE is enough to cause complete oxidization.

A lack of oxygen has negative results on photoignition. Vignes *et al.* [16] found that as the concentration of oxygen decreases, the temperature needed to induce weight reduction (combustion) in MWCNT increases. They also noted that the oxidization of MWCNTs was much more gradual at lower O_2 partial pressures [16]. In fact, Figure 2.11 shows the
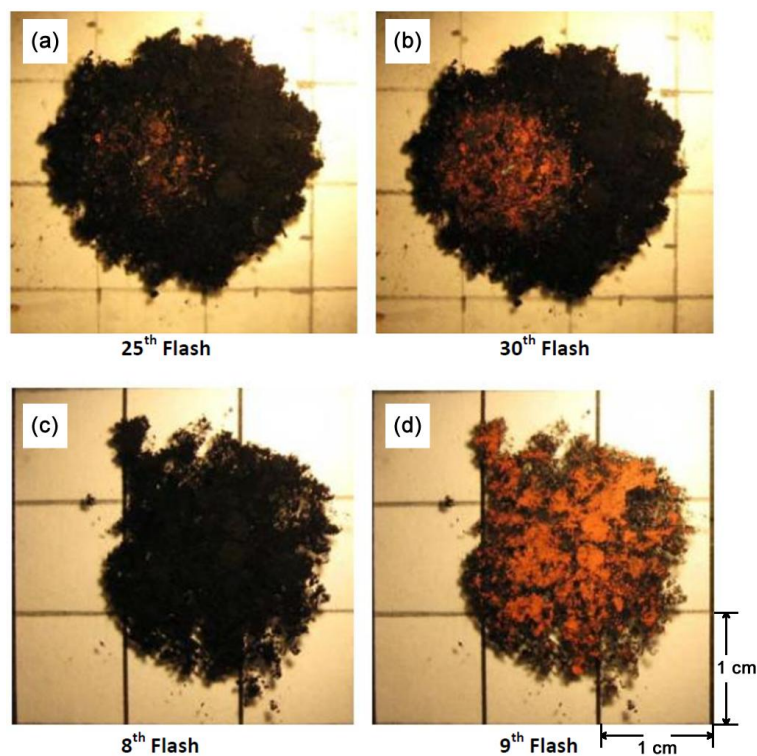
Figure 2.10: Examples of photoignition for 50 wt.% Fe SWCNTs in air and pure O_2. (a) SWCNTs after 25 flashes in air. (b) same SWCNTs sample after 5 addition flashes in air. (c) SWCNTs after the 8 flashes in pure O_2. (d) SWCNTs after the 9th flash in pure O_2 [15].

relative weight of MWCNTs as a function of temperature for different oxygen content in the atmosphere. It indicates that the weight decreased rapidly at $450 - 500^oC$ for MWCNTs in air, with an initial temperature of combustion onset of 452^oC. Note that Vignes *et al.* [16] did not observe the combustion onset temperature for SWCNTs with different oxygen concentrations, only MWCNTs. Combustion onset temperature of SWCNTs was analyzed in the current study and discussed in chapter 3.

However, when the atmosphere is not oxidizing ignition is not observed, and the structural reconstruction observed in the CNTs is radically different [8]. The degree of structural reconstruction in CNTs fibers is dependent on the thermal conductivity of the fluid in which the CNTs are flashed, as shown in Table 2.3 [8]. When the thermal conductivity of the
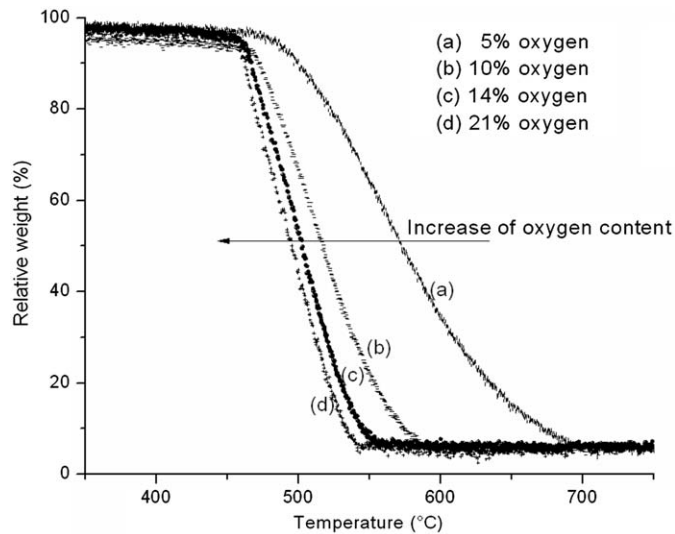
Figure 2.11: Effects of oxygen concentration on MWCNT sample relative weight as a function of the temperature obtained by thermo-gravimetric analysis. [16].

surrounding fluid is too high, the CNTs cannot ignite.

2.3.4 Effect of atmospheric and physical pressure

The effect of sample compaction on MIE was studied by Chehroudi *et al.* [15]. Figure 2.12 shows the effect of sample compaction on the area fraction of oxidization for various flash energies. It is important to note that the lightly compacted samples with 5-15 lbf compaction exhibited significantly better flash photoignition responses than the highly compacted samples with 20-30 lbf compaction.

2.3.5 Effect of solid impurities

Smits *et al.* [37] found that when $6 - 10$ μm grain Fe powder was added to pure CVD-manufactured 0 wt.% Fe SWCNTs it resulted in the combustion of previously unignitable pure carbon SWCNTs. Their observations were similar to that of 50 wt.% Fe arc discharge SWCNTs. Furthermore, note that Fe powder was also capable of photoignition, even in the
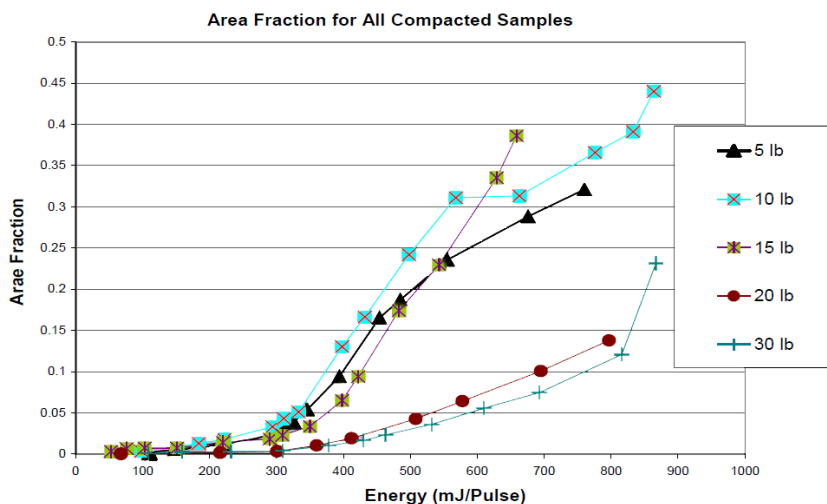
Figure 2.12: Photoignition response of 50wt.% Fe SWCNTs in air with varying sample compactions from 5-30 lbf, flashed with light at successively higher energies [15].

absence of SWCNTs [37].

Unlike solid impurities, liquid impurities greatly hinder SWCNT photoignition due to their rather high heat capacity and impermeability to oxygen [15]. Achieving photoignition of liquid fuels is very difficult due to this complication. In order to attain SWCNT photoignition in liquid fuels, the CNTs must be separated from the liquid until the moment of ignition. Badakshan *et al.* [11] devised a unique solution to this problem. Figure 2.13 shows an encapsulation of a small sample of SWCNTs inside a gelatin capsule which was flashed through the transparent gelatin. This resulted in photoignition and rupture of the gel-cap which sprayed hot SWCNTs onto a fuel spray, causing volumetric ignition of liquid fuel.

2.3.6 Effect of bulk temperature of the CNT bundle

The effect of bulk temperature on photoignition of MWCNTs was first investigated by Vignes *et al.* [16]. The authors performed thermo-gravimetric analysis on MWCNT samples in air for varying temperatures. Figure 2.14 shows the MWCNTs relative weight in 1 bar of air as a function of time at different temperatures. It indicates that there exists a significant

31
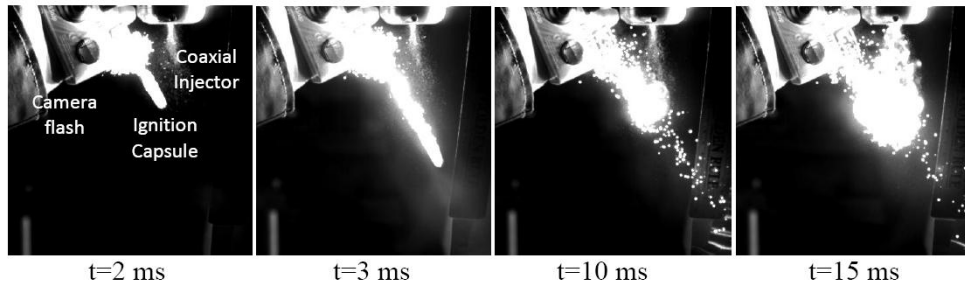
Figure 2.13: Ignition of a 50% hexane, 50% acetone fuel spray via 50 wt.% Fe SWCNT photoignition encapsulated in an ordinary gel-cap. Images were captured at 2000 frames per second with an exposure time of 490 μs [11].
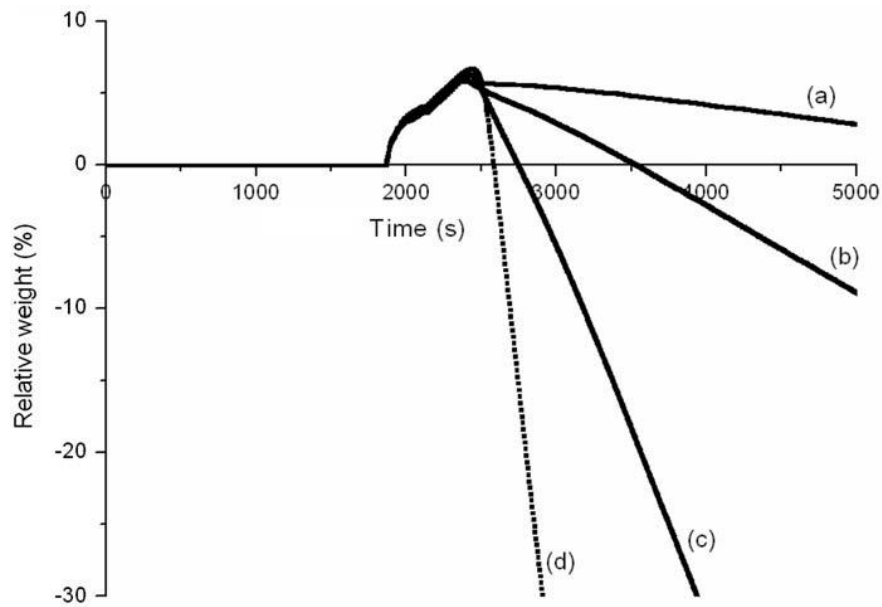
Figure 2.14: MWCNT sample relative weight in a 1 bar air atmosphere over time at a temperature of (a) 450°C, (b) 500°C, (c) 550°C, and (d) 600°C [16].

correlation between the rate at which CNT samples combusted and their bulk temperature. MWCNTs were found to self-ignite at a temperature above 450°C after 2500 seconds.

However, to the best of our knowledge, no studies were performed regarding the effect of

bulk temperature on the photoignition response of SWCNTs or MWCNTs. Determining the effect of bulk temperature on photoignition may give clues to the mechanisms behind CNT photoignition.

CHAPTER 3

Investigation of SWCNT and MWCNT Photoignitable Mixtures

This chapter investigates photoignition of single wall carbon nanotubes (SWCNTs) and multi wall carbon nanotubes (MWCNTs). SWCNTs in air or oxygen atmospheres are known to photoignite when exposed to a flash of light of sufficient intensity. Here, photoignition of MWCNTs alone or mixed with various solid oxidizers and solid fuels was investigated. The most extensive experimental part of this study was concerned with the ignition characteristics and photoignition properties of SWCNT and MWCNT-based photoignitable mixtures. In particular, it investigates the ability of CNTs to initiate further solid fuel combustion reactions, either within a mixture, or placed in a primary/secondary charge arrangement where the photoignitable agent serves as an ignition source for a secondary mixture.

3.1   Materials

In this study, we used (i) Fe-catalyzed 50 wt.% Fe SWCNTs made by DC arc discharge and (ii) xylene-ferrocene catalyzed MWCNTs.

Highly ferrous SWCNTs were obtained from Unidym Corporation, Houston, TX. They had a reported 50 wt.% Fe nanoparticle impurity content. Figure 3.1 shows a SEM micrograph of these SWCNTs. They were black and "fluffy" in appearance and easily dispersed in air due to their low density. This made them difficult to contain and handle.

Moreover, purified HiPco produced SWCNTs were obtained from US Research Nano-materials, Houston, TX. These SWCNTs contained 0 wt.% Fe nanoparticle impurities with
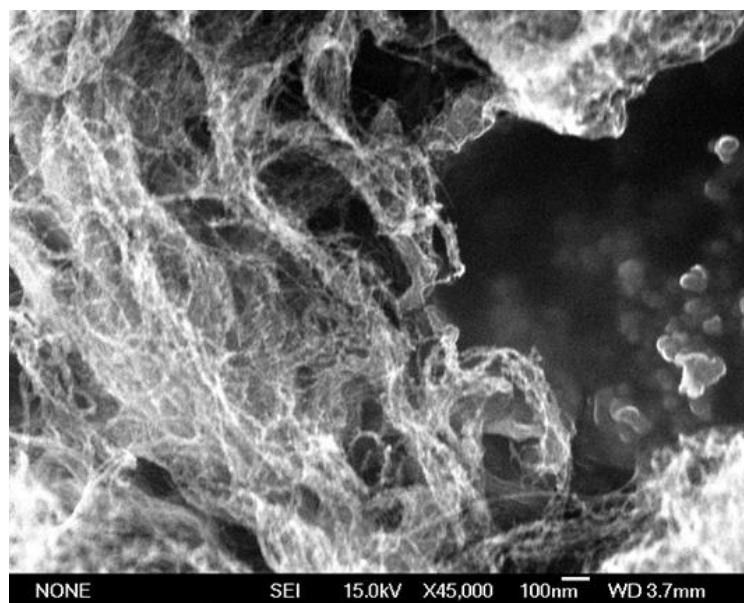
Figure 3.1: SEM micrograph of commercial 50 wt.% Fe SWCNTs used in this study and prepared using the DC arc discharge process.

< 5% graphitic impurities. Figure 3.2 shows a "wall" of densely packed SWCNTs prepared via the HiPco process. The lack of Fe nanoparticles renders them incapable of photoignition, making them an ideal choice as an experimental control. The purification process also compacts the SWCNTs into a "wall" structure, increasing their density and making them much easier to handle than the "fluffy" 50 wt.% Fe SWCNTs.

MWCNTs were also obtained from US Research Nanomaterials, Houston, TX. They had 25-30 wt.% ferrocene nanoparticle impurities [44]. Figure 3.3 shows a SEM micrograph of these MWCNTs. These MWCNTs were reported to be capable of photoignition via flash lamp [44].

Ammonium perchlorate (NH_4ClO_4) and potassium permanganate ($KMnO_4$) were obtained from United Nuclear LLC. These oxidizers were used to accelerate combustion in mixtures with SWCNTs, MWCNTs and other solid fuels. These solid fuels included ferrocene ($Fe(C_5H_5)_2$) obtained from Sigma Aldrich Corp, and titanium hydride (TiH_2) obtained from Fisher Scientific.
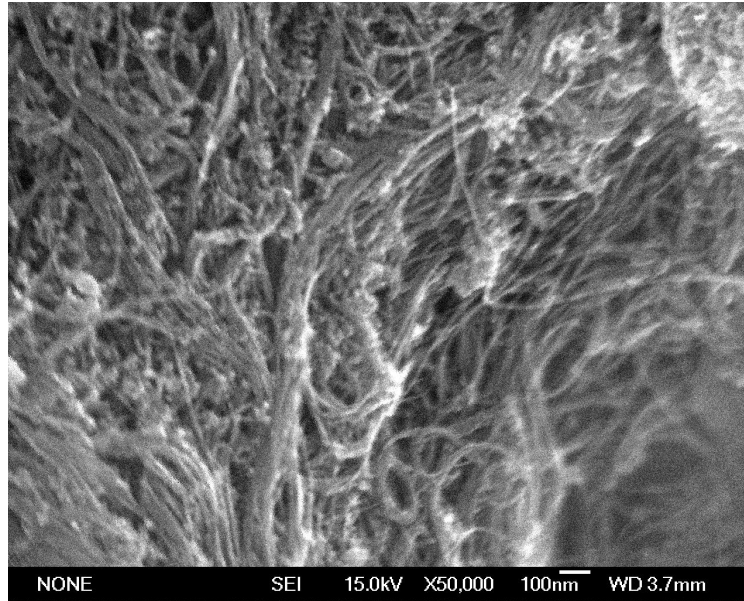
Figure 3.2: SEM micrograph of a "wall" of commercial 0 wt.% Fe SWCNTs used in this study and prepared using the HiPco process.

Various mixtures of CNTs and oxidizers were prepared and tested. First, oxidizers NH_4ClO_4 and $KMnO_4$ were ball milled for 2-3 hours with stainless steel balls in a glass jar. This was performed in order to achieve a powdered oxidizer with a small grain size of approximately -325 mesh (44 μm). All components of the mixture were then weighed and mixed with the photoignition agent in a small glass ball mill with glass balls for 2 minutes before testing. This was performed to ensure the homogeneity of the mixture. It is interesting to note that samples which were hand mixed rather than ball milled did not ignite. Note also that ferrocene and titanium hydride powders were not pre-milled due to their sufficiently small particle size as produced. Table 3.1 shows the compositions of the ten different mixtures investigated.
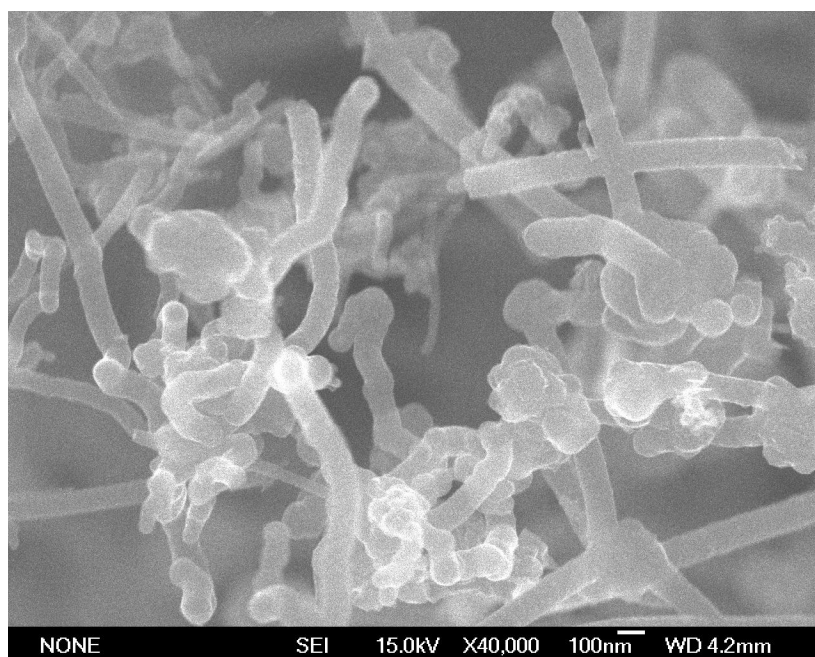
Figure 3.3: SEM micrograph of MWCNTs used in this study containing an estimated 25-30 wt.% ferrocene nanoparticle impurities and prepared using the xylene-ferrocene catalyzed CVD method.

Table 3.1: Compositions of the different samples and mixtures tested in this study.

Mixture	photoignition Agent (wt.%)	Component 1 (wt.%)	Component 2 (wt.%)	Component 3 (wt.%)	Ignition Delay (ms)	Burn Time (ms)	Observations
1	100% MWCNT				$<34\pm17$	204	MWCNT Control Test
2	10% MWCNT	90% NH_4ClO_4			$<34\pm17$	34	Improved energy release
3	6% MWCNT	54% NH_4ClO_4	40% $KMnO_4$		$<34\pm17$	68	Suspected lower MIE
4	6% MWCNT	49% NH_4ClO_4	35% $KMnO_4$	10% $Fe(C_5H_5)_2$	68 ± 17	272	Improved energy release
5	6% MWCNT	49% NH_4ClO_4	35% $KMnO_4$	10% TiH_2	68 ± 17	238	Dramatically improved energy release
6	100% SWCNT				0	7000	SWCNT Control Test
7	10% SWCNT	90% NH_4ClO_4			$<34\pm17$	204	Improved energy release
8	6% SWCNT	54% NH_4ClO_4	40% $KMnO_4$		$<34\pm17$	102	Suspected lower MIE
9	6% SWCNT	49% NH_4ClO_4	35% $KMnO_4$	10% $Fe(C_5H_5)_2$	$<34\pm17$	204	Improved energy release
10	6% SWCNT	49% NH_4ClO_4	35% $KMnO_4$	10% TiH_2	$<34\pm17$	170	Dramatically improved energy release

†MWCNTs contained an estimated 25 wt.% ferrocene nanoparticles

‡SWCNTs contained an estimated 50 wt.% Fe nanoparticles

3.2 Experimental setup

3.2.1 Ignition Experimental Setup

Figure 3.4 shows the experimental setup for testing the ignition capabilities of the SWCNT and MWCNT-based photoignitable mixtures previously described. It consisted of (i) a Xe flash lamp, (ii) a sample holder made from heat resistant materials, (iii) a camera, (iv) a protective enclosure, (v) a 6.30 mm diameter flash aperture, and (vi) a vacuum system for removing exhaust gases. A Xe flash lamp was positioned under a sample chamber surrounded by heat resistant materials including (i) aluminum plate, (ii) a 3/8" thick borosilicate glass window, and (iii) 1/8" thick fiberglass cloth.
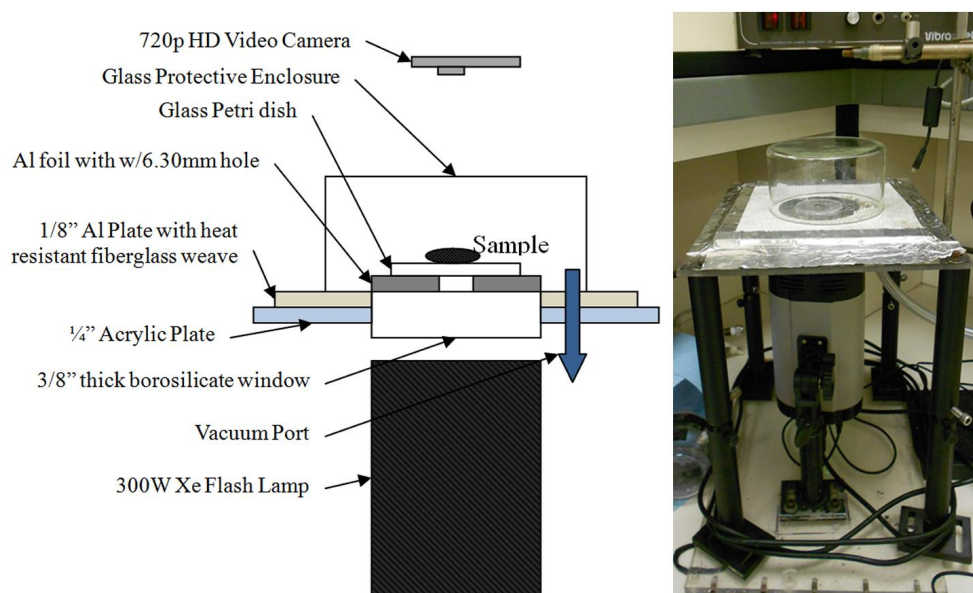
Figure 3.4: (left) Schematic diagram and (right) side view photograph of the experimental setup used in this study.

A vacuum air aspirator (McMaster part number: 13445K81) was attached via teflon vacuum hose to the sample chamber to quickly evacuate the combustion gasses after ignition. Directly below the sample of SWCNT or MWCNT mixture was an aluminum foil disk with a precision 6.30 mm aperture through which the Xe flash light could pass to reach the sample.

Figure 3.6 shows a schematic and photograph of the experimental apparatus.

The Xe flashlamp was a Neewer 300 Ws strobe/flash lamp obtained from Adorama Camera Inc. which was shined through a 3/8" thick borosilicate window. Figure 3.5 shows the emission spectra for the Neewer 300 Ws flash lamp between 200 and 1000 nm [17].
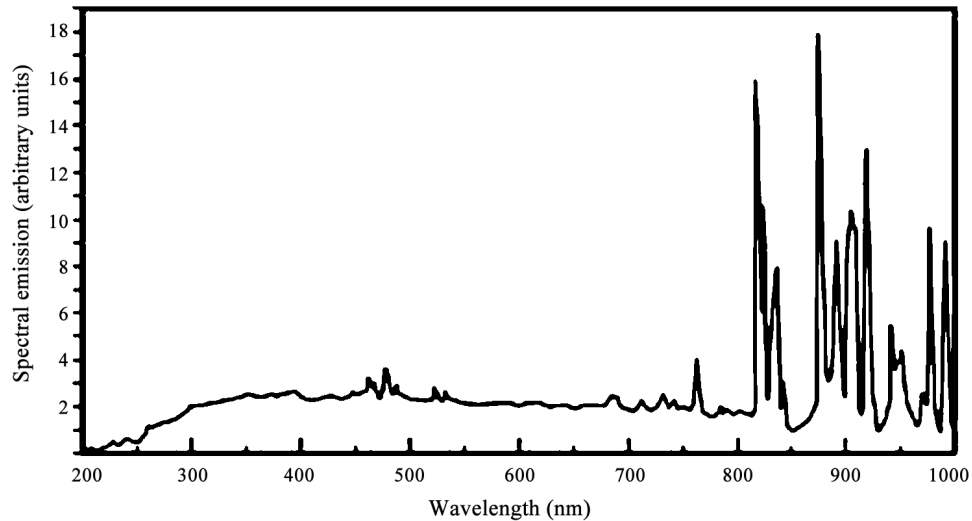
Figure 3.5: Xenon flashlamp emission spectra [17].

A type-K thermocouple, obtained from Omega Engineering Inc was used to measure temperature in the CNTs. Data was collected using a data acquisition system (DAQ) model DAQTEMP 14a from Iotech and DASYLAB software from Measurement Computing Inc.

3.2.2 Minimum ignition energy measurements

Experimental setup

The minimum ignition energy (MIE) of SWCNTs and MWCNTs was investigated in this study to reproduce and confirm the results of Chehroudi *et al.* [15] and to extend their study to MWCNTs and CNTs/oxidizer mixtures. It was hypothesized that by increasing the initial temperature of the CNTs a lower flash energy would be required to induce photoignition. An apparatus was constructed to test this hypothesis. Figure 3.7 shows a diagram of the

40

Figure 3.6: (left) Picture of precision 6.30 mm hole made in aluminum foil and placed in the (right) experimental petri dish.

apparatus used to estimate the minimum ignition energy (MIE) of CNTs. The experimental setup consisted of a glass vial containing a known mass of CNT surrounded by a nichrome heating wire, a Xe flash lamp underneath the sample, a thermocouple for measurement of the CNT bulk temperature, and a thermal energy sensor which was created and calibrated specifically for this test.

Thermal energy sensor

Figure 3.8 shows a schematic of the thermal energy sensor used to measure the minimum ignition energy (MIE). It consisted of a layer of graphite powder deposited on an aluminum film as a liquid suspension of graphite in ethanol sandwiched between two glass disks. The bottom disk was heated until the ethanol had completely evaporated. A type-K thermocouple was secured on the back of the aluminum foil and sandwiched by a second sheet of aluminum foil to double its thickness and increase its thermal mass. Aluminum was chosen for its large thermal conductivity ensuring uniform in-plane temperature in the sensor. The entire apparatus was surrounded by thermally insulating neoprene foam. The thermocouple was connected to a DAQTEMP 14a from Iotech and DASYLAB software was used to collect the data. The acquisition frequency was 20 Hz. The thermocouple was left in the sensor at
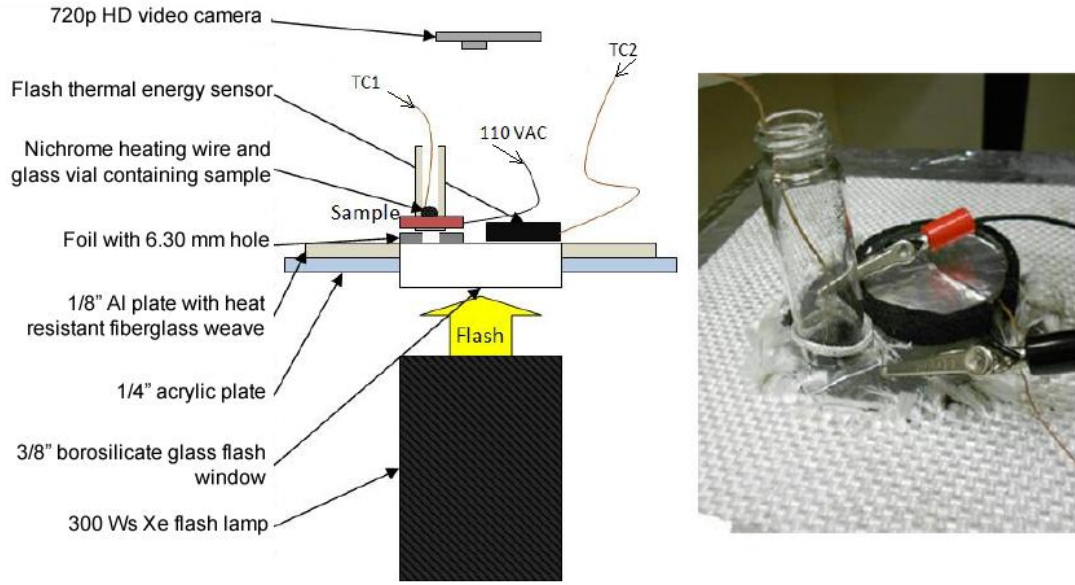
Figure 3.7: Diagram and photograph of the apparatus used to test SWCNT and MWCNT minimum ignition energy dependence on initial bulk temperature.

room temperature for 1 minute and the data was averaged to obtain T_i (71±0.2^o C). There was minimal variation of the thermocouple at room temperature (±0.2^o C) over the course of 1 minute. This error was considered negligible in light of the larger experimental error associated with the construction and inability to calibrate our sensor.

We assumed that the heat conduction rates through the glass plates and insulating foam were significantly lower than the heat conduction rates between graphite and aluminum while the sample was under irradiation from the flash lamp. Thus, the contact resistance between the graphite and aluminum can be neglected. We also assumed uniform incident irradiance on the graphite layer by the flash lamp. In addition, convection was assumed to be negligible compared with the heat flux from the flash and conduction between the graphite and aluminum layers before the maximum temperature was reached at time t_{max}. The thermal energy absorbed by a known area of graphite of total hemispherical absorptivity of $\varepsilon \simeq 0.98$ [19] was assumed to be the same as that absorbed by CNTs ($\varepsilon_{CNT} \simeq 0.99$) [19]. We begin by preforming a thermal energy balance on the sensor as

42
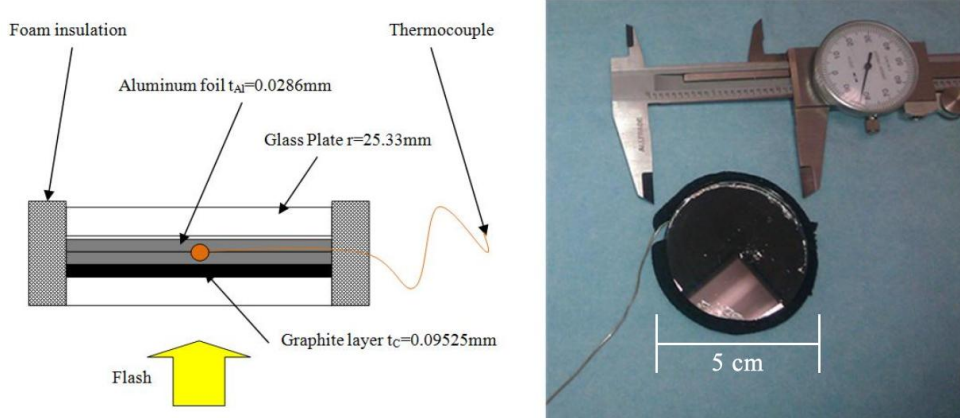
Figure 3.8: Diagram of the flash thermal energy sensor used to measure the total flash energy incident on the SWCNT sample.

$$\frac{\mathrm{d}E}{\mathrm{d}t} = mc_p\frac{\mathrm{d}T}{\mathrm{d}t} = \dot{Q}_{in} - \dot{Q}_{out} \tag{3.1}$$

where $\dot{Q}_{in}$ is the energy absorbed by the sensor and given by $\dot{Q}_{in} = \varepsilon G_{flash}$, where G_{flash} is the total incident irradiance. On the other hand, $\dot{Q}_{out}$ is assumed to be zero. Thus, Equation (3.1) can be written as

$$mc_p\frac{\mathrm{d}T}{\mathrm{d}t} = \varepsilon G_{flash} \tag{3.2}$$

Integrating between initial time $t = 0$ s, corresponding to the beginning of the flash, to final time t_{max} yields

$$\int_0^{t_{max}} mc_p\frac{\mathrm{d}T}{\mathrm{d}t}\,\mathrm{d}t = \int_0^{t_{max}} \varepsilon G_{flash}\,\mathrm{d}t \tag{3.3}$$

Here, $(mc_p)_{eff} = m_{Al}c_{p,Al} + m_C c_{p,C}$ which is the effective heat capacity of the sensor. Equation (3.3) can be written as

$$(mc_p)_{eff}(T_{max} - T_i) = \int_0^{t_{max}} \varepsilon G_{flash}\,\mathrm{d}t \tag{3.4}$$

43

where T_i and T_{max} are the initial and maximum sensor temperatures. After t_{max}, radiation from the flash is no longer provided and convective heat transfer dominates resulting in the cooling of the sensor. If the sensor was perfectly insulated, it would remain at temperature T_{max} for all times t beyond t_{max}. However, this is not the case. Therefore, we must assume that the temperature rise for a perfectly insulated sensor is equal to $\Delta T_{max} = T_{max} - T_i$ for the sensor in this study. It is estimated that this assumption of negligible thermal convection during the time interval 0 to t_{max} carries with it an experimental error of $\pm 0.5^o$ C. We justify this because in the 1 s after T_{max} we see a temperature drop of $\sim 0.5^o$ C per second. Since the rise occurs in ~ 1 s we can estimate an error on the order of the neglected convective temperature loss during the temperature rise leading up to T_{max}. Thus, one can write

$$\varepsilon Q_{flash} = (mc_p)_{eff} \Delta T_{max} \tag{3.5}$$

to determine the MIE (in J/m^2), Equation (3.5) must be divided by the sensor area (A) so that

$$MIE = \frac{Q_{flash}}{A} = \frac{(m_{Al}c_{p,Al} + m_C c_{p,C})}{A\varepsilon} \Delta T_{max} \tag{3.6}$$

where Q/A is the MIE in J/m^2 and A is the total area of the graphite layer ($A = 0.002014$ m^2). The mass of carbon and aluminum samples were determined, by direct weighing as $m_C = 0.2383$ g and $m_{Al} = 0.311$ g, respectively. The specific heat c_p of the thermally conductive materials were $c_{p,C} = 709.75$ J/kg K, and $c_{p,Al} = 896.96$ J/kg K. Finally, we assumed that $\varepsilon \simeq 1$ for graphite and CNT. Applying these values to Equation (3.6) yield the following device specific relation

$$\frac{Q_{flash}}{A} = MIE = 222.432 \Delta T_{max} \quad \text{J/m}^2 \tag{3.7}$$

Calibrations were carried out on the ability of this thermal sensor to measure the power of flashes. To do so, the thermal sensor was placed at a distance ranging from 0 to 70 mm from the flash. The temperature rise $\Delta T = T(t) - T(0)$ was measured as a function of time from a 150 and 300 Ws flash lamp located at various distances from the sensor. Figures

3.9 and 3.10 show the temperature rise ΔT versus time after a single flash from a 150 and 300 Ws flash lamp, respectively. They indicate the temperature rise decreased at all times with increasing distance from the lamp. It is important to note that the 300 Ws flash lamp produced larger ΔT than the 150 Ws lamp at all times for all distances.
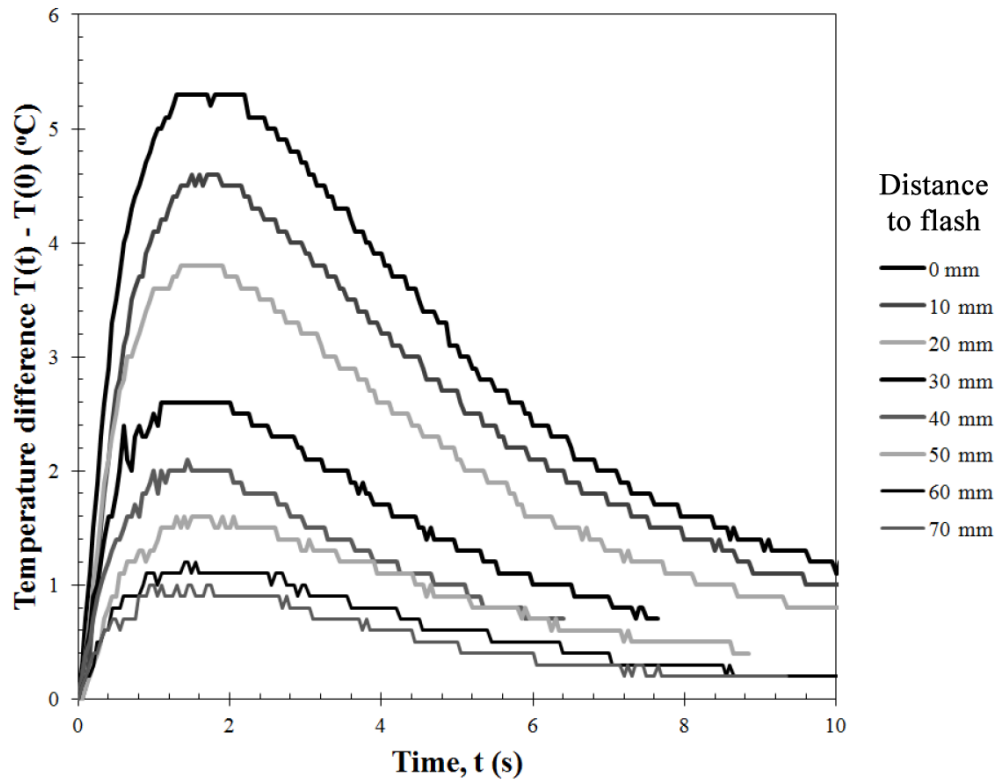
Figure 3.9: Temperature rise ΔT versus time in the flash thermal energy sensor located at various distances from the aperture of a 150 Ws rated Xe flash lamp.

Figure 3.11 plots ΔT_{max}, as a function of the distance between the sensor and the aperture of the Xe flash lamp for 150 Ws and 300 Ws Xe flash lamps. It shows the inverse correlation between sensor distance and ΔT_{max}.

Similarly, Figure 3.12 shows the flash energy per square meter in J/m^2 as a function of distance computed between sensor and flash aperture using Equation (3.7). This illustrates the full range of flash energies offered by our 150 and 300 Ws flash lamp.
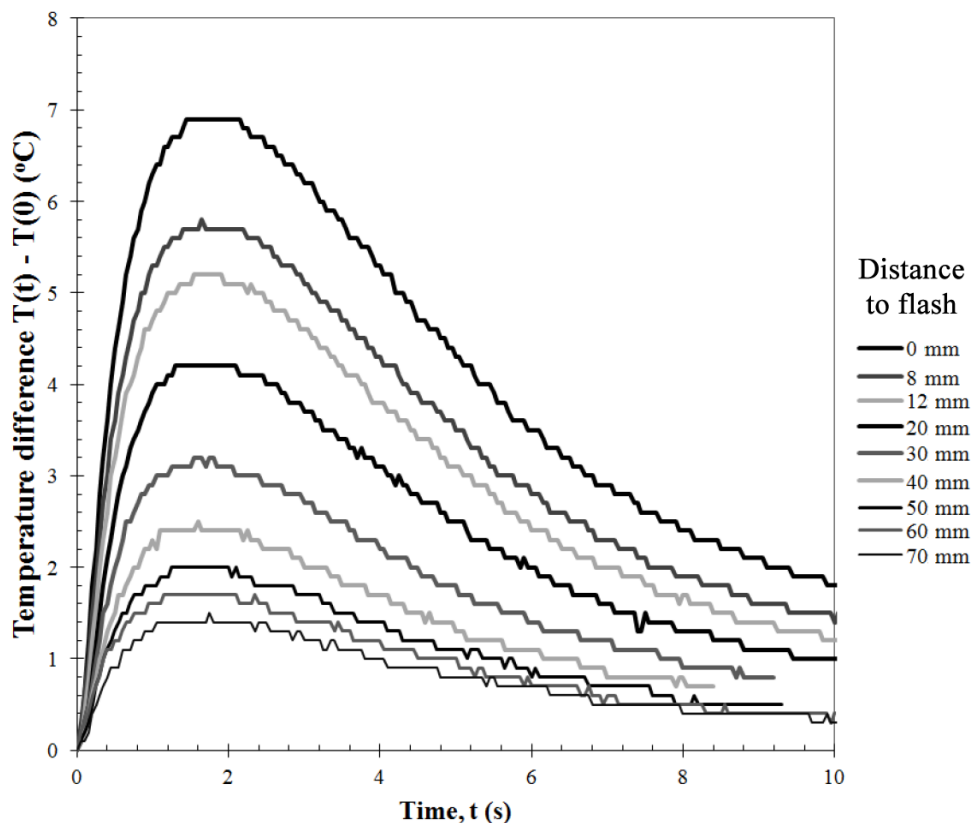
Figure 3.10: Temperature rise ΔT versus time in the flash thermal energy sensor located at various distances from the aperture of a 300 Ws rated Xe flash lamp.

3.2.3 Minimum ignition energy

To test the MIE of SWCNTs, MWCNTs, and NH_4ClO_4 + SWCNT with respect to temperature, a 10 mg sample was placed in the glass vial and slowly raised to temperature using a nichrome heating wire. The temperature was successively raised in increments of 50^oC and flashed with a 300 Ws lamp when the desired temperature was observed on a thermocouple placed in contact with the CNTs sample. If no ignition occurred at the distance attempted, the sample was moved closer to the lamp and the process was repeated with a successively shorter distance until ignition was attained. Once the sample ignited, the vial was removed, cleaned, and a fresh sample was added. The vial was then heated to the next higher tem-
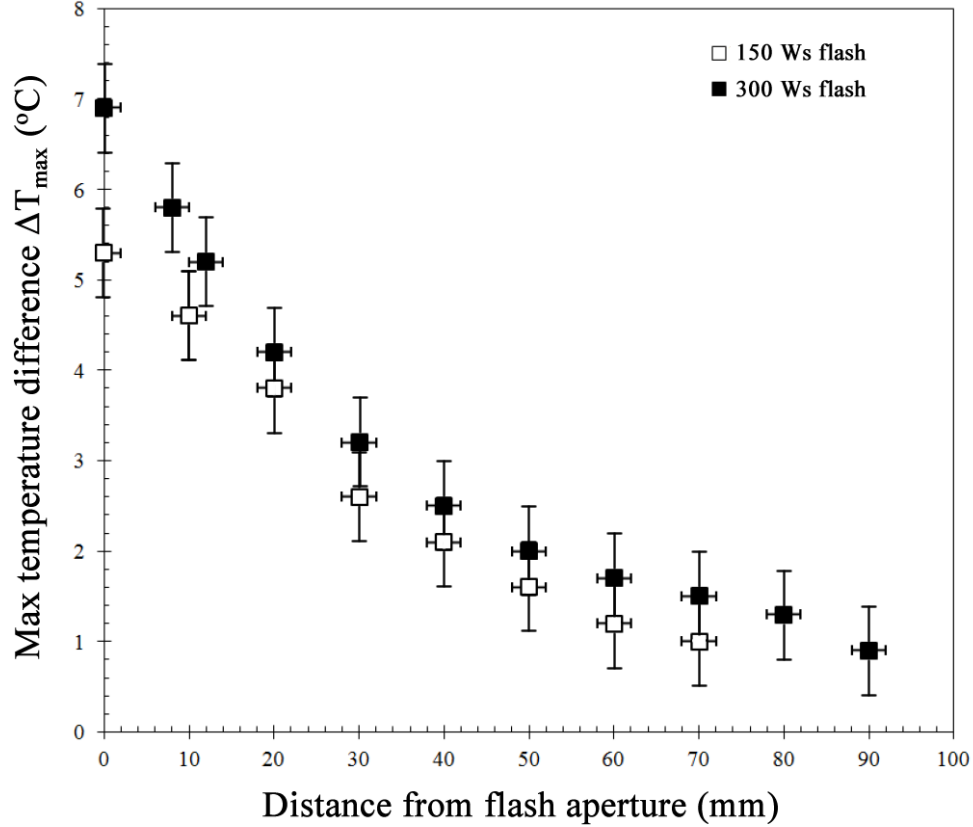
Figure 3.11: Maximum temperature rise ΔT_{max} versus distance of the thermal energy sensor to the flash aperture for 150 Ws and 300 Ws flash lamps.

perature point and the process was repeated until either (a) auto-ignition was observed, i.e., sample ignited from the bulk temperature alone without a flash or (b) the sample was rendered inert.

3.2.4 Critical ignition energy measurements

In the majority of the literature, the MIE of CNTs was expressed in terms of mJ/pulse with a clearly defined flash area or in W/cm^2 [10,15]. However, it was suspected, after the initial tests conducted in this study that the MIE (in J/pulse) depends on the size of the sample and the surface area exposed to the flash. A test was designed to determine the effect of
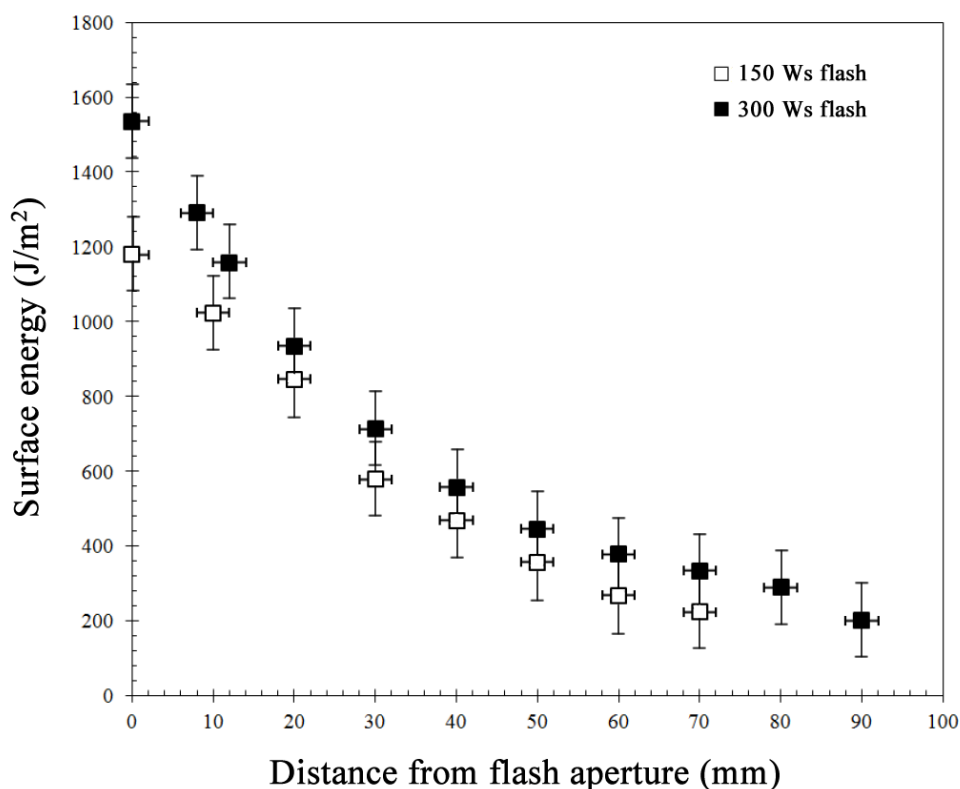
Figure 3.12: Flash surface energy as a function of distance from the flash aperture for 150 Ws and 300 Ws flash lamps.

sample size on the MIE.

Figure 3.13 shows diagrams of the different microscope slides prepared with reflective aluminum foil layer placed on one side. Shapes were cut into this reflective foil layer to allow Xe flash light to reach the CNTs. One foil slide featured rectangular openings while the other had square openings. It was hypothesized that if the samples were placed at a distance of 0 mm from the flash lamp, the intensity per unit area would exceed the MIE threshold and all samples would ignite. However, if MIE was a function of total energy incident on the SWCNTs, instead of energy per unit area, the surface area incident to the flash would determine which samples ignited.
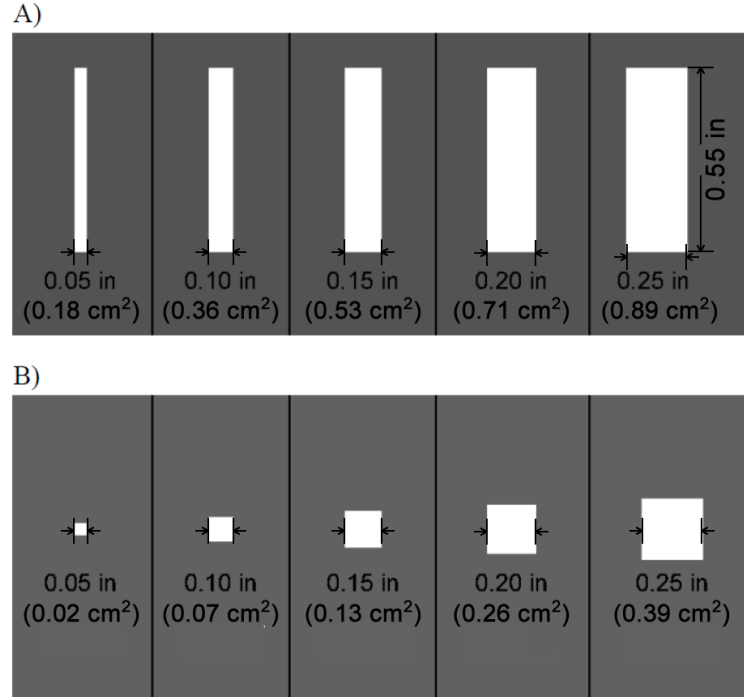
Figure 3.13: (A) Diagram of the rectangular cutout slides. (B) Diagram of the square cutout slides. Grey area represents foil (light blocked), while white represents transparent glass (light passes through to CNT).

3.3 Experimental error and uncertainty

There are several sources of experimental uncertainty associated with the design and analysis of the flash thermal energy sensor used to measure the MIE. Because of our assumption of negligible thermal convection during the time interval 0 to t_{max} an experimental error of $\pm 0.5^o$ C was estimated. We justify this because in the 1 s after T_{max} we see a temperature drop of $\sim 0.5^o$ C per second. Since the rise occurs in ~ 1 s we can estimate an error of $\pm 0.5^o$ C. Because we did not have a calibrated flash energy sensor capable of measuring the Xe flash lamp energy with adequate temporal resolution, a full validation was not possible. Thus, due to the lack of experimental validation of our theoretical model, the sensor could only be realistically used to qualitative analysis and not for true quantitative measurements.

Error was also introduced in the photoignition characteristics of CNTs mixtures section due to the limitations of a 30 frame per second camera. Both Badakhshan *et al.* [11] and Berkowitz *et al.* [9] noted the use of a 1000 fps camera in their experiments enabled them to see critical steps within the first 34 ms of the experiment. For example, the uncertainty in ignition delay time using our experimental setup was ±17 ms, whereas their experimental error in ignition delay was ±0.5 ms.

3.4   Results and discussion

This section will detail the results obtained by testing the previously described SWCNT and MWCNT mixtures. The mixture numbers refer to those presented in Table 3.1. This section also qualitatively discusses the results of the MIE experiments. Finally, the results of the critical ignition energy tests are presented and discussed.

3.4.1   Ignition characteristics of SWCNT and MWCNT mixtures

Effect of CNT type

Figure 3.15 shows a time sequence between 0 and 1000 ms of the photoignition of 25 wt.% ferrocene MWCNTs. The sample was located 0 mm from the flash aperture. It shows a clear combustion of the ferrocene deposits between 0 and 204 ms, with combustion lasting a total of 204 ms. In contrast, figure 3.14 shows a time sequence between 0 and 7000 ms of the photoignition of 50 wt.% Fe SWCNTs. The sample was located 20 mm from the flash aperture. It shows a slow oxidization of the Fe nanoparticle deposits lasting 7000 ms. Also, the volume of black SWCNTs appears to decrease between t= 0 ms and t= 7000 ms. In contrast to pure MWCNTs, pure SWCNTs showed no clear combustion. This may indicate a decomposition of the SWCNT structure in addition to the Fe oxidization. Samples were placed at their respective photoignition agent's minimum ignition distance for a 6.30 mm hole. Samples containing SWCNTs and MWCNTs as a photoignition agent were placed at

a distance of 0 mm and 20 mm from the flash aperture, respectively.
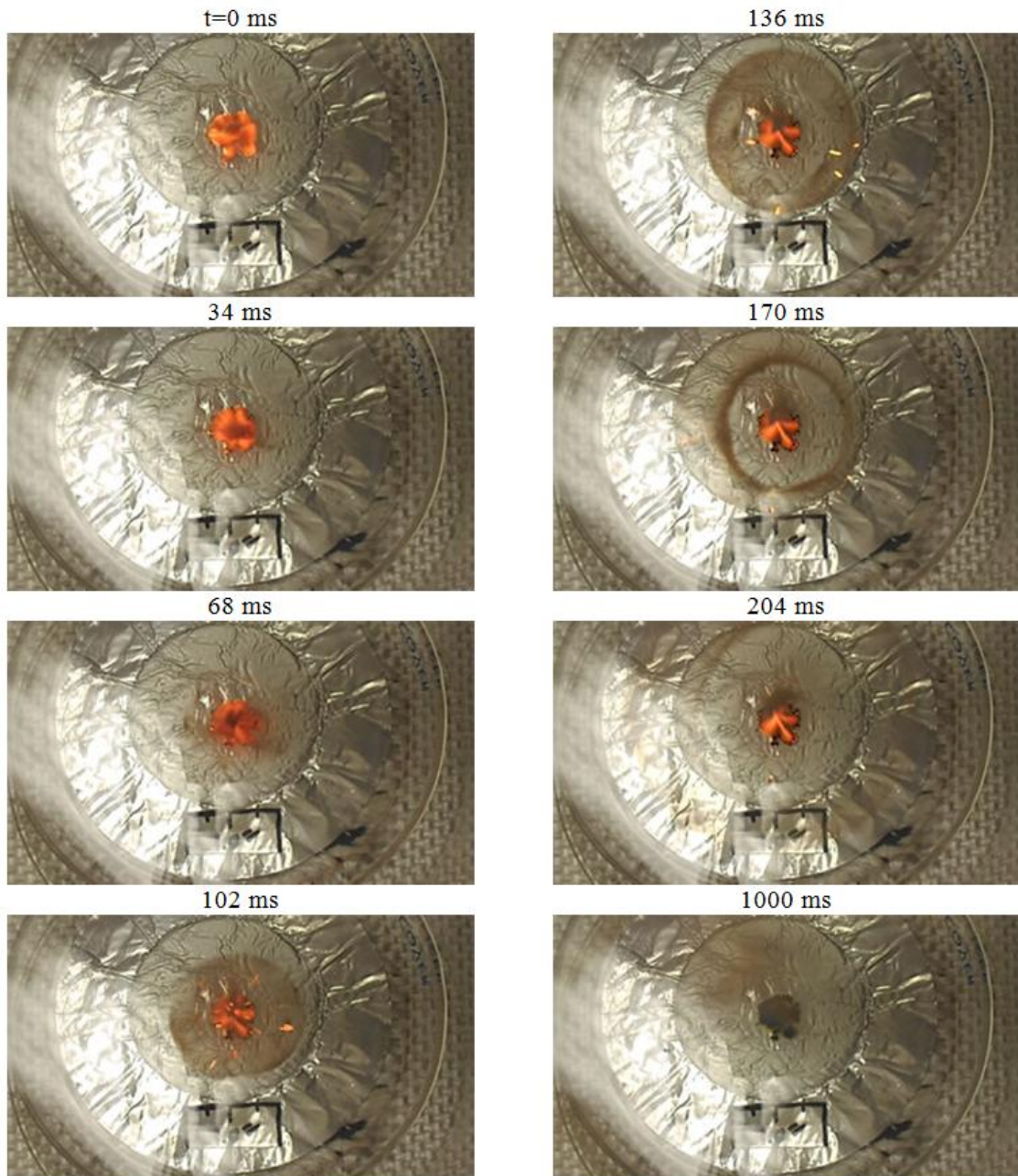
Figure 3.14: Sample 1- 2.5 mg (pure 25 wt.% ferrocene MWCNTs) placed at a distance of 0 mm from the 300 Ws flash aperture through a 6.30 mm diameter circular hole.

Figure 3.15: Sample 6- 2.5 mg (pure 50 wt.% Fe SWCNTs) placed at a distance of 20 mm from the 300 Ws flash aperture through a 6.30 mm diameter circular hole.

Effect of ammonium perchlorate

Figure 3.16 shows a time sequence between 0 and 1000 ms of the photoignition of mixture 2, consisting of a 10 wt.% and 90 wt.% mixture of MWCNT photoignition agent and NH_4ClO_4, respectively. The sample was located 0 mm from the flash aperture. Figure 3.16 shows a very brief combustion for ~ 34 ms which ejected relatively few hot particles. Addition of NH_4ClO_4 to MWCNTs dramatically shortened the combustion time compared to pure MWCNTs. Similarly, Figure 3.17 shows a time sequence between 0 and 1000 ms of the photoignition of mixture 7 consisting of a 10 wt.% and 90 wt.% mixture of SWCNT photoignition agent and NH_4ClO_4, respectively. The sample was located 20 mm from the flash aperture. Mixture 7 shows a slightly longer combustion of 102 ms compared with 34 ms for mixture 2. In contrast to mixture 2, the reaction tended to spark and eject many hot particles for ~ 204 ms. The combustion of SWCNTs in mixture 7 also appeared to be more complete, leaving less residue than the MWCNTs in mixture 2. Overall, adding ammonium perchlorate to SWCNTs and MWCNTs resulted in more energetic reactions than with either pure SWCNTs or MWCNTs alone.
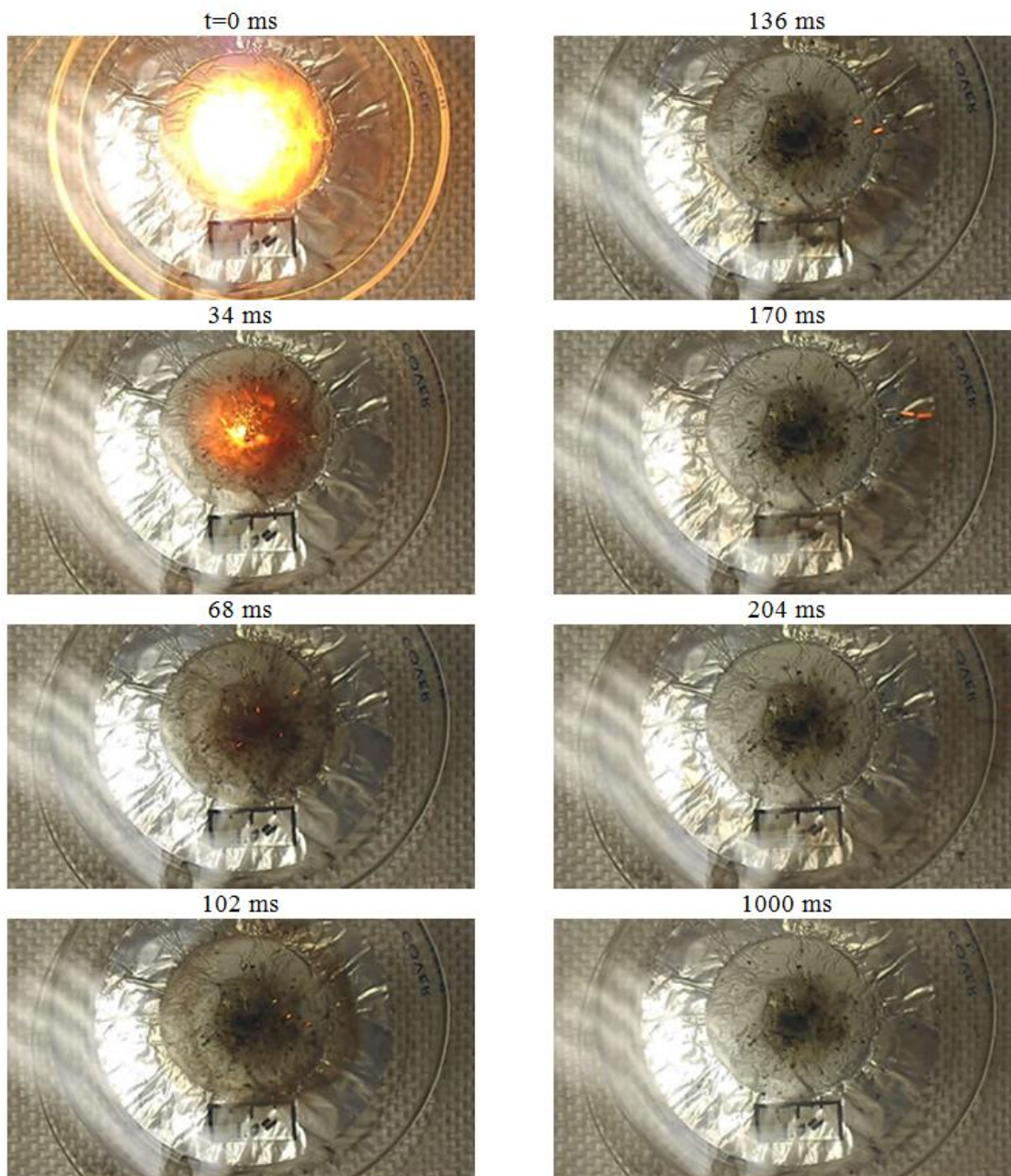
Figure 3.16: Sample 2 - 10 mg (10% MWCNTs, 90% NH_4ClO_4) placed at a distance of 0 mm from the 300 Ws flash aperture through a 6.30 mm diameter circular hole.
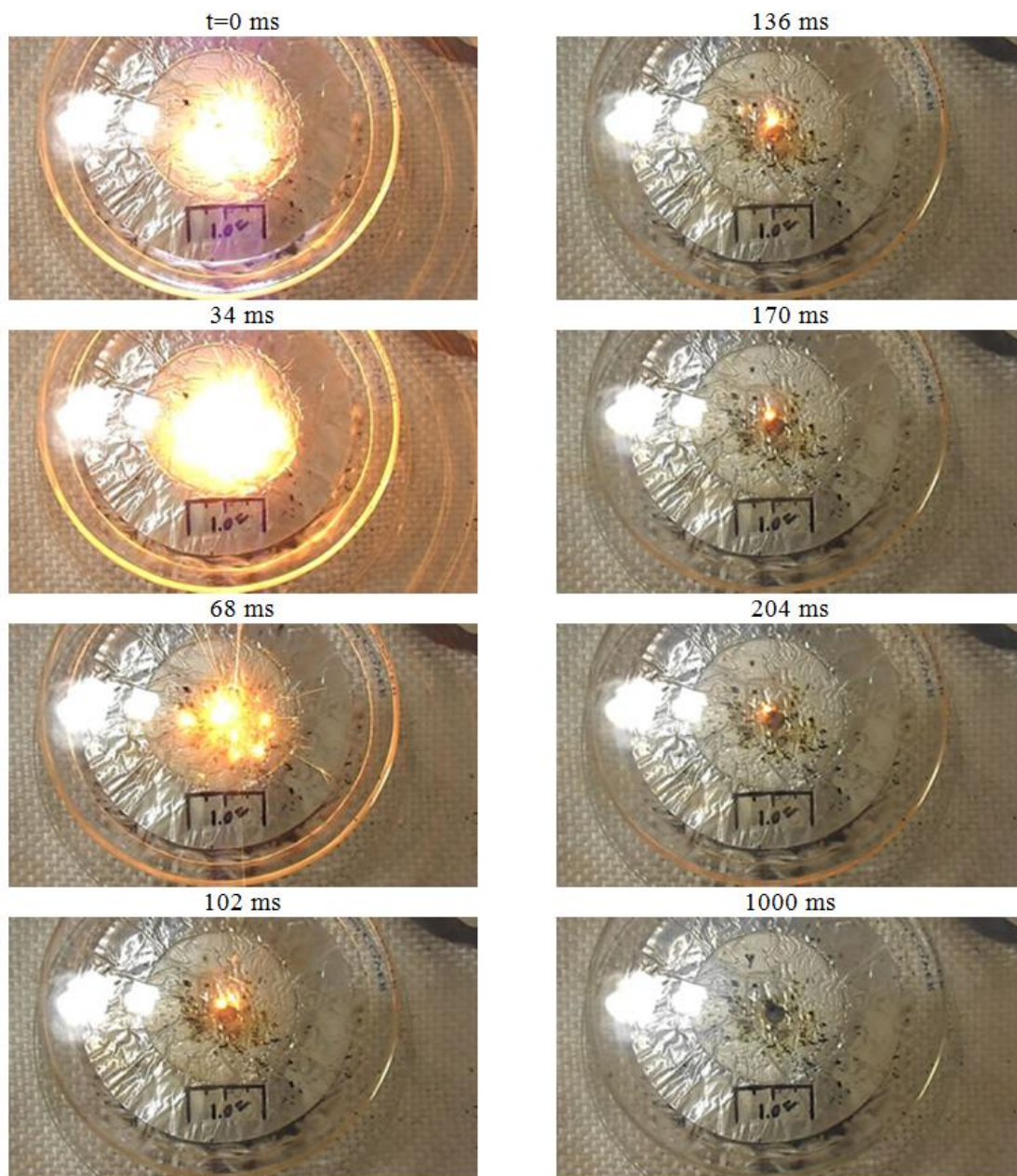
Figure 3.17: Sample 7 - 10 mg (10% SWCNTs, 90% NH_4ClO_4) placed at a distance of 20 mm from the 300 Ws flash aperture through a 6.30 mm diameter circular hole.

Effect of potassium permanganate

Figure 3.18 shows a time sequence between 0 and 1000 ms of the photoignition of mixture 3, consisting of 6 wt.%, 54 wt.%, and 40 wt.% of MWCNTs, NH_4ClO_4, and $KMnO_4$, respectively. The sample was located 0 mm from the flash aperture. It shows a longer duration of combustion than with ammonium perchlorate alone, namely 68 ms versus 34 ms, respectively. Also, there were many hot particles ejected which were not seen in the photoignition of mixture 2. Similarly, Figure 3.19 shows a time sequence between 0 and 1000 ms of the photoignition of mixture 8, consisting of 6 wt.%, 54 wt.%, and 40 wt.% of SWCNTs, NH_4ClO_4, and $KMnO_4$, respectively. The sample was located 20 mm from the flash aperture. Mixture 8 demonstrated a shorter duration of combustion of about 102 ms compared with 204 ms for mixture 7. It also released fewer hot particles. When $KMnO_4$ was added to SWCNTs and NH_4ClO_4, a cloud of red hot gas was produced and can be observed after 68 ms. This was not observed in the case of MWCNTs or SWCNTs with NH_4ClO_4 alone. Due to the photo-decomposition of the permanganate, oxygen gas enabled a more complete combustion of both SWCNTs and MWCNTs.
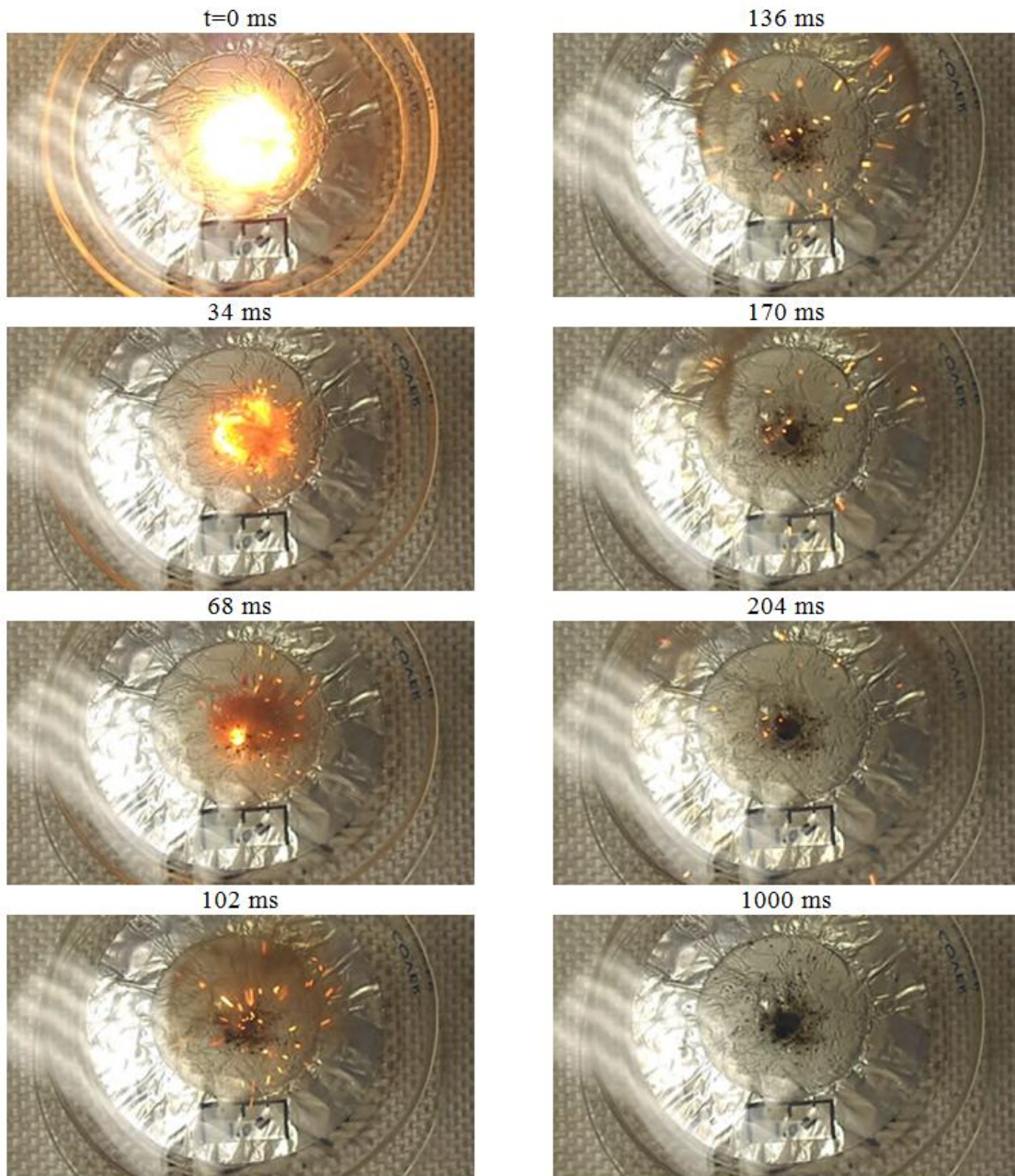
Figure 3.18: Sample 3 - 10 mg (6% MWCNTs, 54% NH_4ClO_4, 40% $KMnO_4$) placed at a distance of 0 mm from the 300 Ws flash aperture through a 6.30 mm diameter circular hole.

Figure 3.19: Sample 8 - 10 mg (6% SWCNTs, 54% NH$_4$ClO$_4$, 40% KMnO$_4$) placed at a distance of 20 mm from the 300 Ws flash aperture through a 6.30 mm diameter circular hole.

Effect of ferrocene

Figure 3.20 shows a time sequence between 0 and 1000 ms of the photoignition of mixture 4, consisting of a 6 wt.%, 49 wt.%/, 5 wt.%, and 10 wt.% mixture of MWCNTs, NH_4ClO_4, $KMnO_4$, and ferrocene, respectively. The sample was located 0 mm from the flash aperture. The addition of ferrocene in mixture 4 lengthened the combustion phase to 272 ms compared with 68 ms and 34 ms in mixtures 3 and 2, respectively. This effect may have been due to the presence of ferrocene serving as an addition to the ferrocene already contained in the MWCNTs. Note that in mixture 4, an ignition delay was present which was most likely due to the release of oxygen gas from the permanganate and/or the sublimation of ferrocene from the MWCNTs. The reaction also left a carbon/iron oxide soot deposit on the camera shield. This served as additional evidences of a fuel-rich combustion when MWCNTs were used in this mixture.

Similarly, Figure 3.21 shows a time sequence between 0 and 1000 ms of the photoignition of mixture 9, consisting of a 6 wt.%, 49 wt.%/, 5 wt.%, and 10 wt.% mixture of SWCNTs, NH_4ClO_4, $KMnO_4$, and ferrocene, respectively. The sample was located 20 mm from the flash aperture. Comparing mixture 9 with mixture 4 shows SWCNTs yield a leaner and faster combustion than MWCNTs when used in this mixture with combustion times of 204 ms and 272 ms, respectively. There was no ignition delay evident when SWCNTs were used, and additionally no soot deposit was left on the camera shield during the photoignition of mixture 9. This served as additional evidences of a more fuel-lean combustion when SWCNTs were used as compared to MWCNTs. The addition of ferrocene in mixture 9 also lengthened the combustion time to 204 ms compared with 102 ms in mixture 8. However, photoignition of mixture 9 did not eject as many hot particles as mixture 7.
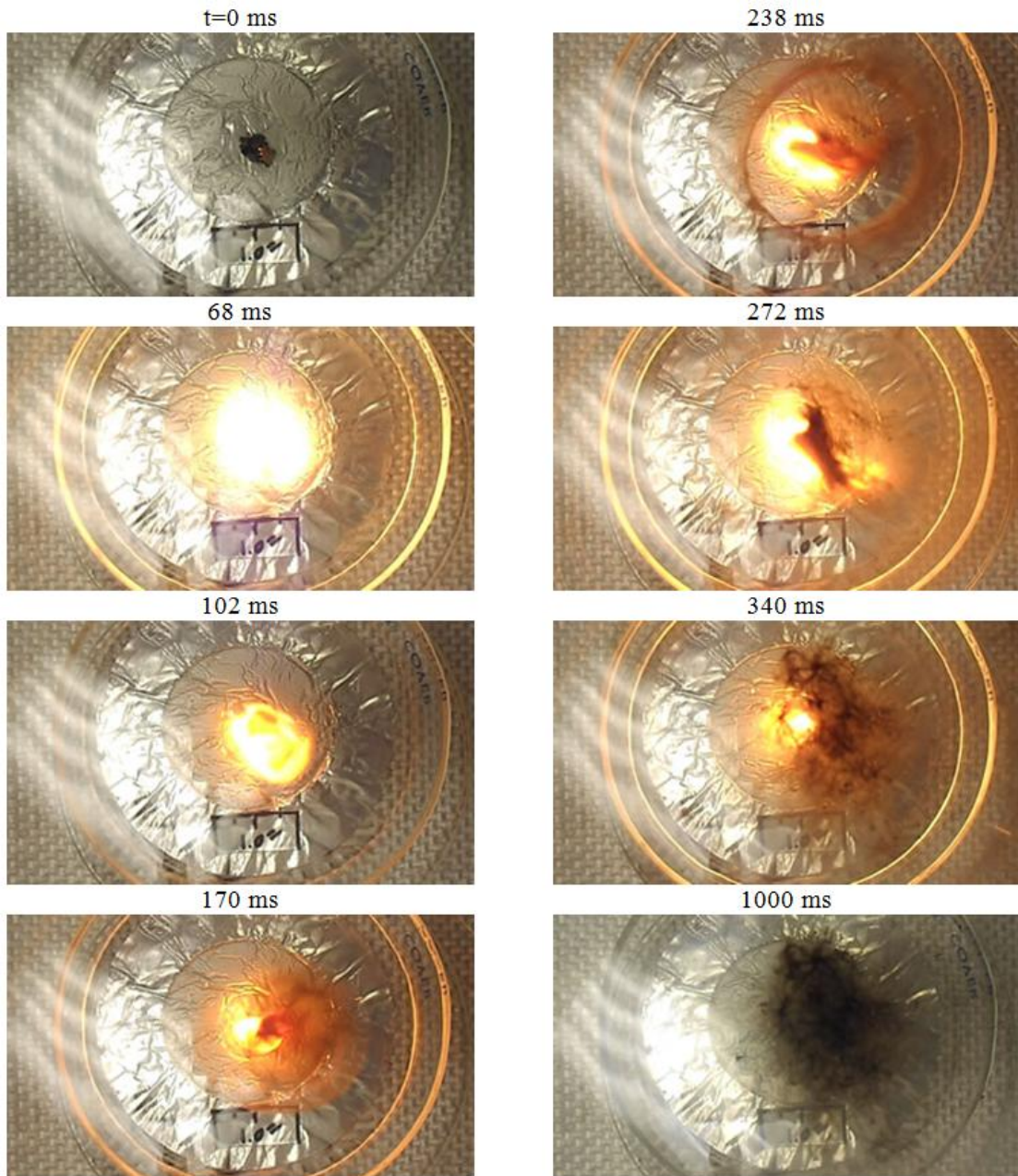
Figure 3.20: Sample 4 - 10 mg (6% MWCNTs, 49% NH$_4$ClO$_4$, 35% KMnO$_4$, 10% ferrocene placed at a distance of 20 mm from the 300 Ws flash aperture through a 6.30 mm diameter circular hole.
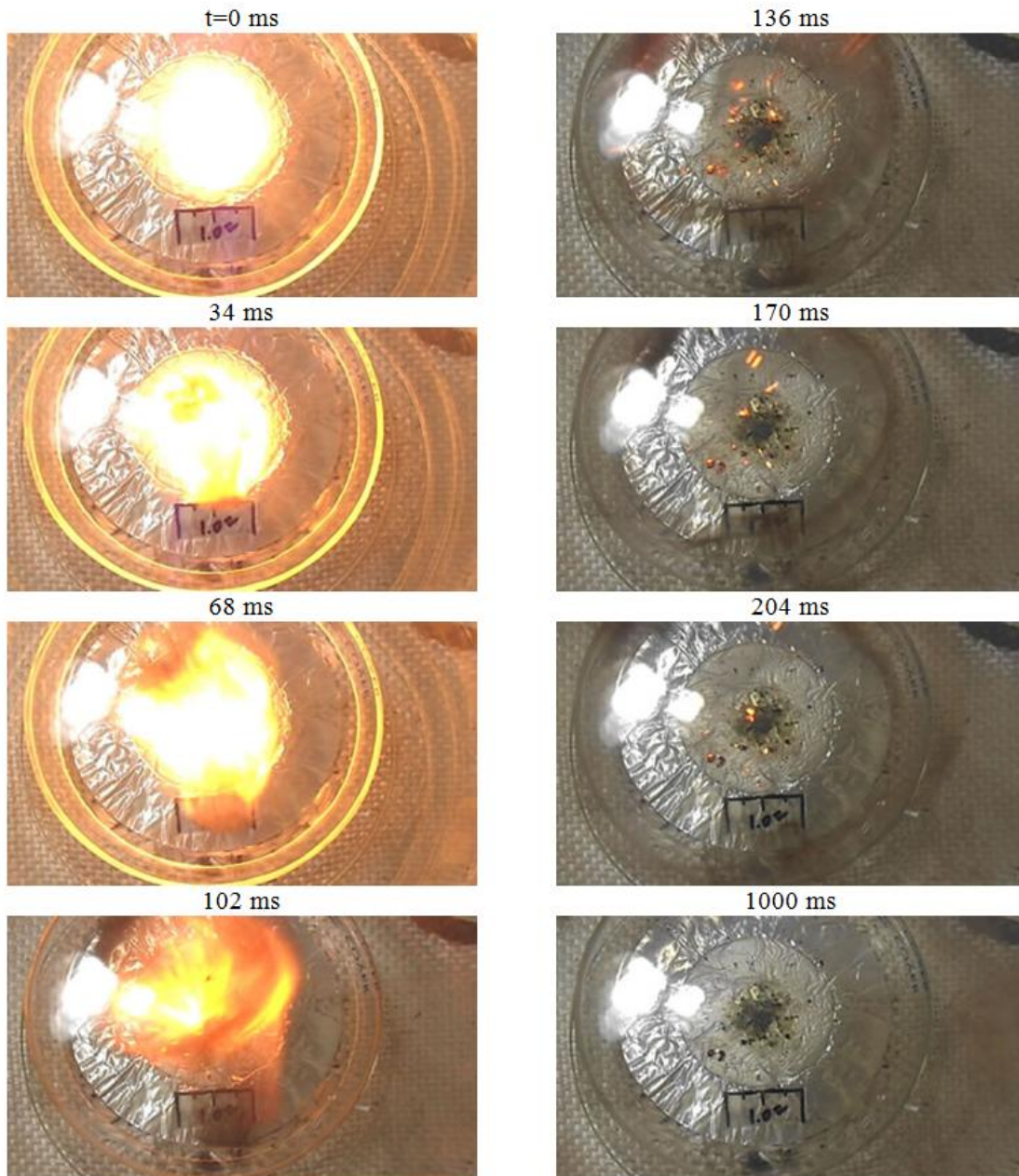
Figure 3.21: Sample 9 - 10 mg (6% SWCNTs, 49% NH_4ClO_4, 35% $KMnO_4$, 10% ferrocene placed at a distance of 0 mm from the 300 Ws flash aperture through a 6.30 mm diameter circular hole.

Effect of titanium (II) hydride
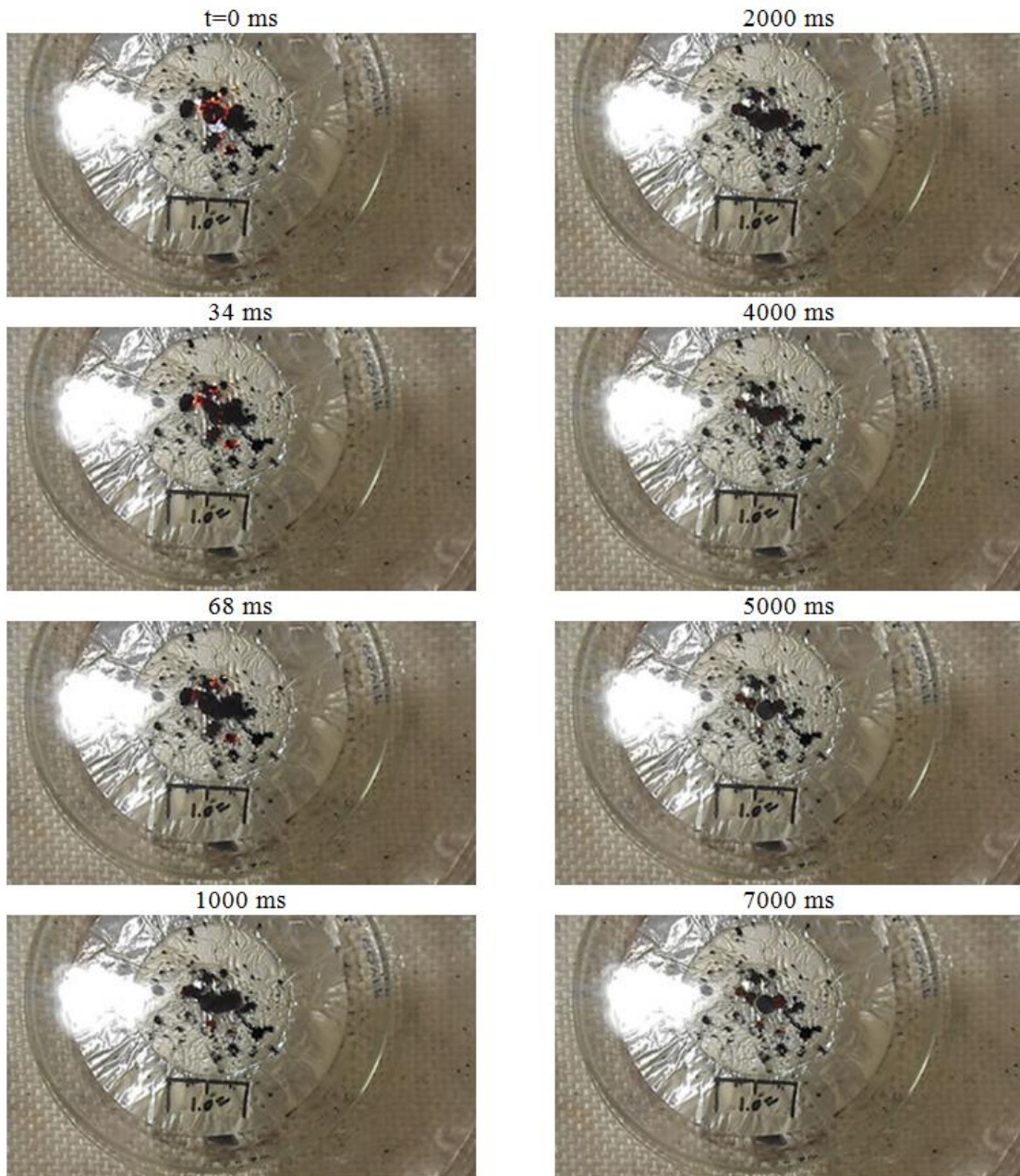
Figure 3.22 shows a time sequence between 0 and 1000 ms of the photoignition of mixture 5, consisting of a 6 wt.%, 49 wt.%/, 5 wt.%, and 10 wt.% mixture of MWCNTs, NH_4ClO_4, $KMnO_4$, and titanium (II) hydride (TiH_2), respectively. The sample was located 0 mm from the flash aperture. The addition of TiH_2 in mixture 5 had little effect on the combustion time in comparison to mixture 4. This may be due to TiH_2 which served the same role as a fuel as filled by ferrocene in mixture 4. In mixture 5 as well as in mixture 4, an ignition delay of $\sim$ 68 ms was present. In contrast to mixture 4 however, mixture 5 left no soot deposits and ejected many hot particles.

Similarly, Figure 3.23 shows a time sequence between 0 and 1000 ms of the photoignition of mixture 10, consisting of a 6 wt.%, 49 wt.%/, 5 wt.%, and 10 wt.% mixture of SWCNTs, NH_4ClO_4, $KMnO_4$, and TiH_2, respectively. The sample was located 20 mm from the flash aperture. Comparing mixture 10 with mixture 5 shows SWCNTs yielded a much leaner and faster combustion than MWCNTs when used in this mixture with combustion times of 170 ms and 238 ms, respectively. Additionally, there was no ignition delay evident when SWCNTs were used. It is important to note the significant thermal energy release seen at 34 ms. At this point the camera's sensor became overwhelmed and the frame appears white. The reaction proceeded for $\sim$ 170 ms before extinguishing itself. The presence of such a large thermal release, specifically with a SWCNT photoignition agent and a titanium (II) hydride fuel was an anomalous result. It is unknown to us at this time why TiH_2 causes such an energy release, but the results necessitate further study.

Figure 3.24 shows four time sequences of SWCNT mixtures in a separate experimental apparatus with different mixture proportions. It shows the photoignition of (a) 2.5 mg of pure 50 wt.% Fe SWCNT. (b) 10 mg of a mixture consisting of 5 wt.%, and 95 wt.% SWCNTs and NH_4ClO_4, respectively. (c) 10 mg of a mixture consisting of 5 wt.%, 45 wt.%, 28 wt.%, and 22 wt.% SWCNTs, NH_4ClO_4, $KMnO_4$, and sucrose, respectively. Finally, (d) 10 mg of a mixture consisting of 5 wt.%, 75 wt.%, and 20 wt.% SWCNTs, NH_4ClO_4 and titanium

(II) hydride, respectively [11]. It demonstrates the repeatability of the TiH_2 effect as seen in mixture 10 of the current study.
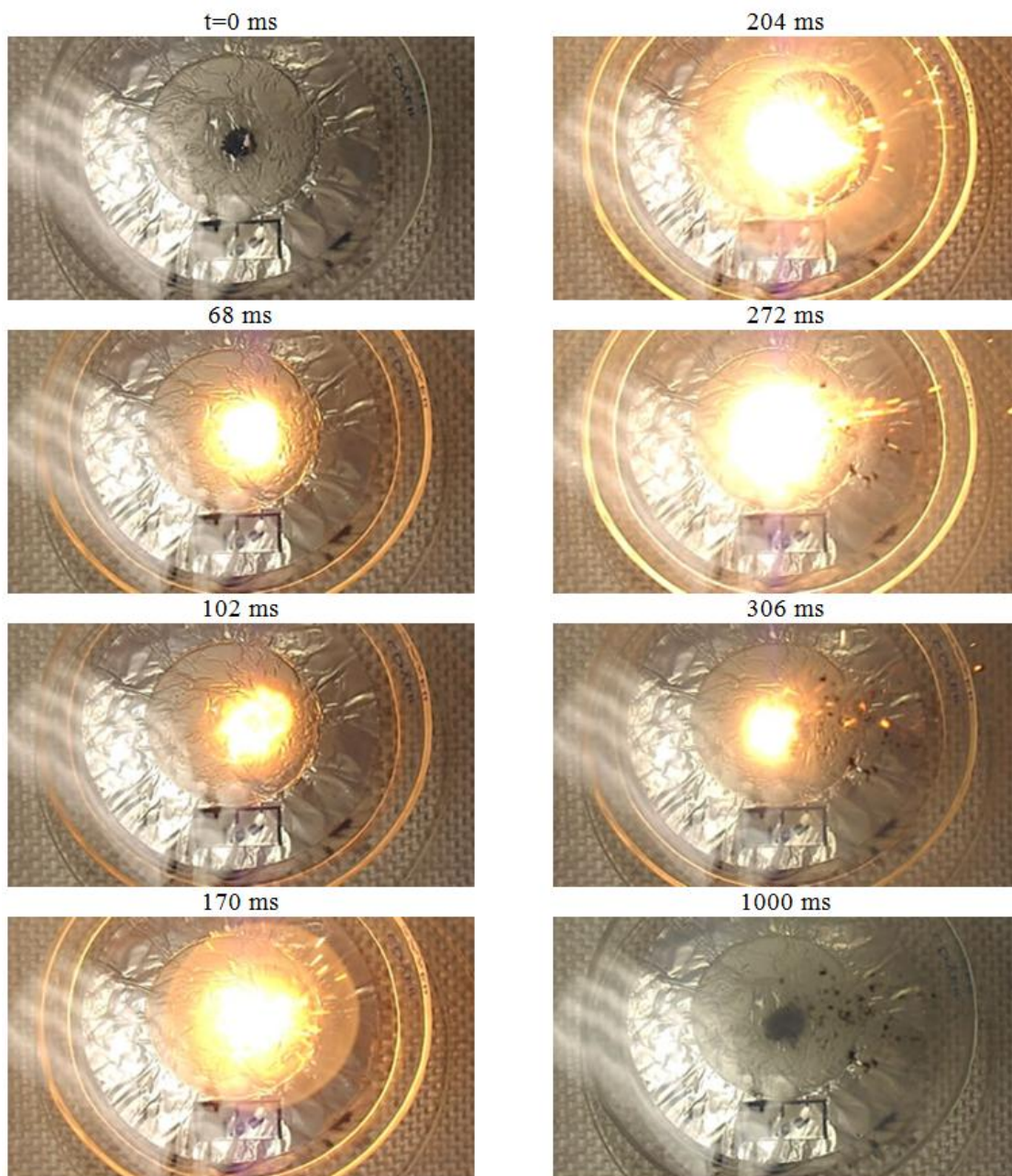
Figure 3.22: Sample 5 - 10 mg (6% MWCNTs, 49% NH_4ClO_4, 35% $KMnO_4$, 10% TiH_2) placed at a distance of 20 mm from the 300 Ws flash aperture through a 6.30 mm diameter circular hole.
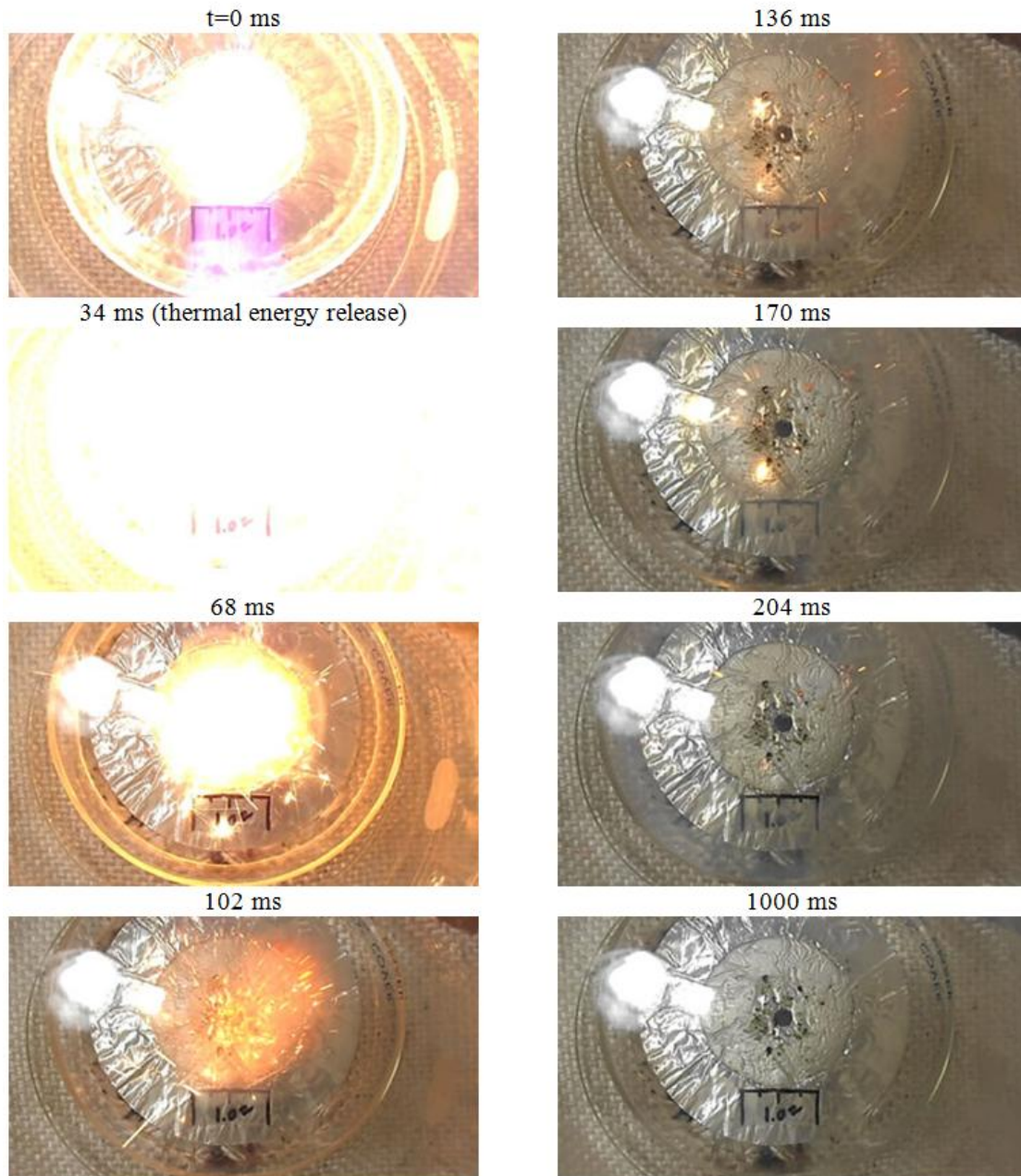
Figure 3.23: Sample 10 - 10 mg (6% SWCNTs, 49% NH_4ClO_4, 35% $KMnO_4$, 10% TiH_2) placed at a distance of 10 mm from the 300 Ws flash aperture through a 6.30 mm diameter circular hole.
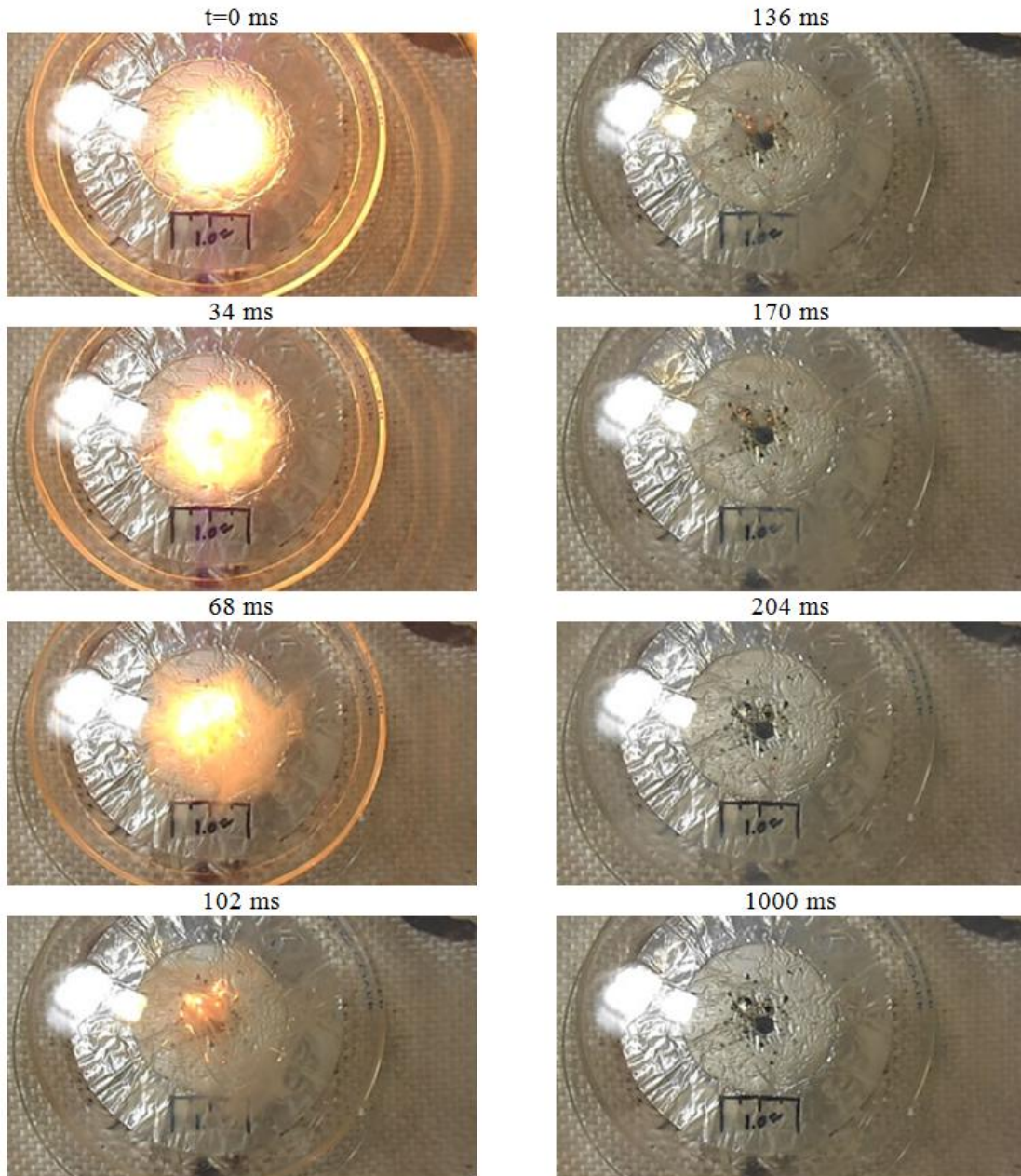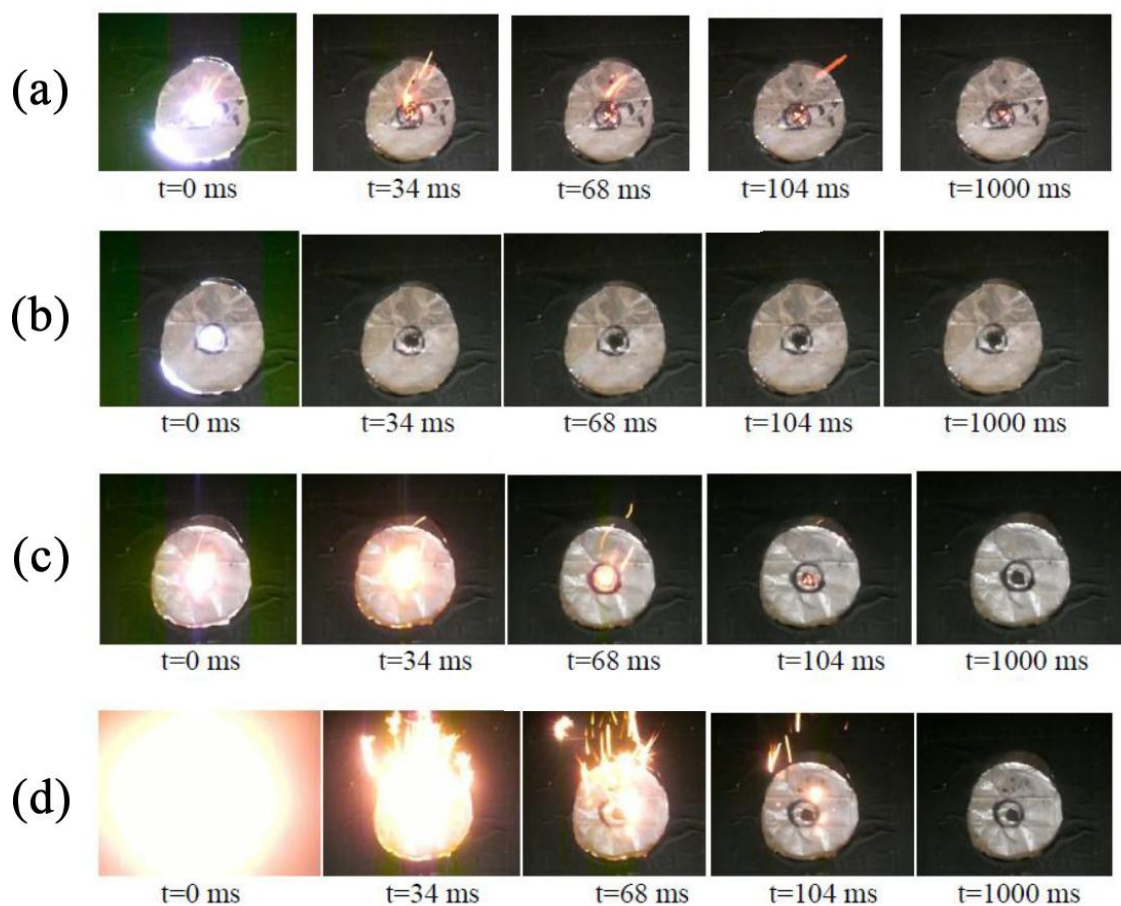
Figure 3.24: Time sequences of the photoignition of SWCNT mixtures placed in different apparatus with different mixture proportions. Shows mixtures consisting of (a) 2.5 mg of pure SWCNT, (b) 10 mg of SWCNTs and NH_4ClO_4, (c) 10 mg of SWCNTs, NH_4ClO_4, $KMnO_4$, and sucrose, and (d) 10 mg of SWCNTs, NH_4ClO_4 and TiH_2 [11].

3.4.2 Minimum ignition energy

First, the minimum ignition energy of SWCNTs and MWCNTs was determined using the thermal energy sensor previously described. The results were compared with the results reported by Chehroudi *et al.* [15]. The authors obtained different MIE values with different pulse widths. They obtained a MIE of 67 ± 10 mJ/cm^2 for 50 wt.% Fe SWCNTs with a 7 ms pulse (85 ± 10 mJ/pulse through a 1.267 cm^2 aperture) and a MIE of 25 ± 5 mJ/cm^2 for 50 wt.% Fe SWCNTs with a 0.2 ms pulse (32 ± 5 mJ/pulse through a 1.267 cm^2 aperture). In the current study we obtained a MIE of 24.5 ± 10 mJ/cm^2 for 50 wt.% Fe SWCNTs at room temperature (7.64 ± 1 mJ/pulse through a 0.312 cm^2 aperture). This shows that our result of 24.5 ± 10 mJ/cm^2 is comparable to the Chehroudi *et al.* result of 25 ± 5 mJ/cm^2 for the same substance and lends credence to our thermal energy sensor data.

Figure 3.25 shows a summary of the MIE versus sample temperature for SWCNTs, SWCNTs/NH$_4$ClO$_4$, and MWCNTs. It indicates (i) pure SWCNTs exhibit a general decline in MIE followed by spontaneous ignition at 350°C, (ii) pure MWCNTs exhibit a decrease in MIE followed by a critical point at 200°C after which they cease to photoignite due to the sublimation of their ferrocene ignitable material, and (iii) SWCNTs/NH$_4$ClO$_4$ showed similar results to the SWCNTs until the mixture spontaneously ignited at 250°C. This was due to the decomposition temperature of ammonium perchlorate at 250°C [45].

Figure 3.26 shows a photograph taken after the MWCNTs were heated to $\sim$ 250°C and the ferrocene had fully sublimed out of the MWCNTs. It indicates small ferrocene crystals growing on the sides of the glass chamber and blue air filter. Since the primary fuel in MWCNTs is the ferrocene catalyst particles present between the MWCNTs, the characteristics of ferrocene play a critical role in the ignition properties of MWCNTs . Unlike the Fe nanoparticles contained in the 50 wt.% Fe SWCNTs, ferrocene has a sublimation temperature of 249°C at atmospheric pressure [46]. Thus, after the MWCNTs were heated to 250°C, the MWCNTs no longer contained any flammable material. This, in order to ignite, they would need to be heated to their CO$_2$ formation temperature ($> 550^o$C) which
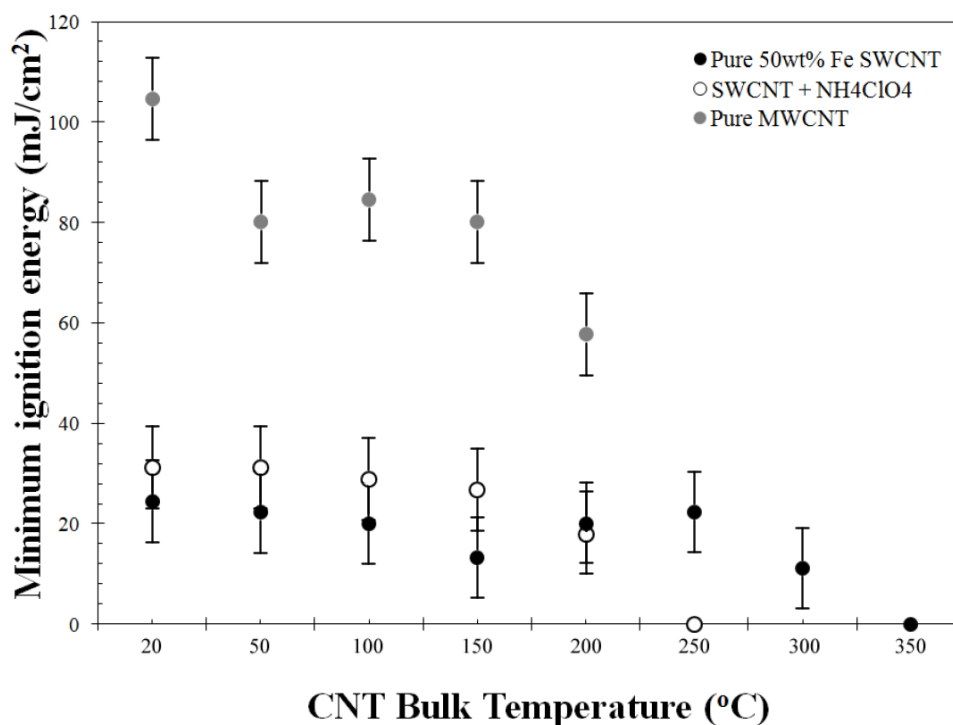
Figure 3.25: Measured MIE versus CNTs bulk temperature for 5 mg samples of SWCNTs, SWCNTs + NH_4ClO_4 solid oxidizer, and MWCNTs. Note that the MWCNT data stops at 200^oC due to CNT being rendered inert by the high temperature.

is a sufficiently higher MIE and was unachievable with our flashing/heating apparatus which was used in the present study.

3.4.3 Critical ignition energy

To test the critical ignition energy of samples of SWCNT mixture 8, both foil-coated slides shown in Figure 3.13 were exposed to a 300 Ws flash at a distance of 0 mm. Figure 3.27 shows the physical results after flashing the slides covered with mixture 8 once at a distance of 0 mm from the flash aperture. Table 3.2 summarizes whether photoignition was observed when flashing both slides at this distance for different slat areas. It is important to note that the photoignition of the CNTs depended on the surface area exposed to the flash but was
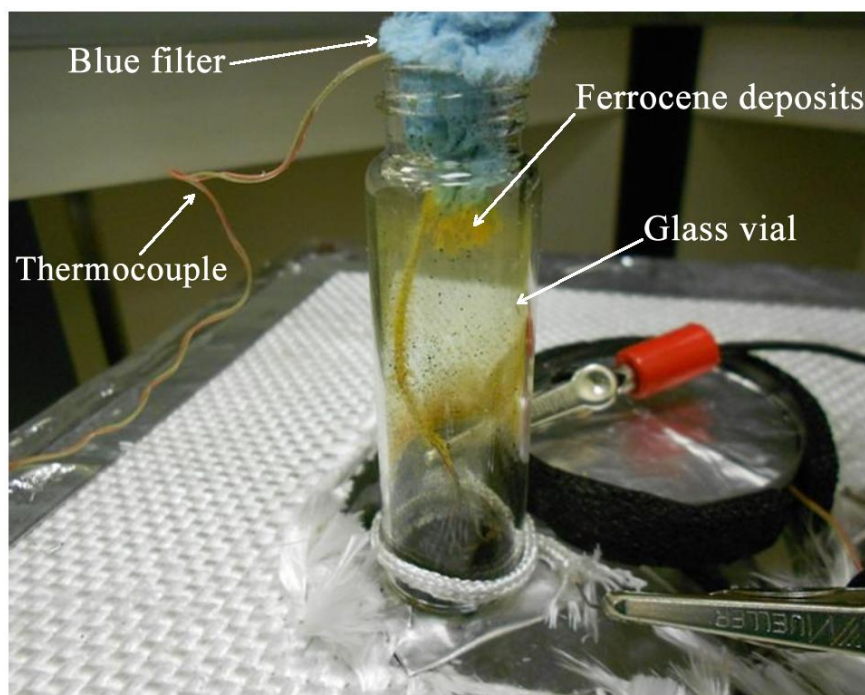
Figure 3.26: Photograph of a glass vial containing pure MWCNTs at 250°C. Dendritic crystals of deposited ferrocene can be seen growing from the walls of the vial and from the blue filter.

independent of the shape of the opening. This is in direct contradiction to the previously held assumption that MIE depends on energy per unit surface area. If the previously used unit of MIE was true (J/cm^2) [10, 11, 15], then we would expect to see all samples ignite, regardless of the area exposed to the flash, however this is not the case. The results indicate that a critical ignition sample surface area of 0.26 cm^2 is required for photoignition at the given flash energy. Meaning samples with smaller surface areas exposed to the flash will not be photoignitable regardless of their shape.

3.5 Conclusions

This chapter investigated photoignition of SWCNTs and MWCNTs both alone and in mixtures with solid oxidizers and fuels including NH_4ClO_4, $KMnO_4$, ferrocene, and TiH_2. The
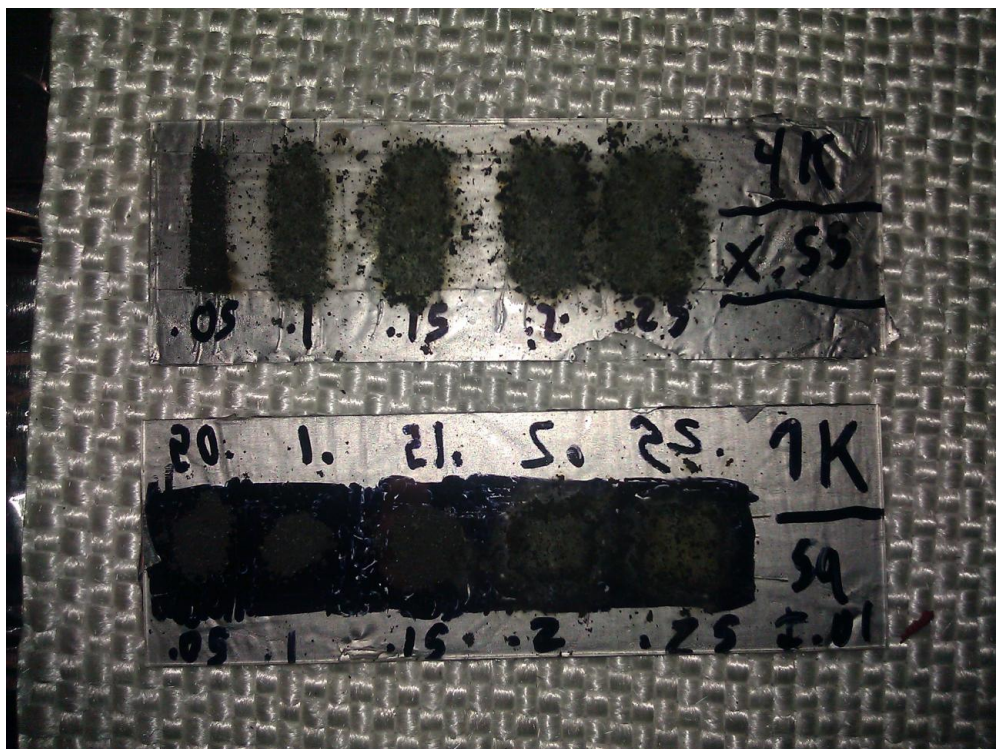
Figure 3.27: Photograph of both microscope slides after exposure to a 300 Ws flash - showing clearly the slats which were able to stimulate CNT photoignition.

addition of NH_4ClO_4 enabled a faster and more energetic combustion. The use of $KMnO_4$ in conjunction with NH_4ClO_4 created an elevated oxygen concentration in the local atmosphere which caused a leaner and more complete combustion. The addition of ferrocene lengthened combustion time for both SWCNTs and MWCNTs. The addition of TiH_2 to a MWCNT mixture had a similar effect to ferrocene but with less soot production. However, an unusually large thermal energy release was observed when TiH_2 was added to a photoignitable mixture containing SWCNTs, NH_4ClO_4 and $KMnO_4$. The MIE of MWCNTs was observed to be significantly higher than that of SWCNTs at elevated temperatures. In addition, at 250^oC the MWCNTs are rendered unignitable. Investigation of the MIE of SWCNTs at elevated temperatures showed a general decline in MIE as temperature increased resulting in their spontaneous ignition at 350^oC. The MIE of a mixture of SWCNTs and NH_4ClO_4

Table 3.2: Summary of CNT photoignition versus size of area flashed.

Slat area	Slat shape	Ignition
0.02 cm^2	square	NO
0.07 cm^2	square	NO
0.13 cm^2	square	NO
0.18 cm^2	rectangular	NO
0.26 cm^2	square	YES
0.36 cm^2	rectangular	YES
0.39 cm^2	square	YES
0.53 cm^2	rectangular	YES
0.71 cm^2	rectangular	YES
0.89 cm^2	rectangular	YES

was also investigated at elevated temperatures and showed a spontaneous ignition at 250°C due to the thermal decomposition of NH$_4$ClO$_4$.

CHAPTER 4

Volumetrically Photoignitable Solid Rockets

Solid rockets normally require electric matches, ferrous spark generators, or liquid-fueled pilot flames for ignition [22]. This makes solid rockets particularly difficult to ignite in vacuum conditions. Hot sparks do not burn in the absence of oxygen, and pilot lights add significant complexity to an ignition system. We considered various designs to demonstrate controllable volumetric ignition of solid rockets using photoignitable CNTs. Photoignition presents an attractive opportunity in the field of solid rocketry due to the self contained nature of the CNT ignition system which needs only a flash of light to initiate combustion at multiple points in the solid fuel.

The goal of this study is to demonstrate the feasibility of a (i) volumetrically ignitable, (ii) re-ignitable, and (iii) thrust vectorable photoignitable solid rocket. Volumetric ignition refers to the presence of multiple ignition points within the fuel volume. Re-ignitable refers to the ability to start, shut down, and restart the motor. Thrust vectoring refers to the ability to adjust the rocket's thrust vector with respect to its velocity or orientation vector. A small prototype rocket was constructed to demonstrate controllability of volumetric ignition. The apparatus and results for testing photoignitable solid rocket capabilities are detailed in the following sections.

4.1   Materials

In the current study, we used (i) Fe-catalyzed 50 wt.% Fe SWCNTs made by DC arc discharge and (ii) xylene-ferrocene catalyzed MWCNTs. Highly ferrous SWCNTs were obtained from

Unidym Corporation, Houston, TX. They had a reported 50 wt.% Fe nanoparticle impurity content. Figure 3.1 shows a SEM micrograph of these SWCNTs. They were black and "fluffy" in appearance and easily dispersed in air due to their low density. This made them difficult to contain and handle. MWCNTs were also obtained from US Research Nanomaterials, Houston, TX. They had 25-30 wt.% ferrocene nanoparticle impurities [44]. Figure 3.3 shows a SEM micrograph of these MWCNTs. These MWCNTs were reported to be capable of photoignition via flash lamp [44]. Ammonium perchlorate (NH_4ClO_4) and potassium permanganate ($KMnO_4$) were obtained from United Nuclear LLC. These oxidizers were used to accelerate combustion in mixtures with SWCNTs, MWCNTs and other solid fuels. These solid fuels included ferrocene ($Fe(C_5H_5)_2$) obtained from Sigma Aldrich Corp, and titanium hydride (TiH_2) obtained from Fisher Scientific.

The Xe flash lamp used for photoignition was a Neewer 300 Ws strobe/flash light obtained from Adorama Camera Inc. which was shined through a 3/8" thick borosilicate glass window obtained from McMaster Inc. The same Neewer 300 Ws flash lamp as that previously used for photoignition experiments in Chapter 3 was used for ignition of the prototypical rockets. Devcon 2-Ton clear epoxy (2-part epoxy) was used to create rigid, strong, and optically transparent bonds.

4.2 Experimental setup

Solid rocket "cells" were constructed to demonstrate a proof of concept for controllable volumetric photoignition. "Rocket cells" were small photoignitable solid rockets capable of stand-alone ignition. Several rocket cells were arranged in a grid and exposed to light through a specific mask. The mask allowed for specific cells in the pattern to be exposed to a Xe flash while others are kept dark. Figure 4.1 shows the components of (A) prototypical "rocket cell", and (B) a 9-cell rocket assembly. Each rocket cell consisted of a glass tube which served as both thermal insulation and structural support. Glass tubes were 1/4" OD borosilicate glass with an ID of 0.215" and were obtained from Fischer Scientific as glass

pipettes which were cut using a SiC glass cutter and liquid nitrogen to achieve a clean break. Only the straight portion of the pipettes was used in the construction of the prototypical rocket cells.

At the bottom of the glass tube, 10 mg of a SWCNT or MWCNT photoignitable mixture containing potassium permanganate (3,4,5,8,9, or 10) was placed into the tube against an optically transparent seal. The transparency of the seal was important so that light could pass through it to ignite the mixture. When mixtures did not contain potassium permanganate, rocket ignition was unreliable and rare with $< 10\%$ success rate. Mixtures containing potassium permanganate had a 90% success rate on average. On top of the CNT mixture, 50 mg of dry solid fuel containing 50 wt.% ferrocene and 50 wt % NH_4ClO_4 was placed. This served as a booster charge for the photoignitable mixture to properly and reliably ignite the solid fuel coating on the tube. A small cotton wad was used to secure the dry components in place. The tube's inside surface was coated with a UVCE (Ultraviolet Curable Epoxy), ferrocene, and NH_4ClO_4 mixture which was UV cured to the inside of the tube.

Ultraviolet Curable Epoxy (UVCE) was prepared from the following components: 70wt.% Sartomer CN975, 20wt.% Sartomer CN373, 9wt.% ethanol (200 proof, absolute), 1wt.% Sartomer brand powdered phenobenzone "Benz-X" Cole-Parmer brand flake phenobenzone was also effective. UVCE was prepared by dissolving phenobenzone in 200 proof ethanol. Ethanol solution was poured into the CN373 and mixed with a glass stirring rod until it was homogeneous. This mixture was then combined with CN975 to form the finished UVCE. The epoxy was cured using a 30 W 365 nm high power UV light emitting diode source, which was effective at curing the epoxy in less than 5 seconds at full power.

The various cells were secured in place vertically by mounting in an aluminum honeycomb. Aluminum honeycomb was used for structural support and was 0.25" cell (2.3 pcf) 0.985" thickness and made from 5052 aluminum alloy, donated by George Franck of TEKLAM Corp, Corona, CA. Figure 4.2 shows a photograph of the honeycomb. It is important to see that the glass tubes fit snugly into the honeycomb cells which held them upright and stable. The optically transparent seals were facing a 3/8" thick borosilicate window through which the
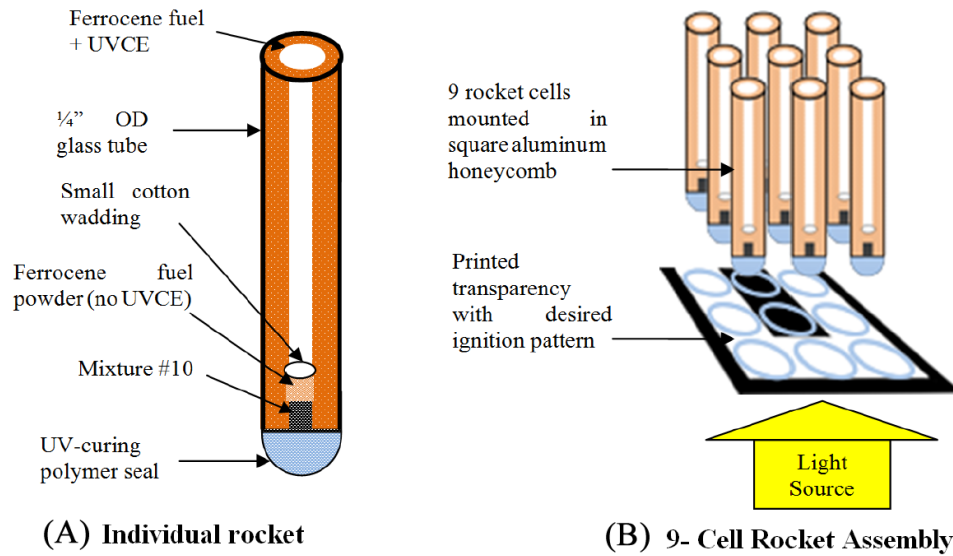
Figure 4.1: Shows (A) a diagram of an individual "rocket cell" and (B) a diagram of a 9-cell volumetric ignition setup meant to demonstrate controlled ignition through a laser printed transparency.

Xe flash lamp could expose the cells without risk of damage to the lamp. Between the rocket cells and the borosilicate window, a pattern was created using a laser-printed transparency sheet. This was designed to expose certain rocket cells to light from the flash and shield other cells.

4.3 Rocket cell assembly

The procedure for constructing the prototypical rocket cells was as follows:

1. The construction of an individual rocket cell began with the cutting of a borosilicate glass tube to between 2.5" and 3" in length. One side was smoothed via heating and will be referred to as the "smooth end". In the final rocket cell, the smooth end was facing down towards the flash lamp.

2. A syringe was used to deposit a thin uniform layer of UVCE onto the inside of the glass tube, from the top of the unsmoothed side to 1/2" away from the smooth end. 1/2" of tube surface was left dry of polymer near the smooth end of the tube.

3. Tubes were dipped and shaken in a ferrocene fuel powder and all wet UVCE surfaces were coated with solid fuel. The fuel consisted of 50 wt.% ferrocene mixed with 50 wt.% powdered NH_4ClO_4.

4. The tube was exposed to UV light until the UVCE cured. The tube was then placed in a secure holder with the smooth end facing up.

5. A small piece of cotton wadding was placed into the smooth end of the tube until it rested 1/4" into the fuel coated section. The size of the cotton wadding was large enough to fully block the tube to prevent powder and CNT from escaping, but small enough to be easily ejected from the tube at the onset of ignition.

6. 50 mg of the same ferrocene fuel used to coat the sides of the tube was poured into the smooth end. If correctly constructed none of the powdered fuel was able to pass the cotton wadding.

7. 10 mg of photoignitable mixture was placed on top of the ferrocene powder through the smooth end of the tube.

8. The smooth end of the tube was then sealed by either (i) applying clear 2-part epoxy resin, (ii) applying and curing UVCE, or (iii) sealing a thin polyethylene film to the end of the tube.

9. The cotton wad was then gently pressed down from the non-smooth end of the tube, until the CNT mixture touched the seal on the smooth end.
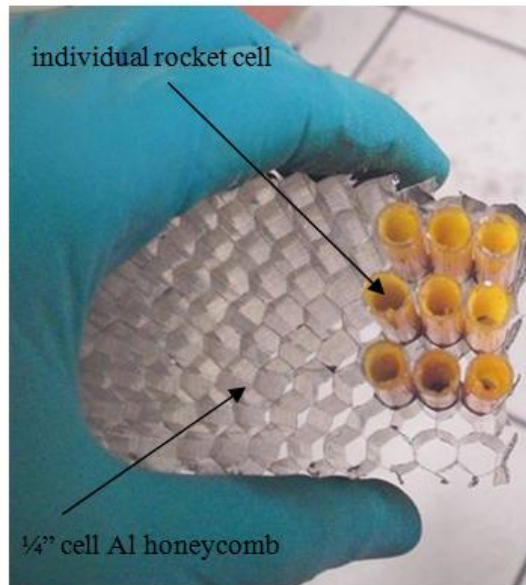
9- Cell Rocket Assembly

Figure 4.2: A photograph of a 9-cell volumetric ignition test showing the rough side of the cells facing up. The sample is intended to be flashed from the bottom and hot gas escapes from the top.

4.3.1 Volumetric solid rocket control test (9-Cell)

The 9-cell solid rocket test was conducted in order to demonstrate controllable volumetric photoignition of solid rockets. Figure 4.2 shows individual rocket cells held by an aluminum honeycomb with the smooth end featuring the optically transparent seal facing down towards the Xe flash lamp. These cells used a thin film of transparent UVCE as the sealant for the smooth end. The photoignition agent was SWCNT mixture 10. 9 cells in total were arrayed in a square to create the rocket in this experimental setup. The reliability of the photoignition reactions were observed.

4.3.2 Volumetric solid rocket re-ignition and vectoring test (15-Cell)

A more advanced design was constructed to demonstrate the capacity for re-ignition, throttling and thrust vectoring with photoignitable rocket cells. The same flashing apparatus as that shown in Figure 3.4 was used for testing the new 15-cell rocket engine. Figure 4.3 shows a schematic of the final 15-cell volumetric solid rocket design along with a picture of the prototypical rocket. A circular platform was chosen instead of a square for ease of machining and to illustrate the capacity for thrust vectoring. The sealant chosen for the rocket cells was 0.001" (1 mil) polyethylene film, backed with a 1/4" thick, 2" diameter borosilicate glass disk and which was secured with transparent 2-part epoxy resin. The photoignition agent was MWCNT mixture 5. An aluminum housing and nozzle was secured over the rocket cells to direct the combined thrust. The printed transparency between the borosilicate disk and flash lamp was used to determine which cells were exposed to the flash which resulted in a varying direction of the hot exhaust gases.

The 15-cell rocket consisted of 3 rows of rocket cells. Row (1) contained 4 cells, row (2) contained 6 cells, and row (3) contained 5 cells. Rows 1 and 3 were intended to demonstrate thrust vectoring, while row 2 was designed to demonstrate re-ignition potential.

The rocket was tested by exposing rocket cells to a Xe flash lamp through a 1/4" thick borosilicate glass disk at the bottom of the rocket motor. Four different experiments were carried out by placing the rocket on a 3" diameter, 3/8" thick borosilicate glass disk which served to protect the flash lamp from damage. The 15-cell testing was carried out by flashing four times. Figure 4.4 shows (a) a diagram of the placement of rocket cells in the 15-cell rocket motor, (b) a plain black transparency covering all cells for the control experiment, (c) a diagram of the first experiment which flashed 4 cells on the left side, (d) a diagram of the second experiment which flashed 5 cells on the right side, (e) a diagram of the third and final experiment which flashed the remaining 6 cells in the central row.

The capability for re-ignition and thrust vectoring of the rocket was assessed qualitatively. If the rocket was able to be ignited, extinguished, and re-ignited as intended (3 times) it would
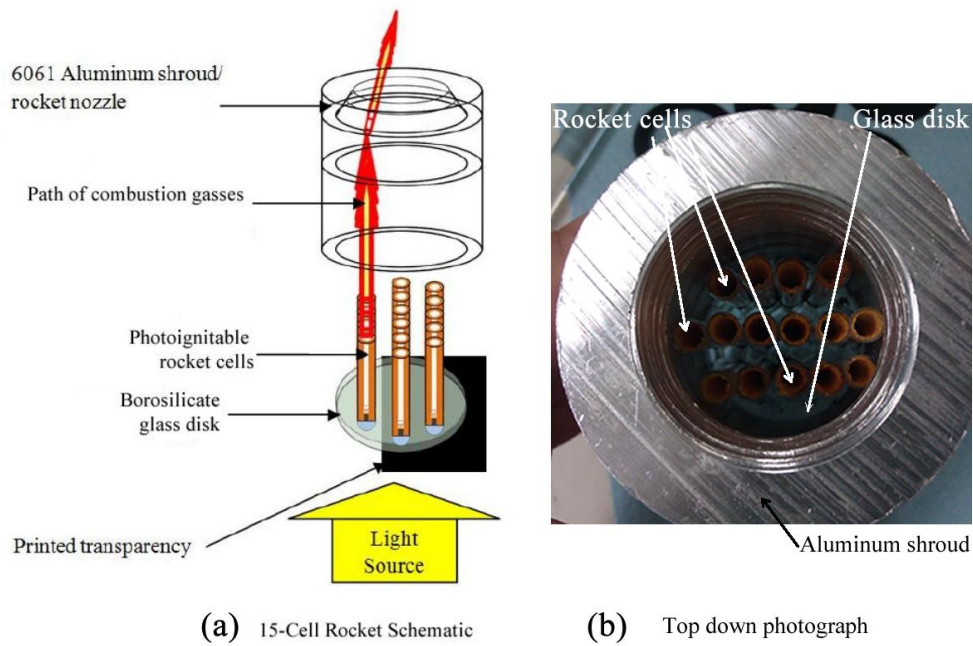
Figure 4.3: Shows (A) a diagram of the 15-cell volumetric solid rocket setup, demonstrating the intended path of hot combustion gasses and (B) a top down photograph of the various components of the 15-cell rocket motor.
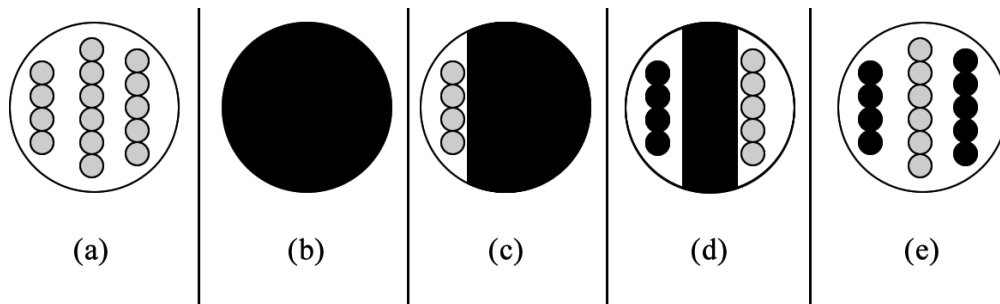
Figure 4.4: shows (a) the overall diagram of the placement of rocket cells in the 15-cell engine, and (b,c,d, and e) the patterns of laser transparencies used in the 4 tests of the engine.

confirm re-ignition of a volumetrically photoignited solid rocket. The general direction of the rocket's exhaust was observed in time sequence images. However, we were not able to study

the rocket's thrust characteristics quantitatively due to equipment limitations. Quantitative thrust analysis for volumetrically photoignited solid rocket motors is suggested as a topic of future study.

4.4   Experimental error and uncertainty

Experimental error was introduced due to the limitations of a 30 frame per second camera and the lack of a suitable high speed camera. Both Badakhshan *et al.* [11] and Berkowitz *et al.* [9] noted the use of a 1000 frame per second camera in their experiments, allowing them to see critical steps within the first 34 ms of the experiment we could not. The uncertainty in ignition delay time using our experimental setup was ± 17 ms, whereas their experimental error in ignition delay was ± 0.5 ms.

4.5   Results and discussion

4.5.1   Volumetric solid rocket control test (9-Cell)

Figure 4.5 shows the 9-cell rocket (a) before, (b) during, and (c) after firing. The 9 cells were assembled to demonstrate photoignition of the letter "U". While the upper right corner cell failed to fire, all other cells functioned as intended. In Figure 4.5 (a) the 9 individual cells are highlighted with circular outlines. Next, (b) shows the combusting rocket cells are highlighted by unfilled black circles and the unignited cells are highlighted by filled black circles. Finally, (c) shows the rocket after combustion ceased, cells which did not ignite are highlighted with circular outlines and cells which did ignite are highlighted with filled black circles. The firing continued for 2100 ms in total before all cells extinguished. The test showed 8 out of 9 cells functioning correctly, which equates to an 89% controllability for this application of volumetric ignition. With an improved photoignitable mixture, and more consistent construction of the rocket cells this success rate could easily be improved close to 100%.
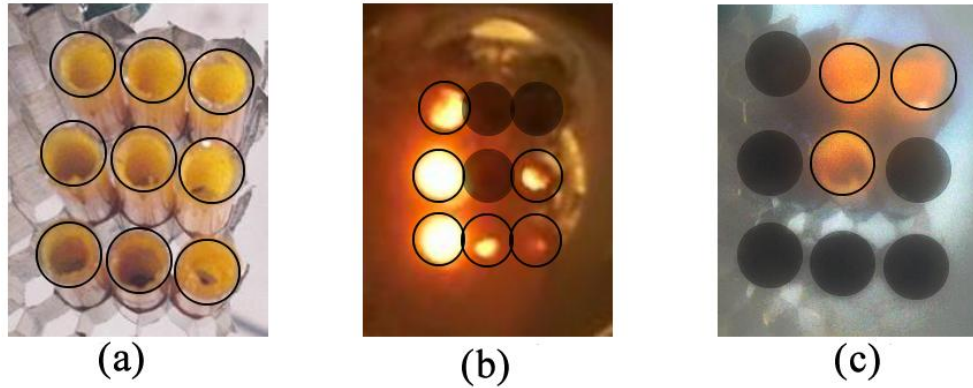
Figure 4.5: The 9-cell rocket (a) before, (b) during, and (c) after firing. The upper right hand corner cell failed to ignite as intended, but all other cells functioned as intended.

In theory, the technology demonstration was a success and with proper equipment and enough time, the design could be scaled up to spell "UCLA". Future work could include production of a large grid of rocket cells capable of producing thrust and digitally throttling the solid rocket cells by varying the number of cells flashed at a given time.

4.5.2 Volumetric solid rocket re-ignition and vectoring test (15-Cell)

After the capability to simultaneously ignite multiple rocket cells was demonstrated with the 9-cell volumetric photoignition test, the capability of the rocket cells to provide thrust vectoring and re-ignition was attempted with a larger 15-cell test. As an experimental control, the 15-cell rocket was first flashed with a fully black laser-printed transparency sheet which covered all cells. This was done to verify that the printed transparency effectively blocked the Xe flash and the cells would not unintentionally fire. The control test was 100% successful, with 0 cells firing. The rocket was then flashed with a transparency sheet which exposed 4 cells on the left side of the rocket to the Xe flash. Figure 4.6 shows a time sequence of the rocket firing. Images at 238 ms and 272 ms after flashing show a leftward deflection of the hot exhaust gasses. However, since there was no force sensor available at the time of its construction, the thrust and moment could not be quantitatively measured. An ignition

delay of 204 ms was observed in this test. Between 0 ms and 107 ms only hot sparks could be observed from the nozzle and after 204 ms a clear exhaust plume was visible. The firing continued for 1700 ms in total before its fuel was exhausted and the rocket extinguished.

Figure 4.6: Time sequence firing of the 15-cell volumetric rocket engine on its first ignition. A leftward deflection of the exhaust gasses is observed between 238 ms and 272 ms after flashing.

84

The rocket was flashed with a transparency sheet which exposed 5 cells on the right side of the rocket to the Xe flash. Figure 4.7 shows a time sequence of the rocket firing. At 204 ms after flashing, one of the cells detonated inside the enclosure. Glass and solid rocket fuel can be observed as it was ejected from the engine in the 272 ms frame. Despite the unexpected detonation, a rightward deflection of hot exhaust gasses was still observed at 34 ms but in all other images the direction of the exhaust gases is inconclusive. In contrast to the first flashing, there was no ignition delay observed in this test. The firing continued for 1300 ms in total before its fuel was exhausted and the rocket extinguished.

Figure 4.7: Time sequence firing of the 15-cell volumetric rocket engine on its second ignition. A rightward deflection of the exhaust gasses is observed at 34 ms after flashing. The detonation of a cell is visible at 204 ms after flashing, and the hot debris ejection can be seen at 272 ms after flashing.

The rocket was flashed with no transparency sheet, exposing the final 6 cells in the central row to the Xe flash. Figure 4.8 shows a time sequence of the rocket firing. These cells all fired correctly with no detonations. At 68 ms and 102 ms after flashing a slight rightward deflection of the hot gases can be observed. However, this could be attributable to the amateur design and construction of the nozzle or rocket cells. The firing continued for 5000 ms in total before its fuel was exhausted and the rocket self extinguished. The abnormally long firing length was most likely due to one cell not igniting with the initial flash but instead igniting from the heat of the other cells' combustion.

t=0 ms t=34 ms t=68 ms t=102 ms t=272 ms
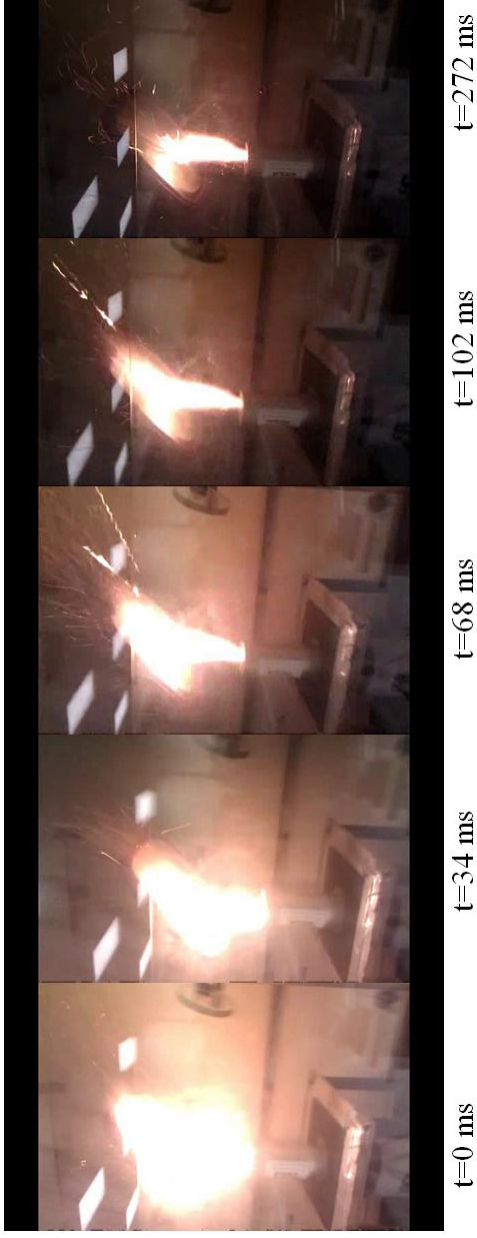
Figure 4.8: Time sequence firing of the 15-cell volumetric rocket engine, on its third ignition. A slight rightward deflection is observed between 68 and 272 ms after flashing. It may be attributable to the amateur design and construction of the rocket.

88

During the final firing, we suspect that one cell failed to photoignite properly. During the second firing one cell clearly detonated. This demonstrates a success rate of 13/15 cells which correctly photoignited, or a success rate of 87%.

4.6 Conclusions

The construction and testing of the 15-cell rocket engine demonstrated a partial proof of concept for thrust vectoring and a full proof of concept for the re-ignitability of photoignitable solid rockets. Further testing using quantitative thrust measurements will be necessary for a full proof of concept of thrust vectoring capabilities. When cells were flashed in parallel their combustion lasted between 1300 and 2100 ms. The number of cells flashed in parallel did not appear to have an effect on their combined burn time. However, an anomaly was observed in the third experimental flashing of the 15-cell rocket which continued combustion for a full 5000 ms. The ignition capabilities of both the 9-cell and 15-cell volumetrically photoignitable solid rocket designs shows great promise for reliable and safe rocket ignition systems based on this technology. The test of the 9-cell volumetric rocket demonstrated an 89% success rate for photoignitable solid rocket cells. The test of the 15-cell volumetric rocket demonstrated a success rate of 87%. We believe that the success rate for photoignitable solid rockets could be improved close to 100% with more repeatable and quality controlled manufacturing of the rocket cells.

CHAPTER 5

Conclusions and Future Work

This chapter aims to summarize the results from the present study and the potentially new applications for photoreactive nanomaterials. Suggestions for future testing and experimentation based on the results from Chapters 3 and 4 are also discussed.

5.1 Conclusions

This study investigated the use of photoignition of SWCNTs and MWCNTs for aerospace applications. Tests were conducted on solid fuel volumetric ignition of SWCNTs to supplement the research of Chehroudi *et al.* [11] and the research of Berkowitz *et al.* [9], which focused on liquid and gaseous fuel volumetric ignition of SWCNTs, respectively. Mixtures of energetic materials and photoignition agents such as MWCNTs and SWCNTs were tested and analyzed. SWCNTs, MWCNTs and NH_4ClO_4/SWCNT samples were analyzed to determine their MIE as a function of bulk temperature using a custom made flash thermal energy sensor.

5.1.1 CNT photoignition

One of the objectives of our study was to assess the dependence of CNT photoignition on atmospheric composition, atmospheric and physical pressure, solid impurities, and bulk temperature of the CNTs bundle. Regarding the photoignition dependence of CNT. The following conclusions can be reached.

    1. Photoignition of both SWCNTs and MWCNTs was found to be dependent on the

oxygen content of the atmosphere. The higher the local oxygen concentration was at the time of flashing, the more complete the combustion was.

2. SWCNTs containing Fe nanoparticles exhibited a different ignition from MWCNTs containing ferrocene. SWCNTs photoignited alone yielded a long oxidization of the Fe nanoparticles but no combustion. MWCNTs photoignited alone yielded a distinct combustion of the ferrocene nanoparticles. SWCNTs photoignited in mixtures yielded a leaner and more complete combustion than MWCNTs which displayed more fuel rich combustion.

3. Solid oxidizers and fuels in mixtures of CNTs played a large role in determining their ability to photoignite. When solid oxidizers were added to mixtures of CNTs, their ignition was much more energetic than that of CNTs alone. Ignition delay times, burn times, and thermal energy release all depended strongly on the presence and compositions of the solid components of the CNTs mixture.

4. It was determined through the MIE characterization tests in Section 3.4.2 that SWC-NTs, MWCNTs and NH_4ClO_4/SWCNTs had vastly different photoignition responses when pre-heated above room temperature. It was clear that the solid impurities such as iron, ferrocene, or ammonium perchlorate had a much greater impact on ignition characteristics at elevated temperature than did the structure of the CNTs. The temperature dependent properties of the impurities were clearly observed at high temperature. For example, ferrocene sublimed at 249° C, NH_4ClO_4 decomposed at 250° C, Fe oxidized without flashing beyond 350° C. However, we saw no decomposition of the pure carbon in CNTs with increasing temperature. We observed evidence that the CNTs acted only as a light absorption medium which supplied the initiation energy to subsequent reactions at the sites of reactive impurities within the CNT bundle such as iron nanoparticles, ferrocene, and/or solid oxidizers.

5.1.2 Photoignitable solid fuel mixtures

Another objective of the current study was to demonstrate photoignition of SWCNTs and MWCNTs when used in solid mixtures with various oxidizers, fuels, and metallic powders. Through qualitative testing of 10 mixtures consisting of SWCNTs, MWCNTs, NH_4ClO_4, $KMnO_4$, ferrocene, and TiH_2 in various proportions, the following was observed.

SWCNTs and MWCNTs were both capable of photoignition, both in pure form and as components in mixtures with various oxidizers and fuel powders. While mixtures containing SWCNTs and MWCNTs differed slightly in ignition characteristics, the effect of solid oxidizers and fuels was much greater than the effect of the type of CNTs used. For example, the addition of NH_4ClO_4 enabled a faster and more energetic combustion of both SWCNTs and MWCNTs. The use of $KMnO_4$ in conjunction with NH_4ClO_4 created an elevated oxygen concentration in the local atmosphere which caused a leaner and more complete combustion of both SWCNTs and MWCNTs. The addition of ferrocene lengthened combustion time for both SWCNTs and MWCNTs. Finally, the addition of TiH_2 caused a large thermal energy release in both SWCNTs and MWCNTs. The only effect of CNT type which could be observed was the incomplete combustion of photoignitable MWCNT mixtures (such as those containing ferrocene), in contrast with identical SWCNT mixtures which had a more complete combustion.

An anomalous result was obtained when titanium (II) hydride (TiH_2) was added as a fuel powder in a mixture consisting of SWCNTs, NH_4ClO_4 and $KMnO_4$. The result was a vastly increased energy release and a more energetic combustion reaction. The energy release was not as pronounced as in a similar mixture containing MWCNTs. It is not clear at this time why TiH_2 had such an effect on the photoignition of such a mixture, or why it produced so much more energy than other fuels. However, the effect was repeatable and pronounced for TiH_2 concentrations of 5 - 20 wt.% in mixtures also containing $KMnO_4$ and NH_4ClO_4. An investigation of SWCNT/TiH_2 mixtures warrants further study.

5.1.3 CNTs for spacecraft propulsion

Our final objective was to demonstrate proof of concept for spacecraft propulsion using CNT-based photoignitable materials.

Volumetric solid rockets were constructed to investigate the controllability of SWCNTs and MWCNTs photoignition. First, 9 photoignitable rocket cells were constructed which contained a mixture consisting of SWCNTs, NH_4ClO_4, $KMnO_4$, and TiH_2 as the photoignition source. "Rocket cells" consisted of (i) a SWCNT or MWCNT photoignition agent, (ii) a ferrocene and NH_4ClO_4 booster charge, and (iii) a UVCE, ferrocene, and NH_4ClO_4 propellant grain. The cells were placed in a square array and were flashed with a "U" pattern. This experiment successfully demonstrated the controllability of the photoignition process in solid rockets.

Furthermore, a prototypical re-ignitable, controllable, and thrust vectoring solid rocket motor was constructed. This experiment utilized 15 photoignitable rocket cells which contained a mixture consisting of MWCNTs, NH_4ClO_4, $KMnO_4$, and TiH_2 as the photoignition source. It successfully demonstrated a proof of concept for re-ignitable solid rockets based on photoignitable nanomaterials. Thrust vectoring was qualitatively observed but could not be quantitatively measured. Quantitative thrust analysis for photoignitable solid rocket cell arrays is suggested as a topic for future study. Future work will now be suggested based on inconsistencies and unanswered questions identified in the literature, and based on the results of the present study.

5.2 Future work

5.2.1 Effect of photon energy on MIE

Table 2.2 shows ignition energy versus wavelength data obtained by Chehroudi *et al.* [10]. However, it can be argued that the results of their study are inconclusive with regards to the effect of light wavelength on MIE. It is suggested that additional work be done to assess the

wavelengths for which CNTs are most responsive to photoignition using optical bandpass filters. In our studies, we found that when light was passed through UV-vis liquid light pipes (77628, from Spectra-Physics, U.S.A) which filtered the Infrared (IR) portion of the light from the Xe flash lamp, ignition was not possible using our 300 Ws lamp, even when the light pipe was placed directly against the flash bulb and the other end against the SWCNTs. Badakhshan *et al.* [15] conducted experiments using a silica fiber optic light pipe and they were easily able to ignite SWCNTs. Silica fiber optic light guides block more UV light allow most IR to pass through. Our findings suggest that the CNT photoignition might be more responsive to IR light. However, because the Xe flash lamp spectra seen in Figure 3.5 has higher emission in the IR wavelengths than UV, it is unknown whether SWCNTs are truly more sensitive to IR wavelengths, or whether it is simply that more energy from the lamp is emitted in those wavelengths. By blocking the IR light, one may be simply blocking the majority of the Xe flash lamp's output and lowering the total energy delivered to the SWCNTs below the MIE threshold.

The effect of higher energy photons on SWCNT photoreactions is unknown. Wavelengths on the order of the SWCNT diameter such as X-rays ($\lambda \sim 0.01$ nm to 10 nm) may have an entirely different effect on SWCNTs than wavelengths on the order of the SWCNT length such as microwaves ($\lambda \sim 1$ mm to 1000 mm) and infrared ($\lambda \sim 0.75$ μm to 1 mm).

5.2.2 CNTs for spacecraft propulsion

A new form factor for solid rocketry could be made possible through use of a system similar to the 9-cell test reported in this study. In space, a throttling solid rocket array with a design similar to the 9-cell rocket could be used to provide limited thrustor capability on small spacecraft. Square photoignitable solid rocket panels could be attached to six sides of a cube-like micro-satellite or spacecraft and used to avoid space debris on short notice. A system of fiber-optic cables leading to a LCD screen and flash lamp could be used to direct flash energy to specific cells. Proof of concept for vacuum ignition of photoignitable rocket cells would first be needed to validate the feasibility of this system.

References

[1] D. Cook, "Simple model rocket launch controller", http://www.robotroom.com/Model-Rocket-Launch-Controller.html, 2010.

[2] U. Sleytr and B. Wien, "Nanotechnology, the convergence of scientific disciplines", http://pchem.univie.ac.at/en/materials-science-centre-of-nanotechnologies/.

[3] S. Iijima, "Helical microtubules of graphitic carbon", *Nature*, vol. 354, pp. 56– 58, 1991.

[4] G. L. Hornyak, H. F. Tibbals, J. Dutta, and J. J. Moore, *Introduction to Nanoscience and Nanotechnology*, CRC Press, Boca Raton, FL, 2009.

[5] S-kei, "Plasma CVD reactor diagram", commons.wikimedia.org/wiki/File:PlasmaCVD.PNG, 20 Sep 2008.

[6] Ltd. Rigaku Mechatronics Co., "Arc discharger contributing to nanotechnology", http://www.rigaku.co.jp/rms_en/application/appli02.html, 2006.

[7] D.Z. Guo, G.M. Zhang, Z.X. Zhang, Z.Q. Xue, and Z.N. Gu, "Visible-light-induced water-splitting in channels of carbon nanotubes", *The Journal of Physical Chemistry B*, vol. 110, no. 4, pp. 1571– 1575, 2006.

[8] P.M. Ajayan, M. Terrones, and A. de la Guardia, "Nanotubes in a flash-ignition", *Science*, vol. 296, pp. 705, 2002.

[9] A. Berkowitz and M. Oehlschlaeger, "Photo-induced ignition of quiescent ethylene/air mixtures containing suspended carbon nanotubes.", *Proceedings of the Combustion Institute*, vol. 33, pp. 3359– 3366, 2011.

[10] B. Chehroudi, "Minimum ignition energy of the light-activated ignition of single-walled carbon nanotubes (SWCNTs)", *Combustion and Flame*, vol. 159, no. 2, pp. 753 – 756, 2012.

[11] A. Badakhshan, S. A. Danczyk, D. Wirth, and L. Pilon, "Ignition of liquid fuel spray and simulated solid rocket fuel by photoignition of carbon nanotubes utilizing a camera flash", JANNAF Liquid Propulsion Conference, 2011.

[12] R. Manaa, A. Mitchell, and R. Garza, "Flash ignition and initiation of explosives-nanotubes mixture.", *Journal of the American Chemical Society*, vol. 127, pp. 13786– 13787, 2005.

[13] T. W. Bastian and S. J. Roberts, "Multi-burn solid fuel restartable rocket and method of use", US Patent No. 4357795, Nov. 9, 1982.

[14] S. Tseng, N. Tai, W. Hsu, L. Chen, J. Wang, and C. Chiu, "Ignition of carbon nanotubes using a photoflash.", *Carbon*, vol. 45, pp. 958– 964, 2007.

[15] B. Chehroudi, S. Danczyk, and A. Badakhshan, "Distributed ignition using SWCNTs with applications in aerospace and future automotive engines", *Recent Patents on Space Technology*, vol. 2, pp. 67 –75, 2010.

[16] A. Vignes, O. Defaud, L. Perrin, D. Thomas, J. Bouillard, A. Janes, and C. Vallieres, "Thermal ignition and self-heating of carbon nanotubes: From thermokinetic study to process safety", *Chemical Engineering Science*, vol. 64, pp. 4210– 4221, 2009.

[17] B. Giles, "Experimental optical methods, xenon flashlamp spectra", http://utopia.cord.org/cm/leot/course04_mod04/4_fig22.jpg.

[18] R. J. Brown, P. J. Brewer, and M. J. Milton, "The physical and chemical properties of electroless nickel-phosphorus alloys and low reflectance nickel-phosphorus black surfaces", *Journal of Materials Chemistry*, vol. 12, pp. 2749– 2754, 2002.

[19] Duane Johnson, "Absorptivity & emissivity table 1 plus others", http://www.solarmirror.com/fom/fom-serve/cache/43.html, 2010.

[20] "CVI Miles Griot filters", http://www.cvimellesgriot.com/.

[21] "Edmund optics filters", http://www.edmundoptics.com/products/.

[22] G. P. Sutton and O. Biblarz, *Rocket Propulsion Elements, Eighth Edition*, Wiley, Hoboken, NJ, 2010.

[23] R. Clark and R. Sheldon, "Dusty plasma based fission fragment nuclear reactor", *American Institute of Aeronautics and Astronautics*, vol. 41, pp. 4460, 2005.

[24] D. Goebel and I. Katz, *Fundamentals of Electric Propulsion*, Wiley, Hoboken, New Jersey, 2008.

[25] C. D. Brown and AIAA education series, *Spacecraft Propulsion*, AIAA, Washington, DC, 1996.

[26] R. Varvill and A. Bond, "A comparison of propulsion concepts for SSTO reusable launchers", *The Journal of the British Interplanetary Society*, vol. 56, pp. 108– 117, 2003.

[27] G. L. Hornyak, H. F. Tibbals, J. Dutta, and J. J. Moore, *Introduction to Nanoscience and Nanotechnology*, CRC Press, Boca Raton, FL, 2009.

[28] M.J. Bronikowski, P.A. Willis, D.T. Colbert, K. A. Smith, and R.E. Smalley, "Gas-phase production of carbon single-walled nanotubes from carbon monoxide via the HiPco process: A parametric study", *Journal of Vacuum Science Technology A: Vacuum, Surfaces, and Films*, vol. 19, no. 4, pp. 1800 –1805, 2001.

[29] M. Meyyappan, L. Delzeit, A. Cassell, and D. Hash, "Carbon nanotube growth by pecvd: a review", *Plasma Sources Science and Technology*, vol. 12, pp. 205– 216, 2003.

[30] Z. Shi, Y. Lian, X. Zhou, Z. Gu, Y. Zhang, S. Iijima, L. Zhou, K. T. Yue, and S. Zhang, "Mass-production of single-wall carbon nanotubes by arc discharge method", *Carbon*, vol. 37, pp. 1449– 1453, 1999.

[31] Z. Xu, X. Bai, Z. L. Wang, and E. Wang, "Multiwall carbon nanotubes made of monochirality graphite shells", *Journal of the American Chemical Society*, vol. 128, no. 4, pp. 1052– 1053, 2006.

[32] A.L. Sundar Rao, *Photodecomposition and absorption spectrum of potassium permanganate*, Indian Academy of Sciences, The Bangalore Press, Bangalore, India, 1937.

[33] Y. Yamamoto and M. Nishimura, "Association of two manganese atoms with the reaction center of photosystem ii in a highly active O_2-evolving photosystem ii preparation", *Biochimica et Biophysica Acta (BBA) - Bioenergetics*, vol. 724, no. 2, pp. 294 – 297, 1983.

[34] S. Desilets and P. Brousseau, "Flash ignitable energetic material", US Patent No. 20080066835A1, March 20, 2008.

[35] S. Gilje, S. Dubin, A. Badakhshan, J. Farrar, S. A. Danczyk, and R. B. Kaner, "Photothermal deoxygenation of graphene oxide for patterning and distributed ignition applications", *Advanced Materials*, vol. 22, pp. 419– 423, 2010.

[36] I. V. Blonskij, M. S. Brodyn, V. A. Tkhoryk, A. G. Filin, and J. P. Piryatinskij, "The photoacoustic effect in porous silicon: peculiarities of its manifestation and its application to the investigation of optical and thermal properties of materials", *Semiconductor Science and Technology*, vol. 12, pp. 11– 12, 1997.

[37] J. Smits, B. Wincheski, M. Namkung, R. Crooks, and R. Louie, "Response of fe powder, purified and as-produced hipco single-walled carbon nanotubes to flash exposure", *Materials Science and Engineering*, vol. A358, pp. 384– 389, 2003.

[38] G. P. Sutton and O. Biblarz, *Rocket Propulsion Elements, Eighth Edition*, Wiley, Hoboken, NJ, 2010.

[39] P. A. Czysz and C. P. Rahaim, "comparison of SSTO launchers powered by an RBCC propulsion system and a pulse detonation wave propulsion system", *Proceedings of 6th International Symposium on Propulsion for Space Transportation of the 21st Century*, pp. 14– 16, 2002.

[40] S. Hong and Myung S., "Nanotube electronics: A flexible approach to mobility", *Nature Nanotechnology*, vol. 2, pp. 207 – 208, 2007.

[41] B. Peng, M. Locascio, P. Zapol, S. Li, S. L. Mielke, G. C. Schatz, and H. D. Espinosa, "Measurements of near-ultimate strength for multiwalled carbon nanotubes and irradiation-induced crosslinking improvements", *Nature Nanotechnology*, vol. 3, pp. 626 631, 2008.

[42] K. Mizuno, J. Ishii, H. Kishida, Y. Hayamizu, S. Yasuda, D. N. Futaba, M.otoo Yumura, and K. Hata, "A black body absorber from vertically aligned single-walled carbon nanotubes", *Proceedings of the National Academy of Sciences*, vol. 106, no. 15, pp. 6044–6047, 2009.

[43] D. A. Rains, "Laser initiation of solid propellant rocket ignition", *JANAF-ARPA-NASA Solid Propellant Group*, vol. 3, pp. 71–82, 1962.

[44] US Research Nanomaterials, "Flash-ignited multi-walled carbon nanotubes", http://www.us-nano.com/inc/sdetail/314, 2011.

[45] L. Liu, F. Li, L. Tan, L. Ming, and Y. Yi, "Effects of nanometer Ni, Cu, Al and NiCu powders on the thermal decomposition of ammonium perchlorate", *Propellant, Explosives, Pyrotechnics*, vol. 29, pp. 34– 38, 2004.

[46] D. R. Lide, *CRC Handbook of Chemistry and Physics*, CRC Press, Boca Raton, FL, 86th edition, 2005.